EXPERIMENTAL AND NUMERICAL QUANTIFICATION OF EV AND PHEV BATTERY PACK THERMAL ISOLATION STRATEGIES

by

Joseph Brennan

A Thesis Submitted in Partial Fulfilment of the Requirement for the Degree of

Masters of Applied Science in Automotive Engineering

in

The Faculty of Engineering

University of Ontario Institute of Technology

October 30, 2015

Abstract

The objective of this thesis is to quantify the effects of passive thermal management achieved through augmenting thermal isolation incorporated into an electrified vehicle's energy storage system by design. Temperature changes within the cells are to be minimized over the typical 24 hour daily cycle when exposed to extreme ambient climates. Productionized thermal management solutions take the approach of increasing heat transfer through augmented system power to maintain cell temperatures in their operating range under demanding conditions. The intent of this work is to provide feasible design alternatives that reduce active battery thermal management requirements and thereby parasitic power losses for an electrified vehicle by applying fundamental engineering design principles.

Considering a production intent vehicle envelope as a packing constraint, various methods of increasing thermal isolation are explored. Techniques are evaluated based on their overall effectiveness, as well as their ability to be packaged efficiently within a production energy storage system. Consequent cost and mass increases are considered as limiting factors when presenting the design alternatives.

Keywords:

Electric Vehicle, Energy Storage, Thermal Management System, Plug-In Hybrid, Finite Element Analysis, Computational Fluid Dynamics

Author's Declaration

I hereby declare that I am the sole author of this thesis. This is a true copy of the thesis, including any required final revisions, as accepted by my examiners. I understand that my thesis may be made electronically available to the public.

Dedication

I would like to dedicate this thesis to my parents Rick and Marilyn Brennan for their encouragement, and my fiancé (now wife) Lauren Uebrueck who simply did not allow me to give up.

Acknowledgements

I would like to acknowledge my faculty advisor Dr. Greg Rohrauer for giving me the opportunity and inspiration to complete this thesis. With his guidance I was able to develop a deeper understanding of electric vehicle battery thermal management and more broadly electric vehicle design. The support gained through EcoCar: The Next Challenge (With headline sponsorship by General Motors and US Department of Energy, administered by Argonne National Labs) and through a grant from Automotive Partnerships Canada, NSERC APC 386787-09, made this endeavor possible.

Contents

Table of Figures

List of Tables

List of Abbreviations

A	Ampere
BAS	Belt Alternator Starter
BMS	Battery (charge) Management System
BTMS	Battery Thermal Management System
C	Charge Rate: 1C = 1 hour for complete charge
CAD	Computer Aided Design
CAE	Computer Aided Engineering
CARB	California Air Resource Board
CFD	Computational Fluid Dynamics
CNG	Compressed Natural Gas
DOD	Depth Of Discharge
EPA	Environmental Protection Agency
EREV	Extended Range Electric Vehicle
ESS	Energy Storage System
EV	Electric Vehicle
FCEV	Fuel Cell Electric Vehicle
FE	Finite Element
FEA	Finite Element Analysis
FFEV	Full Function Electric Vehicle
FWD	Front Wheel Drive

GHG	Green House Gas
HEV	Hybrid Electric Vehicle
IC	Internal Combustion
LFP	Lithium Iron Phosphate
Li-ion	Lithium Ion
LMO	Lithium Manganese Oxide
LPH	Litres per 100 kilometres
MPG	Miles per Gallon
MSRP	Manufacturers Suggested Retail Price
NiCd	Nickel Cadmium
NiMH	Nickel Metal Hydride
NMC	Lithium Nickel Manganese Cobalt Oxide
PCM	Phase Change Material
PHEV	Plug-In Hybrid Electric Vehicle
Q	Heat Work (J)
$\bar{Q}$	Rate of Heat Transfer (W/s)
RWD	Rear Wheel drive
SEI	Solid Electrolyte Interface
SMC	Sheet Molded Compound
SOC	State Of Charge
T	Thermal Time Constant (s)

TE	Thermo-Electric Unit
USDOE	US Department of Energy
V	Volt
VRLA	Valve Regulated Lead Acid
W	Watt
Ω	Ohm

Chapter 1. Introduction

As global emissions and fuel economy targets become stricter the fraction of the automotive market belonging to partially and fully electrified vehicles is rapidly on the rise. Designing and building electrified vehicles presents manufacturers with new cost and packaging challenges. Electric vehicles (EVs), and partially electrified vehicles must be able to provide similar range, refueling time, and overall value as their more traditional internal combustion (IC) engine powered counterparts. Keeping range and refueling time competitive with IC powered vehicles leads to utilizing more advanced cell chemistries with higher energy densities and charge rate capabilities. Battery systems capable of providing such attributes are costly and therefore this makes it difficult for electrified vehicles to remain cost competitive. Currently in the US and Canada, as in other parts of the world, government incentives exist to help offset this cost increase. However as incentives are reduced and eventually taken away, manufacturers must find the means to produce electrified vehicles which are truly cost competitive.

Electrified and partially electrified vehicles are commercially available today in various forms. Hybrid vehicles (HEV) come in both strong and mild variants. Mild HEVs either replace or augment the traditional 12V starting battery allowing the IC engine to be turned off while the vehicle is coasting or stationary. Strong HEVs perform the same functions as mild HEVs but add the ability to augment tractive force to the vehicle's powertrain. The purpose of this is to increase fuel economy by permitting the IC engine to be downsized and thereby spend a greater portion of time operating at high load. This puts it closer to its optimal efficiency point. Both types of HEVs generally feature a relatively small ESS that is not critical to vehicle's function and therefore ESS use can be limited or even eliminated if cell temperatures are such that they would sustain damage under load. Plug-in hybrid electric vehicles (PHEV) perform the same functions as strong HEVs but add the ability for the battery system to substitute as the primary source of tractive energy for up to a given range. They feature a larger ESS that can be recharged and operated in a charge depleting mode. Generally speed and acceleration is curtailed when operating using only the electric ESS. Extended range electric vehicles (EREV) further the proposition by making the electric

motor and ESS combination large and powerful enough to act as the primary source of propulsion. EREVs generally feature a small IC engine which does not provide tractive force directly but instead acts primarily to generate electricity, recharging the cells within the ESS. This gives EREVs the attributes of an EV, while eliminating the consumer range anxiety developed from lack of fast re-charge ability when longer trips are planned. They do however have the disadvantage of higher complexity and parts count compared to a full function EV. As EREVs and EVs rely primarily on the electric ESS for vehicle power, they feature the high capacity battery packs that must operate anytime the vehicle is driven. Battery thermal management is of higher importance in these vehicles compared to other partially electrified forms, as the battery cannot simply be bypassed. This type of application is the focus of the research presented.

In order to reduce battery capacity loss and increase its cycle life, a battery thermal management system (BTMS) is employed to maintain cells at optimal operating temperature. These systems while necessary to ensure consumer satisfaction regarding vehicle life (system longevity and capacity fade) represent an additional cost, mass, and packaging challenge for manufacturers. The BTMS needs to be designed such that it is capable of protecting the ESS from heat generated within the cells, transferred from other vehicle components, and emanating from ambient influence.

Generally a BTMS is sized by calculating the cumulative peak of all heat sources and then designing a system that can extract, or in the case of cold ambient conditions add, an appropriate amount of heat to maintain the cells within the ESS at their optimal operating temperature. Lithium-ion (Li-ion) cell chemistry is commonly used in EVs as they exhibit good energy and power density. Their optimal operating temperature is in the range of 15 to 30 °C [1]. Cells are able to operate ~ 10-15 °C outside of this range in either direction however aging effects begin to increase. At lower temperatures cells are not able to deliver energy as effectively and also suffer from premature aging when exposed, and especially when utilized in extreme cold environments [2]. This is aside the well-known hot exposure ageing effects.

In order to maintain cells within their optimum operating temperature range, energy needs to be removed from the ESS and used by the BTMS, this leads to a reduction in vehicle range

and thereby efficiency which can become significant in the case of extreme ambient environments. Optimally a system would be designed such that it requires the least amount of energy to maintain optimal ESS temperature without increasing cost or vehicle mass. One such way to partially achieve this objective is to increase the thermal isolation of the ESS.

1.2 Thesis Goals

The goal is to minimize the power requirements of a battery thermal management system through increasing the thermal isolation of the battery pack. The system examined shall be constrained within the packaging of a production vehicle. For this a Chevrolet Volt EREV is targeted as reflective of the production vehicle environment. Minimization of thermal management power needs is attained through added thermal isolation or incorporating features such that the amount of heat energy required to maintain the battery within its optimal temperature range is minimized. The practical metric used to quantify this minimization of the thermal management system energy needs is the reduction of temperature rise when exposed to heat, as characterized by the characteristic time constant following a step input.

1.3 Approach

The optimization of pack design for thermal isolation does not follow traditional engineering design methodologies in some key respects. **Error! Reference source not found.** Figure 1-1 shows the actual design development methodology followed. In this case much of the preliminary analysis and concepts to be explored were identified and shown to be viable through UOIT's (University of Ontario Institute of Technology) EcoCAR project. Throughout the competition, the author along with other members of UOIT's EcoCAR team developed an ESS for a full function electric vehicle (EV). This included both a BTMS and a pack designed for high thermal isolation while maintaining structural rigidity. In such a proof of concept it was identified that for the case of a massive battery in an EV designed for long range, the

biggest heat source in fact was not from cycling of the pack, but rather from its exposure to ambient conditions. The condition is a consequence of the surface area to volume ratio of the pack coupled with its thermal mass. It led to the development of a BTMS aimed at protecting the cells within the ESS from the ambient environment. An active liquid cooling system design was hence converged upon and the ESS was insulated to protect cells from the surroundings. However within the EcoCAR design prototype, gains were never quantified from the point of truly evaluating the thermal isolation approach and quantifying the expected energy savings. This design had evolved from the need to provide sufficient thermal management within the very limited remaining packaging space and it led to the concept of utilizing insulation as a means of reducing BTMS size and power requirements.

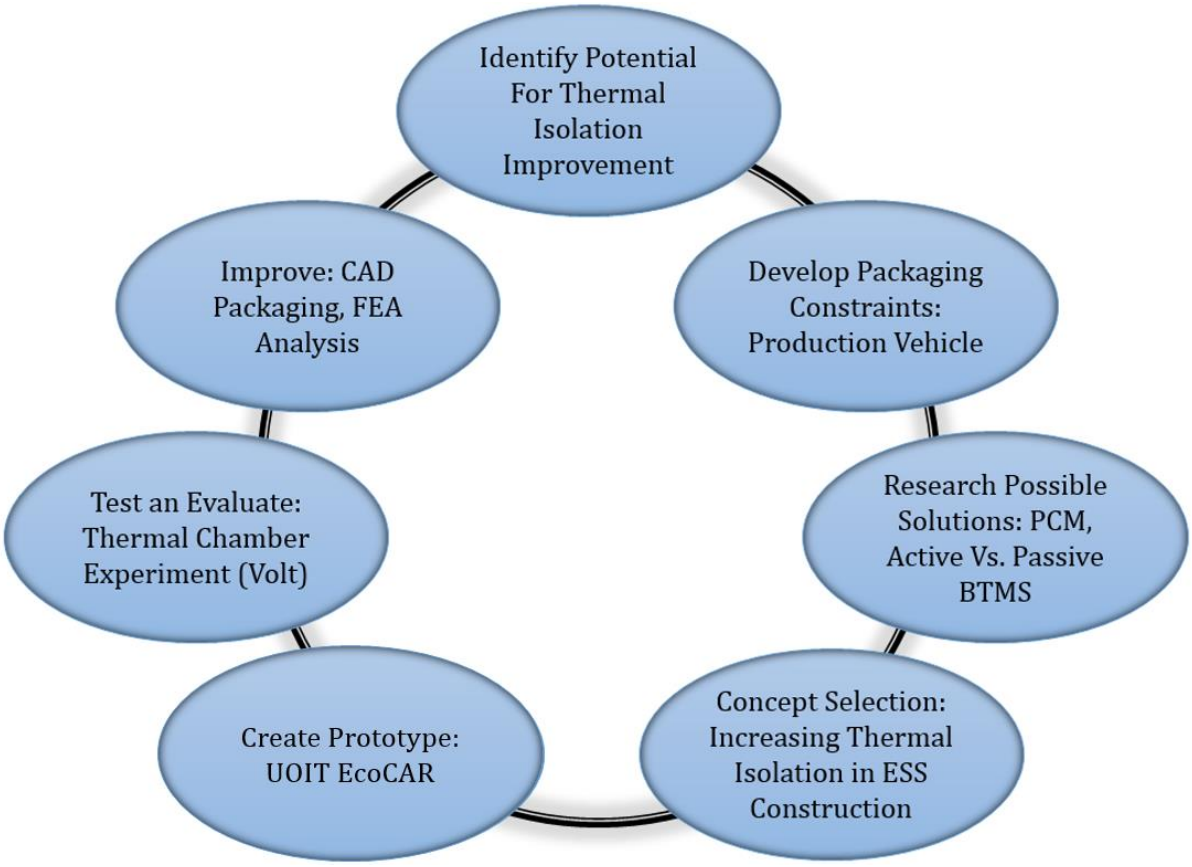

Figure 1-1, Concept development using engineering design

The gains anticipated with the EcoCAR concept were later analyzed and quantified through HVAC research development work carried out on a production Chevrolet Volt ESS. It was realized the design constraints were similar, and that a bit of added insulation would easily

shift the ambient heat flux to thermal mass ratio towards the same condition as those found with the EcoCAR pack, albeit the less favorable surface area to volume ratio of this smaller battery. This later research project's objectives and deliverables were to identify areas within the HVAC system where energy reductions were possible and thermal management system efficiency could be gained. Multiple students were engaged in the endeavor, each focusing on different means towards thermal management improvements. The portion outlined in this thesis centers on the quantification of the gains that added insulation provides as a means of reducing BTMS energy requirements. In this work experimental quantification of increasing the thermal isolation by the addition of varying amounts of insulation, as first displayed in the EcoCAR prototype, is undertaken. Constraining the design requirements further is the development of a proof of product within an existing production environment, rather than a more open-ended conceptual prototype. This restricts the addition of insulation with competing factors like space for passengers, adding extra cells, increased system cost, and ultimately return on investment potential.

Considering the temperature rise and fall throughout a day, typically high temperatures are experienced near midday, while low temperatures occur after midnight. Aside from extreme cold and extreme hot environments, average conditions over the day will often actually fall within an optimal range for Li-ion cell operation. Figure 1-2 shows temperature data for Phoenix Arizona which would be considered an extremely hot environment. The daily temperatures through the hot season (center of chart) can be seen to swing between 25 and 45 °C, but the nighttime is mitigating. If a pack could be constructed in such a way that temperature rise from ambient is minimized through the hot portion of a 24 hour temperature cycle the BTMS power requirement could be greatly reduced. The same can be said for a cold environment in the north where the temperature drop needs to be minimized through the coldest portion of the day, generally nighttime.

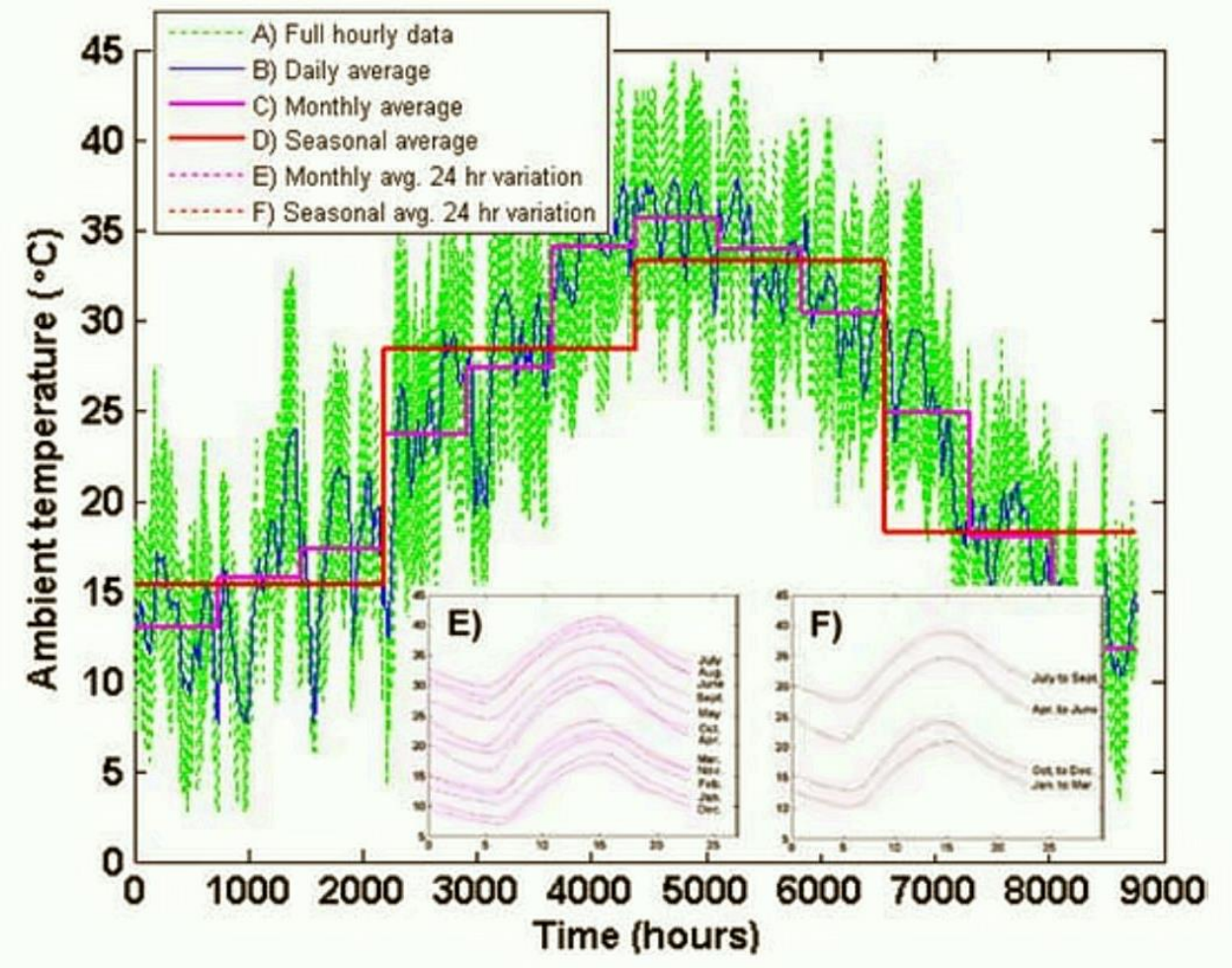

Figure 1-2, Phoenix Arizona temperature data [3]

The EcoCAR prototype and the testing later conducted on a production Chevrolet Volt led to concept selection and refinement of methods to increase thermal isolation within an ESS. Realizing the constraints of a production packaging solution, and limited to implementation within a production environment, cost and mass minimization may still be derived through computer modeling efforts. At least, that was the premise held moving forward. The concepts examined were packaged within the production system dimensional constraints using computer aided design (CAD) tools, and the designs evolved were then analyzed thermally via finite element analysis (FEA). Although chronologically the traditional engineering design process was not followed, being that solutions originally developed for one case were transposed onto another and extended, the key factors were ultimately fully examined in the development of final recommendations.

1.3.1 Concept Selection

There are many directions to be explored in the optimization of a BTMS. The focus of this thesis is on decreasing BTMS power requirements through optimizing pack construction via incorporating thermal isolation specifically, and considering structural requirements in the more general sense. Colleagues at UOIT have focused on optimizing the total HVAC system through exergy analysis, improving the efficiency of miniature thermoelectric based independent thermal management systems, and introducing PCM as a latent heat storage means to passively manage cell temperatures. Other related investigations are underway, including detailed experimental verification of different heat flux findings elicited in the present work, along with modeling the entire vehicle's BTMS requirements through dynamic drive cycles, and exploring synergies between all the methods combined. Therefore the scope of this thesis remains on minimizing the BTMS power requirements through the optimization of ESS design by increasing thermal isolation, while remaining within certain allowances of typical vehicle mass production constraints and necessary cost compromises this entails.

When developing technical solutions within industry, often a design matrix is used to help with concept selection. Table 1-1 shows a design matrix for increasing the thermal isolation of an ESS. The ideas are evaluated using a Pugh matrix where each concept is scored as it relates to a category. The score is calculated based on the total of positives (+), and negatives (-) assigned across all of the categories. N means the design change has no effect upon the category and is assigned a score of 0. Items which score negatively may be eliminated, and those with positive or neutral scores get evaluated further.

As the design considers a production environment to be important, the addition of cost and mass is weighted heavily. Both these categories are assigned a weighting of two. The effectiveness of each solution is assigned a weighting of 3, as it is the most important aspect when considering implementation of the design. Any items that can increase thermal isolation or "Effectiveness" that are either cost or mass neutral should be considered. Insulation materials evaluated as to their strengths relative to other approaches might score greater overall than competing solutions as shown. The individual concepts surrounding the

insulation approach were evaluated and quantified using methods described in this thesis. Because the design is considered to be a production environment ready solution, care is taken when evaluating the packaging feasibility of the proposed solutions. Addition of insulation materials is severely limited by the packaging space available and thus constrained as such.

Table 1-1, Concept selection design matrix

Modification (Weighting)	Complexity (1)	Cost (2)	Mass (2)	Effectiveness (3)	Packaging Feasibility (2)	Score
Optimize Module Construction	N	N	N	+	N	3
Optimize Thermal Bridging	-	N	N	+	N	2
Adding Thermal Insulation to entire ESS	---	-	-	+++	-	2
Addition of PCM	--	-	-	++	N	0
Insulated ESS Cover & Material	-	-	-	++	N	1
Increase BTMS Energy Efficiency	-	-	N	+	N	0

Chapter 2. Background

In order to be able to develop a model in which to optimize the design parameters of an electrified vehicle's ESS it is important to examine and comprehend the manufacturing and technological limitations that presently exist. Understanding historical vehicle electrification efforts allows for better future predictions. With such a background it is then possible to set about optimizing the pack parameters to best suit the design needs for future products.

At the dawn of the automobile, EVs were a direct competitor to IC engine vehicles. However due to a plentiful oil supply and quick refueling capabilities, the IC powered vehicles quickly dominated the automotive marketplace for decades to come. Interest in EVs was not renewed until much later in the late 20th century when fears of oil supply limitations, and environmental concerns spawned a renewed interest. These 1990's vehicles were heavy, unreliable, expensive, and slow charging. As the oil supply fears abated, EVs once again disappeared from the marketplace. A decade later during the early years of the 21st century, electrification re-emerged in the automotive marketplace in the form of HEVs. As technology progressed, HEVs have now become quite commonplace. PHEVs, EREVs, and pure EVs have also in recent years become rather common. This can be credited to several factors, primarily improvements in battery technology, rising fuel prices, environmental regulations, and government incentives.

However while market penetration is improving, vehicle electrification, especially EREV and EV technology, is still in its infancy. Many of the current examples are over-engineered in an attempt to get to market quickly and ease consumer apprehensiveness of unproven technology. However as the marketplace matures, there is incentive for manufacturers to improve design efficiency, both to lower costs and maximize EV range. The ESS normally represents the largest fractional cost and mass of an EV. It is also one of the few components that are not common with IC powered vehicles. This makes it an obvious place to start with efficiency improvements.

One way to improve overall efficiency is to decrease parasitic power losses within the ESS. Parasitic power losses are defined as any energy removed from the ESS that is not used towards developing vehicle tractive forces. Power train losses are well researched and largely common with IC powered vehicles. Energy losses throughout the cabin have also been well covered. Focus should then be put on improving the ESS efficiency; this thesis focuses on optimizing construction for greater battery thermal management efficiency. It allows for power reduction of the BTMS and reduced frequency of operation. The thermal efficiency gains within the ESS, aside from reducing parasitic losses, have a secondary attribute of improving vehicle reliability due to the decreased exposure of cells to extreme ambient conditions, and thereby augmenting its useful lifetime.

2.1 Electric Vehicle History

At the end of the 1980's to the late 1990's electric vehicles received their first significant modern day investment. At this time rising fuel prices and the scare of limited fossil fuel reserves along with government policy focused attention on alternative energy. Major vehicle manufacturers instigated development of electric vehicles, driven by the California ZEV program [4]. Some were brought to market on limited length leases and others were put on the road in product test fleets. This was the first time, almost since the beginning of the automobile era, where initiatives were underway to make electric vehicles truly marketable. Many of the systems and technologies that were developed during this era are still being used on electric vehicle concepts today.

Exploring the historical learnings from previously built and current production EV ESSs allows for better design optimization. Understanding how and why packs are manufactured and configured in specific ways leads to a better optimization effort. Many manufactured packs focus heavily on modularization so parts may be shared across multiple ESS configurations to maximize manufacturing tool usage, decreasing part counts and thereby attaining overall cost efficiency. It is important that any improvements made to maximize thermal isolation are synergistic with the manufacturing process.

2.1.1 Vehicles of the Late 20th Century

General Motors, Ford, Chrysler, Toyota, Nissan, Honda, Volkswagen and others all made a foray into the EV market between the late 1980s and 1990s. General Motors built the EV1, Toyota an electric RAV4, Ford built the Ecostar EV, and Ranger truck. Chrysler had their Grand Caravan (EPIC) EV. Other interesting examples exist, none at a production level comparable to their IC powered counterparts. These test fleets did however prove that EVs could be significantly functional in the modern automotive marketplace.

General Motors began working on the EV1 in 1992, and later released the vehicle to the public in 1996, as a 1997 model year product [5]. The vehicles were not sold outright, but

instead available through a leasing program. Upon expiration of the leases the vehicles were returned to the manufacturer to be scrapped. This caused some controversy among EV enthusiasts, and actually inspired the documentary "Who Killed the Electric Car" [6]. However by the termination of the leases the vehicle ESS's were far too costly to maintain.

The first iteration of the EV1 used a VRLA battery in the ESS. The system was nominally 312 volts, with 16 kWh of total capacity. The VRLA pack was very heavy, with the ESS alone representing 1100 lb. of the gross vehicle weight [7]. The EV1 had a range of 85 miles (~ 135 km) per charge on a fresh battery pack. This was considered sufficient as the average American drives around 30 miles (~ 50 km) per day [8]. The assumption was that 60+ miles (100 km) of range would be acceptable for the majority of American commuters.

In order to offset the weight of the ESS, wherever possible the vehicle's components were made from composite materials and aluminum rather than steel. Further efforts to improve range were made when General Motors released the second generation ESS equipped with Nickel Metal Hydride (NiMH) cells rather than VRLA. NiMH chemistry represents a significant improvement in energy density and life but it is also very costly. The cells were 85 Ah instead of 53 Ah, which when assembled in the same structural pack gave the vehicle a range of 140 miles (225 km) [9]. By 2003 all leases had expired on the EV1s and the program became dormant; similarly other manufacturers terminated their test fleets.

Figure 2-1, General Motors EV1 [5]

FIGURE 2-2, TOYOTA RAV4 EV [10]

In the late 1990's Toyota was equally developing electric vehicle platforms. In powering their vehicle they also switched to NiMH batteries. Toyota chose to release their test fleet in America with the more expensive NiMH technology on a small SUV. They also employed a synchronous AC motor which spins up to 4600 RPM, a much lower rate of speed then the 3-Phase AC induction motor technology that the EV1 was equipped with [10]. The motor that Toyota used was about half the power of its competitors but very efficient, it allowed the RAV4 EV to reach 96 km/h in about 20 s, yet its top speed was still 125 km/h [10].

The RAV4 EV had a range of 153 km which was deemed appropriate for the vehicle's intended purpose. As a limitation of the technologies of the time, the vehicle's NiMH pack was rather heavy and recharge times were quite long (~7 hrs). The car was primarily sold to utility companies and government agencies, although a few hundred went into private hands. It featured an (expensive) improvement in the NiMH chemistry which featured lower internal resistance and less heating on charge but this enabled the sufficiency of forced air cooling rather than active refrigeration. Many remain drivable today, a testament to its design.

Ford also released a limited production EV early on. However instead of VRLA, or NiMH cells, they chose to use Sodium Sulfur cells and later Sodium Nickel Chloride "Zebra" cells. This

was a technology pioneered by Ford Motor Company in the 1960's [11]. The cells had an energy density higher than other available technology at the time. The downside being that the cells required high temperatures in order to operate efficiently (~300 °C). For safety and thermal efficiency the cells were contained in a double walled vacuumed casing [11]. The pack created using these cells powered a utility van named the Ecostar. The small utility van was marketed as an in town delivery/utility vehicle. Due to the inherent downside of maintaining a battery pack at high temperatures, and the corrosiveness of hot sodium, this technology sees only niche use today. After initial trials with VLRA, Ford later switched over to NiMH when it electrified its Ranger pickup truck for the ZEV program, using the same Panasonic battery as in the RAV4-EV.

Chrysler took a similar approach with its EPIC minivan. After some early field trials with NiCd and NiFe, they resorted to a NiMH battery supplied by SAFT, this variant incorporated liquid cooling passages directly into the battery casing.

2.1.2 Early 21st Century Examples

In the early 21st century, rising fuel prices, government regulations/incentives, and battery technology improvements led to a renewed interest in IC alternatives. During this timeframe Elon Musk invested in a small automotive upstart and became the CEO of Tesla Motors. The company went on to produce an EV sports car named the Tesla Roadster which was based off the composite chassis of the Lotus Elise, albeit with extreme modification & adaptation.

The Tesla Roadster was one of the first modern era production electric vehicles. Thanks to improved Li-ion battery technologies over the previous decade, it was able to reach a range of over 320 km with a 450 kg battery pack [12]. This is a significant improvement from the earlier GM-Ovonic technology based NiMH batteries which allowed a roughly half as powerful vehicle to reach 225 km. The Tesla Roadster entered production with a Li-ion

battery pack that consists of almost 7000 cylindrical consumer electronics 18650 format Li-ion cells. Although the number presents a packaging challenge, Tesla felt it was outweighed by the cost effectiveness of a mass produced cell size. Nissan attempted a similar implementation in a late 1990's ZEV era program employing larger Sony Li-ion cells to power their EV (Nissan Altra). However at the time the technology was still too expensive, and fraught with unknowns.

Tesla's vehicle was released in 2008, at a price point of $109 thousand USD. Although expensive, it was considered relatively cheap for a vehicle which featured such advanced technology. A reason Tesla commanded a high price was due to clever marketing in releasing it as a sports coupe. The roadster is able to reach 60 mph from a standstill in about 4 seconds thanks to a 185 kW 3-phase AC induction motor [13]. The vehicle is also based on an aluminum/composite chassis. Weighing in at only 1238 kg – the 450 kg battery pack alone is still roughly a third of the total curb weight [12]. Tesla then released an electric sedan called the model S with improved specifications. Tesla has since gone on to become a publicly traded company, and has plans for more offerings. These include a sport utility named the Model X, and a more affordable compact EV to be released soon.

For the 2011 model year, two significant electrified vehicles entered the marketplace. Nissan began selling its EV Leaf, and Chevrolet its EREV the Volt. The Tesla Roadster, Nissan Leaf, and Chevrolet Volt each represent a different approach to vehicle electrification. What makes the Leaf significant is its entry point price. The original MSRP of the LEAF was around $33 thousand USD, which with government price incentives allowed one to be bought for roughly $25, 000 [14].

The LEAF's battery pack uses Li-ion battery chemistry similar to Tesla vehicles; however the construction of the cells differs. They use a prismatic pouch type cell in which the cell's interior is stacked as sheets and then enveloped in a protective laminate pouch. Without a metal casing the cells are lighter and cheaper to produce in the long run, however the design is less robust and therefore the cells have to be protected within a "sardine can", as seen in Figure 2-3.

Figure 2-3, Leaf battery cross section [14]

A unique feature of the Nissan LEAF is its recharge capabilities. It can be charged by a 400 volt 3-phase AC charger up to an 80% State of Charge (SOC) in about 15 minutes [15]. However such sources are not so readily available hence the LEAF is normally charged off standard single phase 240 V or 120 V household outlets over a period of hours via the standard J1772 connector. The fact that it may quick charge however is useful in making the technology future viable, as quick charging stations become more wide spread. The LEAF's pack consists of 48 modules shown in Figure 2-3, each contains four 35 Ah cells. This gives the LEAF's 24 kWh pack enough capacity to propel it 160 km on the LA4 driving cycle [14]. An LA4 drive cycle is a rather easy cycle in comparison to real world driving and therefore the practical range of the LEAF is shorter, typically 110 km. Also, only about 20 kWh of the pack's capacity is actually used as the SOC window is limited for battery longevity. This limitation of the SOC window is common in all EV's, but not necessarily to identical extent.

General Motors released its EREV; the Chevrolet Volt near the same time as the Leaf. This vehicle has two significant features: Active liquid cooling (refrigeration) / heating (electric) for the battery pack, and a range extending IC engine. The active cooling system helps to protect the Li-ion cells, which are pouch types in the Volt's case. The cells are only covered by a thin electrically isolative envelope hence they cool effectively. GM was able to package these in such a way that a metallic cooling plate is touching each individual cell. This proved wise, as Nissan's air cooled design has had significant warranty claims associated with battery capacity degradation due to hot environment exposure.

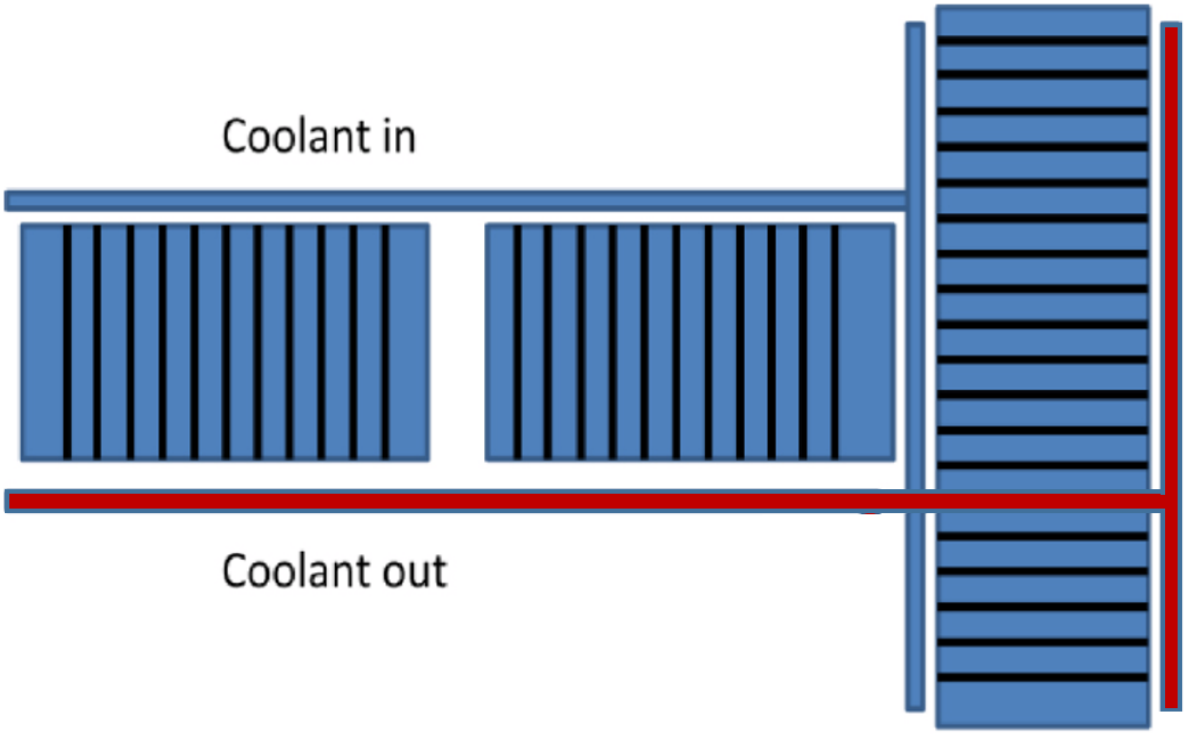

Figure 2-4, GM VOLTEC cooling system schematic [16]

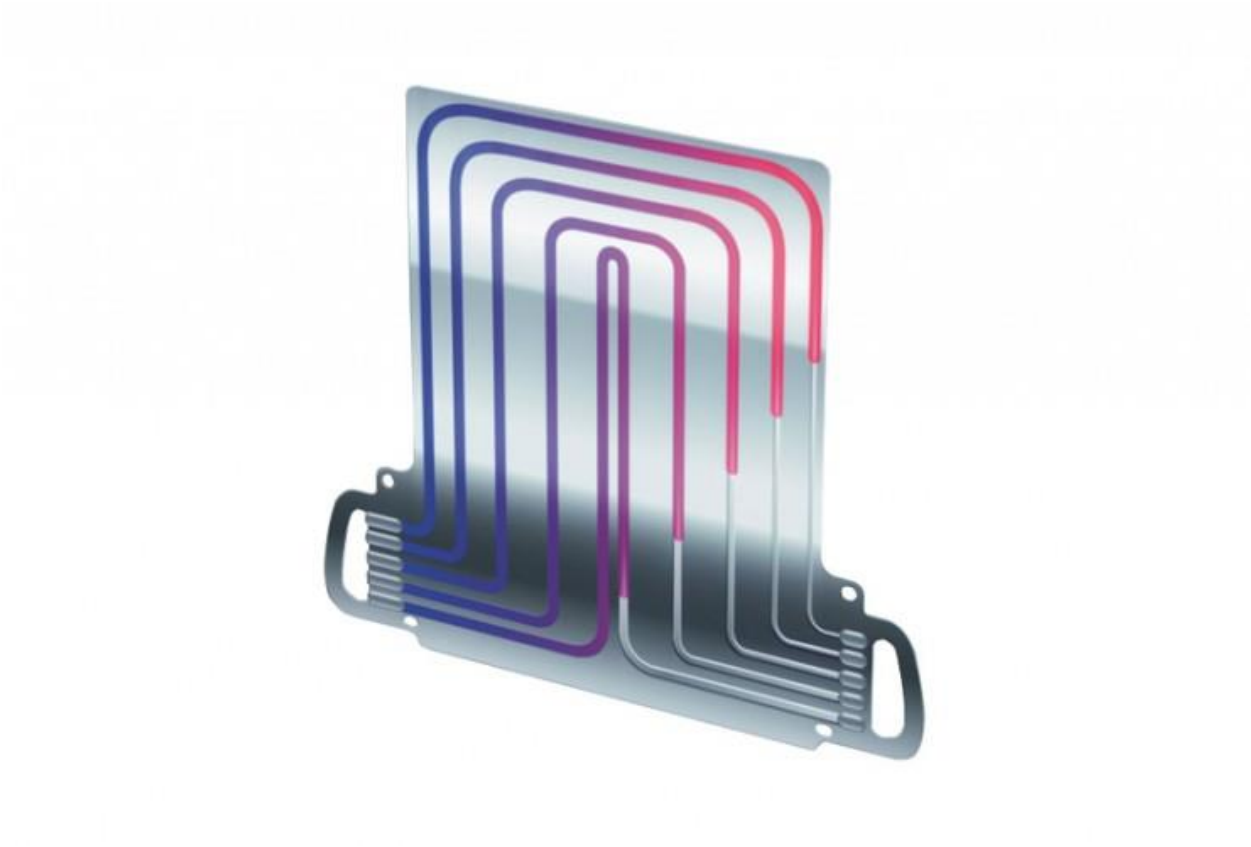

Figure 2-5, VOLTEC cooling plate [17]

The IC range extender concept has also shown itself to help the Volt customer gain the confidence of driving an electric car. The IC engine will run only when the vehicle transitions into charge sustaining mode [16]. This can happen either by the driver selecting charge sustaining to save the battery charge for later use, or automatically as the battery gets depleted to a low SOC. Since the vehicle can be run indefinitely (given there is fuel in the tank) without having to charge the pack, the Volt offers its buyer more versatility then its EV competitors. This will be true until such time that the infrastructure exists to recharge batteries at practically the same rate IC vehicles can be refueled at the gas pump.

General Motors is currently in the process of releasing the second generation Volt which employs a pack that was designed in an iterative sense to the one in the first generation. The same basic module structure is also used in other GM vehicles. Being one of the larger volume "energy" batteries on the market currently, the VOLTEC battery structure used in GM's

EREVs was selected to develop a baseline and to test improvements for thermal isolation in this thesis endeavor.

The Model S released in 2012 was Tesla's initial attempt at building a ground up design pure EV sedan, with variants being offering from 40 kWh to 85 kWh of energy storage [18]. Prices ranged from $59 900 USD to just past $100 000 USD, however many states offered government incentives bringing the total cost a little lower. The 40 kWh variant was dropped in 2013 due to poor demand [19]. Initially only the top end 85 kWh model offered "supercharging" capabilities as a standard feature. All current models now incorporate it by default. Superchargers are the Tesla branded quick charging station which they have begun installing across the United States. Such stations are able to charge vehicles at a rate of 135 kW, giving them a useable range of 290 km after 30 minutes of charging [20]. Tesla has also experimented with battery swapping where the customer can opt to quick swap their pack for a fully charged one. This however has seen limited success compared to the "superchargers" but it does allow for very easy and efficient battery service. As of June 2015 Tesla has surpassed 70 000 units sold making the model S a considerable success.

Various examples mentioned represent different approaches to vehicle electrification. More established manufacturers have begun offering EVs and EREVs with varying success. Different approaches to electrification include PHEVs, HEVs, and fuel cell electric vehicles. EVs, EREVs, PHEVs and fuel cell electric vehicles generally contain the largest batteries in terms of capacity (in descending order) and their ESSs are the focus of this thesis.

2.2 Production Costs

Production costs remain a significant drawback of alternatively powered vehicles when compared to their internal combustion driven counterparts. In vehicles such as PHEVs, and EREVs the ESS and electric drive system are in addition to IC drivetrain components and therefore constitute an additional cost. In EVs the electric powertrain replaces the IC engine and other drivetrain components; however the energy storage is through a battery rather than fossil fuels and has to be paid up front in the initial cost of purchase. This initial price

increase is somewhat offset by the low cost of electricity versus that of gasoline energy. However for many of these vehicles, especially those with greater EV range, the payback period can exceed the useful life of the vehicle. At the present time this is still somewhat offset by various government incentives in North America that allows alternative powered vehicles to remain somewhat cost competitive. However the long term viability relies on both the price of fossil fuels rising, and the cost of battery systems to lower. With lengthened payback periods to overcome the initial cost, battery pack longevity is also an equally important concern.

Figure 2-6 provides an estimate of price premium for IC alternatives in the year 2035 based on 2007 dollars. Figure 2-7 outlines a similar study given a 2015-2020 time frame, each based on the electric range of the vehicle. The EV (Battery Electric) featured in figure 2-6 assumes a 320 km range while the PHEV correlates to the PHEV40 (40 miles or 64 km of electric range) outlined as a 2015 model in figure 2-7. DOH (degree of hybridization) in figure 2-7 refers to the ratio of motor power to total vehicle propulsion power [21]. The exact price premiums will likely fluctuate from the estimates provided; it is apparent that PHEVs, and EVs will continue to come at a price premium. A discrepancy arises where the 2035 PHEV has a 16 kWh pack with 11.6 kWh useable energy. The 2015 PHEV40 estimates a pack of 19 kWh capacity and 11.2 kWh hours of useable energy. Such studies use varying assumptions for pack costs/kWh in future models and the fraction of useable energy (ΔSOC) that can be extracted while still attaining pack longevity. Figure 2-8 estimates a 15 year lifespan of the various PHEV models shown in Figure 2-7; measuring the fuel savings against a similar IC powered vehicle. The initial cost recovery time for a 64 km electric range PHEV is shown to be about seven years based on 24,000 km (15,000 mile) accumulated annually.

	RETAIL PRICE INCREASE [$2007]	
VEHICLE TYPE		
	Cars	Light Trucks
Current Gasoline SIE* retail price	$19,000	$21,000
Incremental relative to current Gasoline SIE:		
Current Diesel	$1,700	$2,100
Current Turbo Gasoline	$700	$800
Current Hybrid	$4,900	$6,300
2035 Gasoline SIE	$2,000	$2,400
2035 Gasoline SIE retail Price	$21,600	$23,400
Incremental relative to 2035 Gasoline SIE:		
2035 Diesel	$1,700	$2,100
2035 Turbo Gasoline	$700	$800
2035 Hybrid	$2,500	$3,200
2035 Plug-in Hybrid	$5,900	$8,300
2035 Battery Electric	$14,400	$22,100
2035 Fuel Cell	$5,300	$7,400

Figure 2-6, Vehicle price premium estimate: 2035 [22]

Vehicle	Curb Mass (kg)	Engine Power (kW)	Motor Power (kW)	DOH	Battery Energy (kWh)	P/E Ratio (1/h)	SOC Window	Fuel Cons. (L/100km)	Elec. Cons. (Wh/km)	Retail Cost (US$)
CV	1429	122	---	---	---	---	---	10.3	---	23,392
HEV0	1412	77	36	32%	1.5	32.8	37%	7.4	---	26,658
PHEV2	1412	77	36	32%	1.5	32.8	37%	7.2	7	27,322
PHEV5	1445	78	41	34%	3.5	15.7	39%	7.0	17	28,365
PHEV10	1481	79	42	35%	6.6	8.5	41%	6.5	32	29,697
PHEV20	1531	81	43	35%	11.8	4.9	47%	5.7	58	31,828
PHEV30	1569	82	44	35%	15.9	3.7	53%	5.0	78	33,533
PHEV40	1598	83	45	35%	19.0	3.2	59%	4.5	96	34,839
PHEV50	1618	84	45	35%	21.6	2.8	66%	4.1	108	35,857
PHEV60	1636	84	46	35%	23.6	2.6	73%	3.7	120	36,681

Figure 2-7, Vehicle price premium estimate: 2015-2020 [21]

Battery electric vehicles and HEVs elicit an increase in cost from an incremental infrastructure standpoint. Widespread adaptation of the technology would likely stress the grid beyond its present capabilities Additional power generation stations could be built over time as the take up rate on EVs increases. A larger infrastructure challenge is faced by fuel

cell powered vehicles which are also an alternative. Additionally within a fuel cell the catalyst platinum is estimated at 22% of the fuel cell's overall cost [4]. If this catalyst can't be replaced, or at the least significantly reduced, it will be hard for fuel cells to reach cost targets, preventing such vehicles from dropping below a certain price point. Generally FCEVs use a battery system to help handle current draw for heavy loads such as acceleration. They therefore require the integration of a battery ESS, further increasing the cost differential shown in Figure 2-6.

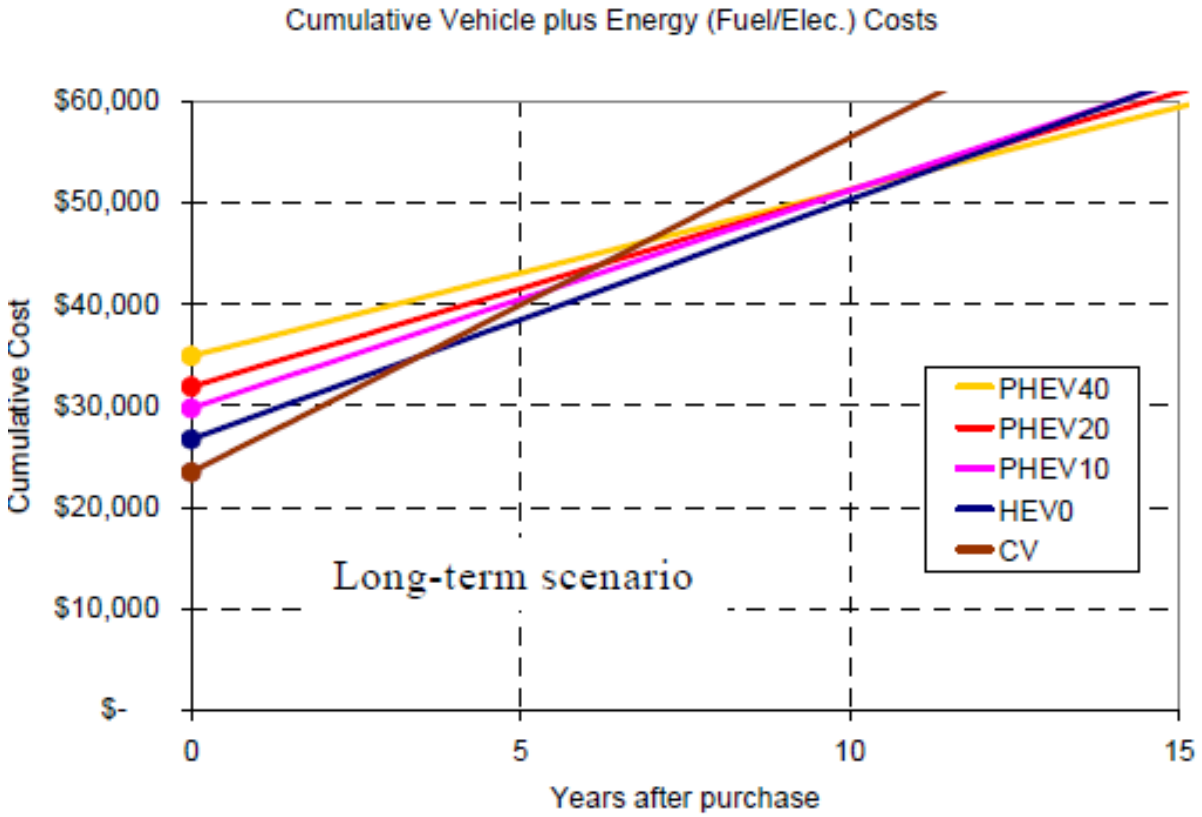

Figure 2-8, Cumulative cost comparison [21]

A study on zero emission vehicles ZEVs in 2010 estimated that battery pack cost will not drop below $300/kWh in the long term [4]. However similar work done by an electric vehicle manufacturer suggests otherwise. Tesla motors puts cell costs below $150/kWh at production rates of 25K units per year [22]; this correlates to a ~$200/kWh pack cost. Figure 2-9 shows a price trend for the cells that Tesla motors used to build their Roadster EV's battery pack in 2008, a distinct drop in price and increase in energy density is evident.

More recently the same company announced a "Giga-factory" which Tesla claims can produce cells for as low as $100/kWh [53]. While this reduction trend may not continue at the same rate, it does suggest that much of the market price associated with automotive lithium ion cells is in fact largely due to the R&D efforts combined with relatively low production volume.

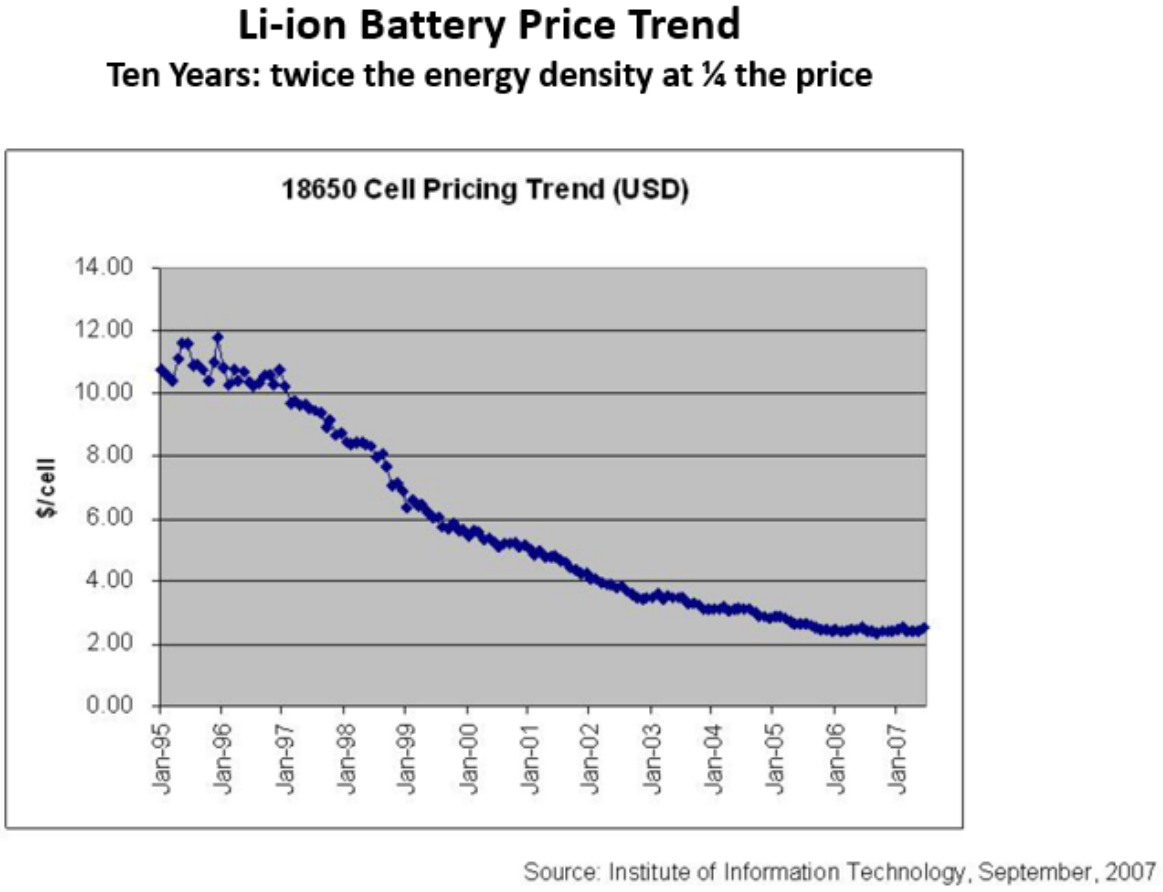

Figure 2-9, Cell price trend [22]

There is a case to be built for decreases in cost via increasing energy density. If batteries are developed that can be manufactured at the same real cost but offer twice the energy density, then a vehicle with identical range could be manufactured at about half the cost given the number of cells required. Some HEV's are still built using NiMH, largely because it is proven technology. With energy density, reliability, and cycle life increasing while costs creep lower, Li-ion cell variants are quickly becoming the energy source of choice.

2.3 System Efficiencies

Electric vehicles can offer significant efficiency improvements over internal combustion engines. The vehicle's energy conversion efficiency can be up to 90% while an efficient internal combustion engine comes in at about 37%. Well-to-wheel efficiency is more important; electric vehicles and plug in hybrid electric vehicles gain advantage in a total well-to-wheel analysis for energy consumed and greenhouse gasses produced in almost all cases. Only $C0_2$ intensive electricity production via coal would lend favor to IC engine propulsion.

Process Fractional Efficiency for:	Intrnl Combust. Gas-engine	Mild Hybrid	Strong Hybrid	Strong Hybrid PHEV	Series Hybrid	Series Hybrid PHEV	All Electric Car
ICE Drive Power (direct to wheels)							
-Highway	0.25	0.27	0.27	0.27	- - -	- - -	- - -
-City	0.15	0.2	0.33	0.33	- - -	- - -	- - -
Total for Gas (avg)	0.2	0.235	0.3	0.3	- - -	- - -	- - -
On-Board Generated Electric Drive Power (ICE generated, wheels driven via electric motors)							
-Generator engine (ICE)*	- - -	0.3	0.32	0.32	0.45	0.45	
-Generator Loss	- - -	0.93	0.93	0.93	0.93	0.93	
-Battery Storage Loss	- - -	0.98	0.98	0.98	0.98	0.98	- - -
-Electric Motor Loss	- - -	0.92	0.92	0.92	0.92	0.92	- - -
-Regenerative braking	- - -	1.25	1.4	1.4	1.5	1.5	- - -
Total for Electric (collective)	- - -	0.31	0.38	0.38	0.57	0.57	
Assumed percent direct gas drive	100	75	50	50	0	0	0
Total for on-board generated	0.2	0.25	0.34	0.34	0.57	0.57	- - -
Grid Electric Drive Power							
-Battery Storage Loss		0.98	0.98	0.98	0.98	0.98	0.98
-Electric Motor Loss		0.92	0.92	0.92	0.92	0.92	0.92
-Regenerative braking		1.25	1.4	1.4	1.5	1.5	1.5
Total for Grid Electric	- - -	1.13	1.26	1.26	1.35	1.35	1.35

	Gas ICE	Mild Hybrid	Strong Hybrid	Strong PHEV	Series Hybrid	Series PHEV	Totally EV
Assume percentage grid power use	0	0	0	60	0	80	100
Miles / gallon	25	31.86	42.23	42.23	70.75	70.75	- - -
Miles / dollar**	10.00	12.74	16.89	40.54	28.30	81.12	89.00
Relative Weight	2000	2200	2300	2500	1775	1900	2300

Now adjust for weight to get final mileage figures

	Gas ICE	Mild Hybrid	Strong Hybrid	Strong PHEV	Series Hybrid	Series PHEV	Totally EV
Miles / gallon	**25.00**	**28.96**	**36.72**	**33.78**	**79.72**	**74.47**	- - -
Miles / dollar**	**10.00**	**11.58**	**14.69**	**32.43**	**31.89**	**85.39**	**77.39**

** Assumes $2.50/gallon and $0.75 electrical cost for 1 gallon equivalent (i.e. 10kW-hrs)

Figure 2-10, Vehicle efficiency comparison [23]

Figure 2-10 gives some typical efficiency numbers of various vehicle architectures, comparing fuel efficiency, drivetrain efficiency, and electric range classes. The information is based on a series PHEV with a 60 mile electric range and an electric vehicle with a 200 mile range [23]. There is however more to total vehicle efficiency. By doing a complete well-to-wheel analysis, one can also factor the total energy consumption of the vehicle including

its manufacture, raw material usage, and disposal. This gives an accurate assessment to best compare architectures from cradle to grave.

The results of a well-to-wheel analysis are dependent on the region that the vehicle is deployed in. For electric and hybrid vehicles charged off of the grid the efficiency numbers depend on how the power is being generated. In Canada where power is largely from nuclear and hydro, very little greenhouse gases are produced. However in some parts of the US where electricity is mostly generated by burning fossil fuels (particularly coal) greenhouse gasses increase.

Looking at total vehicle efficiency, a distinct advantage can be seen in EVs over fuel cell vehicles. For fuel cell electric vehicles (FCEV), hydrogen may be created through electrolysis using grid electricity or more commonly by steam methane reforming. It is then compressed into a holding tank, and turned back into electricity through a fuel cell, temporarily stored in an electrical ESS, and then converted back into mechanical work through an electric motor. The total efficiency of this cycle is about ~12% for electrolysis. If the source of H_2 is natural gas via steam methane reforming, the cycle efficiency is increased to ~25% [24]. Energy for EVs is taken directly from the grid, and put into an electrical ESS, and then converted into mechanical work through an electric motor. The total efficiency of this chain can be approximately 75-86% [25]. However the power must still be produced cleanly at source and is heavily dependent on that component. Nonetheless it generally exceeds the hydrogen pathway in virtually every case. The powertrain efficiency of both vehicle types is roughly the same as they use similar propulsion systems. The efficiency gain in deploying a pure EV is significant, and the infrastructure is pre-existing for refueling although still far from optimal. The drawback is the time associated with refueling. A FCEV can have hydrogen pumped into its tank at fuel stops in as little as five minutes while an EV needs to be plugged in from 30 minutes to 8 hours, per full “refuel” depending on the charging capabilities.

In order to find the total efficiency gains, well-to-tank must be analyzed in each case. In countries such as Canada, ZEVs offer much larger gains over traditional vehicles as the electricity generation is far cleaner.

2.4 Cell Technology

When designing an EV or PHEV battery selection is imperative as there are various choices with different power and cost profiles. Different cell chemistries have attributes that make them superior/inferior to others depending on the intended use. For instance lead acid cells are the cheapest to produce and do not require a sophisticated charge control system, however they have poor power density and cycle life (~400 deep discharge cycles). These are still used in most vehicles for the starter, and auxiliary systems. NiMH batteries have a better energy density then lead acid and have good cycle life (~1400 deep discharge cycles). They are however more costly and require a Battery Management System (BMS) to charge. They also suffer from self-discharge, and charge memory effects. The other choice that has become popular is Lithium ion cell chemistry. These feature excellent energy density and low internal resistance. They are temperature sensitive, costly, and require a sophisticated BMS. Cells come packaged in three general forms; as prismatic units, in cylindrical form, or in flat pouches.

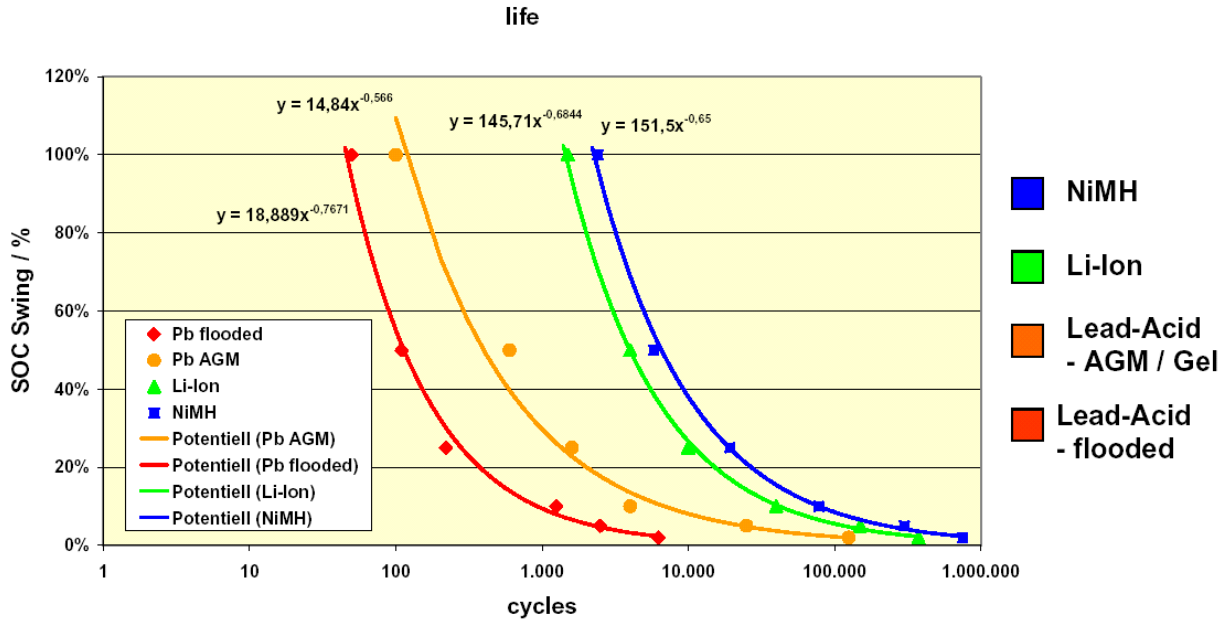

Figure 2-11, Battery comparison [8]

Other alternative chemistries such as Sodium Nickel Chloride, and Lithium Polymer Electrolyte type cells have been tested. Limited life along with thermal management

drawbacks have deemed them inferior and complicated to use in the automotive marketplace. There are a great many variants of anode, cathode, and electrolytes for Li-ion chemistry cells. Most of which suffer from low cycle life or high cost of production thus making them unsuitable for automotive use. Manufacturers must choose chemistries carefully for EVs to deliver the desired range, while hitting cost and longevity targets.

2.4.1 Lead Acid Batteries

Valve regulated lead acid batteries (VRLA) were used in past electric vehicles such as the first generation EV1 from GM. They are simple to integrate and can succeed with simple thermal management (forced air cooling). They also do not require complex electronics for active battery management, as with lithium ion cells. VRLA are able to charge and discharge fairly rapidly with moderate efficiency and heat generation. Aside very poor power density, their major drawback is poor cyclic life. This quickly outweighs any initial cost advantage.

Referring to Figure 2-11, their cyclic life is far inferior to other cell chemistries. Energy density is roughly ~30 Wh/kg, which means that a 10 kWh pack (suitable size for a PHEV) would weigh around 300 kg. While still widely used for auxiliary system, and engine starting, lead acid batteries have been replaced by chemistries with much higher energy densities for PHEV, and EV use. Their prime deployment remains golf carts, forklifts, floor cleaners, and similar low speed applications or where weight is immaterial as in stationary applications such as uninterruptable power supplies.

2.4.2 Nickel Metal Hydride and Nickel Cadmium

Nickel Cadmium (NiCd), Nickel Iron (NiFe) and Nickel metal hydride (NiMH), cells are successive evolutions of the same basic chemistry and were first to replace VRLA cells in electric vehicles. NiMH batteries are more commonly employed on electrified vehicles and therefore will be the focus of discussion. In production vehicles they can reach up to 70 Wh/kg. This is effectively more than twice that of lead acid batteries. They come at a huge

price premium, but are robust and at cost parity at present with Li-ion once the full system is considered.

NiMH cells do have a tendency to self-discharge. They also exhibit what is called a memory effect. This means that if they are not cycled fully the cell will have some tendency to remember the point to which it was last discharged, and will subsequently tend to only discharge to that point easily before seeing a jump in internal resistance. The battery can be refreshed through deep cycling however it will never quite regain its full initial capacity once a strong memory effect has been established [17].

NiMH cells also tend to be less efficient than other chemistries at delivering charge. They have a greater internal resistance than Li-ion cells; and therefore generate more heat during cycling. This becomes an issue for a large battery pack. These can heat up, eventually causing thermal runaway if overcharged. Many packs made of NiMH cells do not have liquid cooling, or even significant active cooling. In hybrid vehicles cabin air is forced through the pack using a blower. Their evolution to survive 65 °C operating temperatures enables such schemes, at least in small packs for HEV's that exhibit a lot of surface area per unit volume.

	NiCd	NiMH	Lead Acid	Li-ion	Li-ion polymer	Reusable Alkaline
Gravimetric Energy Density (Wh/kg)	45-80	60-120	30-50	110-160	100-130	80 (initial)
Internal Resistance (includes peripheral circuits) in mΩ	100 to 200[1] 6V pack	200 to 300[1] 6V pack	<100[1] 12V pack	150 to 250[1] 7.2V pack	200 to 300[1] 7.2V pack	200 to 2000[1] 6V pack
Cycle Life (to 80% of initial capacity)	1500[2]	300 to 500[2,3]	200 to 300[2]	500 to 1000[3]	300 to 500	50[3] (to 50%)
Fast Charge Time	1h typical	2-4h	8-16h	2-4h	2-4h	2-3h
Overcharge Tolerance	moderate	low	high	very low	low	moderate
Self-discharge / Month (room temperature)	20%[4]	30%[4]	5%	10%[5]	~10%[5]	0.3%
Cell Voltage (nominal)	1.25V[6]	1.25V[6]	2V	3.6V	3.6V	1.5V
Load Current - peak - best result	20C 1C	5C 0.5C or lower	5C[7] 0.2C	>2C 1C or lower	>2C 1C or lower	0.5C 0.2C or lower
Operating Temperature (discharge only)	-40 to 60°C	-20 to 60°C	-20 to 60°C	-20 to 60°C	0 to 60°C	0 to 65°C
Maintenance Requirement	30 to 60 days	60 to 90 days	3 to 6 months[9]	not req.	not req.	not req.
Typical Battery Cost (US$, reference only)	$50 (7.2V)	$60 (7.2V)	$25 (6V)	$100 (7.2V)	$100 (7.2V)	$5 (9V)
Cost per Cycle (US$)[11]	$0.04	$0.12	$0.10	$0.14	$0.29	$0.10-0.50
Commercial use since	1950	1990	1970	1991	1999	1992

Figure 2-12, Cell chemistry comparison [26]

2.4.3 Lithium Ion, and Lithium Polymer

Li-ion cells have become the norm in the PHEV, EREV, and EV market. Their superior energy density outweighs all other aspects of NiMH. There are many variations of anode/cathode materials used with different attributes. Three main packaging formats exist; (1) Lithium ion polymer pouch cells which are small and slightly flexible; these exhibit a lot of surface area

which lends to better cooling. Their relatively floppy nature requires they be restrained and well protected in a battery pack. (2) Another common type are cylindrical cells, where the cell layers are turned into a jelly roll like construction and put inside a metal casing. These resemble traditional batteries used in consumer electronics and are mass produced. Their main advantage is that the cell is contained in a metal casing for robustness. Cooling becomes an issue for the larger sizes (~50 mm ϕ) due to the thermal mass increasing disproportionally to the surface area. (3) The third common format is a prismatic plastic cased package exhibiting a cross of characteristics from the previously described formats.

Li cells are currently the most expensive battery chemistry however real costs associated with the chemistry are potentially low. Economies of scale and production level increases are all driving cell costs down. With substitution of some of the more expensive raw materials, Lithium cells could become very cost effective [27]. Materials used in the anode and cathode are what make up a significant portion of the real cost. However finding inexpensive alternatives that provide the same stability, and energy density characteristics has proven difficult. Significant research needs to be done in order to keep the cell performance yet put them at a more competitive price point.

Common Li-ion cell chemistries are Lithium Manganese Oxide (LMO), Lithium Nickel Manganese Cobalt Oxide (NMC), or Lithium Iron Phosphate (LFP) cathodes coupled with a Graphite, Carbon Silicon, or Lithium Titanate anode. LFP is a common choice for HEV "power" batteries due to durability, while LMO batteries offer better energy densities and are commonly used in EV "energy" batteries. Graphite is the most common cathode material being employed today. Lithium Titanate offers superior power performance but reduced energy at a high cost. Research is continually being conducted to improve the anode/cathode materials. New variants offer higher energy densities, or higher power, while others are focusing on low cost; usually the drawback is low cyclic life. All types of cells have their place in the market. In order for a cell chemistry to be used in the automotive industry it must maximize energy density at the required power level without sacrificing cycle life or cost. Extreme reliability is also a key factor for automotive application, and achieving this requires special factories and production systems that go well beyond consumer electronics product standards.

Replacing the cobalt (expensive) in the cathode with iron phosphate also improves the safety but at a cost to energy density. The chemical bond between the iron and the oxygen within the cathode is stronger than that of the cobalt based cell and therefore makes the battery more stable in extreme conditions [28]. This also allows them to be charged and discharged at much faster rates. Some variants (example A123) have a continuous rate capability of about 30 C and can be pulsed up to 100 C [28], where "C" represents a multiple of the Amp-hr rating of the battery. They claim a life of around 3000 cycles at full depth of discharge (DOD) which is more than the standard cobalt cathode. Their only real drawback is a lower operational voltage. High C rate cycling and high cycle life characteristics make such cells suitable for use as a "power" battery, meaning the battery's primary function is to provide as much power as possible vs an "energy" battery that is purposed to store the maximum amount of energy at full charge. They find their use in HEV's.

For EVs energy density is paramount, as the vehicle's only energy source is the battery. Therefore the pack should hold enough charge to propel the vehicle over a suitable range, be able to charge quickly and efficiently, and remain economical enough to provide a payback in operational cost. An EV needs cells with much higher energy densities than a HEV or a PHEV. For this LMO, and NMC chemistries are much better suited. While they are able to hold significantly more energy per unit mass then LFP chemistries, they feature inferior sustainable rates of energy delivery. Charging/discharging at continuous rates above 2 C can damage the cells. Lithium-Sulfur (Li-S) cells offer double the energy density over a standard lithium ion cell using a Cobalt cathode. They are capable of storing ~350 Wh/kg and are able to be charged and discharged safely at rates up to 3 C [29]. Currently the largest drawback to these cells is their low cycle life (~400 cycles). However manufacturers are continuing development to improve performance on these and similar advanced types, for example by utilizing methods to stabilize additions of silicon to the anode.

Lithium manganese oxide and many other mixed metal oxide variants are being experimented with in order to improve the energy density, safety, and power of the Li-ion based chemistry. With further improvements to cathode, anode and electrolyte materials, along with decreasing cost over time, EVs could eventually become commonplace in the market.

2.5 Battery Thermal Management

Due to the large cost and long payback period associated with building battery packs for EVs and PHEVs, great care must be taken in protecting the cells from the environment and through charging/discharging cycles. However any additional cost or weight gain needs to be minimized in order to maintain a competitive MSRP. Manufacturers attempt to gain consumer confidence through lengthy warranties. In order to minimize warranty costs the reduction in battery life must be minimized. The two largest culprits that decrease battery life are large SOC swings, and temperature excursions. The SOC swing is easily managed through the BMS which balances cells and controls their cutoff voltage. Temperature control however is more difficult and must be regulated through a Battery Thermal Management System (BTMS). Li-ion cells tend to be sensitive to both high and low temperatures. Temperatures of 50 °C can begin to cause permanent damage, rapidly increasing the rate of battery aging through loss of active materials via build-up at the solid electrolyte interface layer (SEI) [1]. This also increases internal resistance. At cold temperatures, cells are unable to charge/discharge at normal rates. Attempting to cycle at higher C rates (C rate measures the rate of charge where 1 C is equivalent of a full charge completed in 1 hour) will cause lithium plating, which permanently damages the cell and can eventually lead to internal shorting across the separators [1]. As the ambient environment in which an electrified vehicle is operated varies, the only way to ensure that the cells remain at near optimal thermal conditions is through thermal management of the ESS.

Lithium Ion chemistries are also sensitive to the amount of capacity used per cycle, battery charge management systems (BMS) can help balance the electrical load, to not overstress individual cells. By monitoring each cell and balancing the voltage between individual cells they can ensure that each is cycling to the same depth of discharge (DOD). Letting the cells reach too high a voltage can have a strong negative effect on cell life not only while cycling but also during storage [1]. As well as monitoring and balancing cell voltages, the BMS also tracks cell/module temperatures; shutting down the pack and thereby the vehicle if cells are

operating beyond their limits electrically or thermally. In hot or cold environments without a BTMS, cells can quickly exceed their thermal limits potentially leaving the vehicle stranded.

There are options for thermally managing an ESS. The appropriate choice relies on the type of vehicle and the associated price point in the market. Thermal management can be broken into two types; (forced) ambient air and active refrigeration. With ambient air, vehicle cabin or outside air thermally manages the batteries and the scope of operation is limited. Active refrigeration/heating takes readings from the interior of the pack and through a control system regulates the inlet temperature of the air or liquid coolant flowing through the battery pack in order to maintain it at a desired temperature. The largest attribute of passive cooling systems are relatively low complexity and cost. However being reliant on ambient conditions causes them to be ineffective when conditions are not optimal. These systems tend to be used in either mild hybrids or strong hybrids that can be driven solely by the internal combustion engine. The cell usage can be bypassed and only the internal combustion engine employed when the cells are not at a desirable state. Independent active cooling systems offer the advantage of acting independent to the vehicle's main HVAC system. This allows them to be sized appropriately to address the ESS's needs. They are however more costly than systems linked to a heat pump or A/C unit shared with the passenger compartment. Such independent systems are optimal for vehicles that can't be run off the internal combustion engine when the battery is not at an acceptable operating temperature. The other advantages of active systems are their ability to pre-heat and cool the batteries before the main contactors are closed. Therefore the batteries will only be used in a narrow temperature range greatly increasing their useful life. Though one may focus on cooling when speaking of a BTMS, it must be pointed out that heating ability is equally important for northern climates. Active systems are normally bi-directional and heating ability is usually inferred though not explicitly stated in the many discussions that follow when relating to heat transfer or thermal isolation in the general sense.

Although all cooling and heating systems will fall into the category of active or passive thermal management there are many different variants that can be integrated into a vehicle.**Error! Reference source not found.** Figure 2-13 outlines some configurations that can be used for ESS thermal management. There are also many different ways in which to

pass coolant through a battery pack including semi active systems that share the vehicle heat exchangers but pass dedicated fluid through the pack. Most such systems are deployed in hybrid electric vehicles where there are pre-existing thermal systems for the IC engine and passenger compartment. Such components do not necessarily exist in full electric vehicles and therefore narrow the options available.

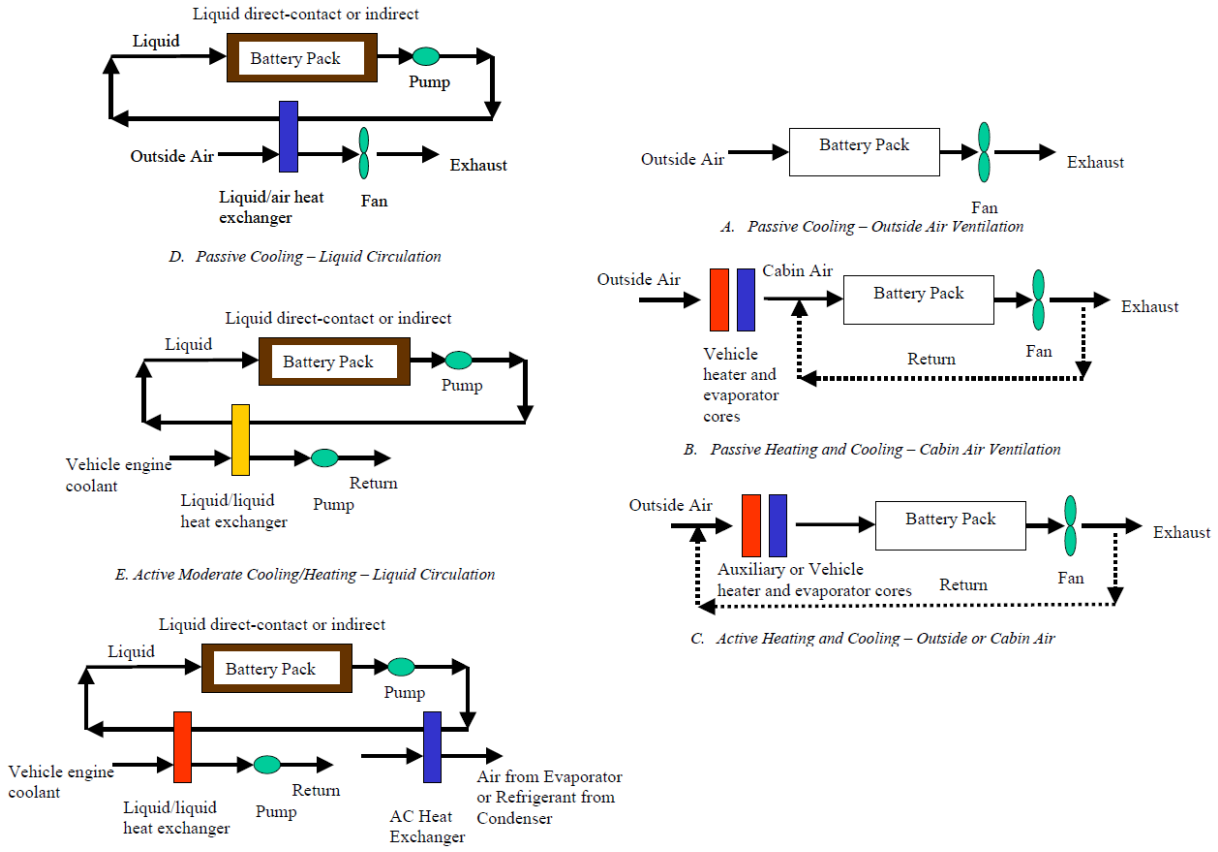

Figure 2-13, Various active and passive cooling systems [30]

Using air as the cooling medium for the cells in a passive system is the most inexpensive way to cool a battery pack, it is however also the most ineffective. It requires a much larger flow rate and pumping power to achieve the same cooling, and becomes ineffective when ambient conditions are further outside of the ESS's optimal operating range. Active liquid cooling achieves superior thermal management at the expense of complexity, cost and mass. Active air cooling systems blow air over the battery pack relying on direct contact with the cells to shed the heat. Active liquid cooling requires cooling lines, a pumping system and heat

exchanger plates between the cells and coolant. Either system requires a large amount of cell surface area to be in contact (directly or indirectly) with coolant. A third option is to use an electrically non-conductive fluid (oil) to bathe the cells. This maximizes the cell's exposure to coolant, but is impractical.

It is possible to partially take advantage of an oil bath type system by using Phase Change Material (PCM). PCM can absorb/reject heat from the cells by changing between a solid and a liquid. The material can be tuned such that the melting temperature of the PCM helps to handle peak thermal loads from the cells. While PCMs can store a large amount of heat per unit volume during the change from solid to liquid, they tend to have poor thermal conductivity, particularly once melted. This can make it difficult to remove the stored heat from the PCM material or control rapid jumps in cell surface temperature once the PCM has melted.

2.5.1 Active Air Cooling

Air cooling using conditioned air from the passenger compartment, or from ambient is a common way to provide temperature control within an ESS. Vehicles using air cooling will generally monitor cell temperature and control the speed of a fan which ducts air through the pack. Air cooling systems have a smaller component count, and are relatively simple to integrate compared to liquid systems. However air has poor thermal conductivity, and heat capacity which makes it an ineffective choice for larger ESSs. For larger packs high flow rates are needed to provide enough cooling capacity which then leads to large parasitic losses. For better temperature control heat exchangers can be added to heat or cool the air as it enters the pack.

Air cooling can be improved by making use of parallel air channels. By ducting the air through multiple paths, greater temperature uniformity can be produced without increasing the flow rate. In a series cooling configuration the air will absorb heat quickly near the inlet, there will then be no additional heat capacity remaining, leaving the cells near the outlet uncooled. While helped by parallel flow, the primary concern still remains.

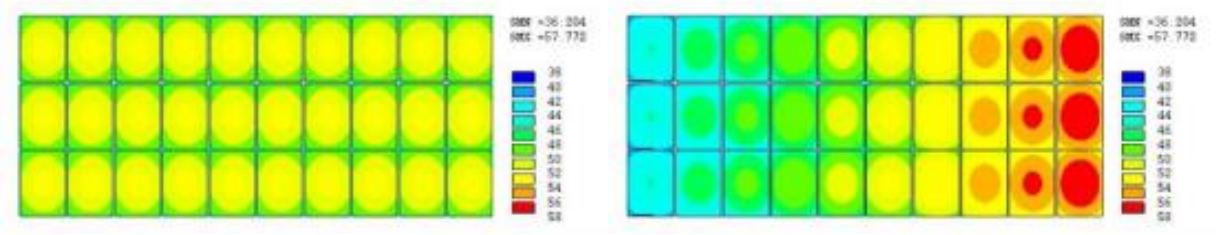

Figure 2-14, Left: parallel flow, Right: series flow [8]

In order to make use of air as a coolant, it must be drawn from either the vehicle passenger compartment or ambient environment. Then if needed, conditioned to the appropriate temperature, before being pushed or drawn through the ESS using fans and ducting. Such a system removes significant energy from the pack when called upon to curtail large temperature differences. For the case of an EV in a hot ambient environment, pack capacity may need to be used to keep cells from reaching dangerously high temperatures. Temperature uniformity is hard to maintain in air cooled battery packs. High flow rates approaching turbulent may be required to create acceptable temperature uniformity due to air's low thermal conductivity and specific heat capacity [8].

Air cooling systems have difficulty extracting enough heat to keep a thermal event (fire) from propagating to nearby cells especially in power dense packs such as lithium ion [31]. In order to prevent this from happening, the heat exchanger and blower units must be significantly overpowered adding more cost and weight. To work around this issue either a coolant with a better heat capacity can be used or an additional system might be added that specifically handles intense heat loads.

Property \ Coolant	Air	Mineral Oil	Water/Glycol
Density ρ (kg/m^3)	1.225	924.1	1069
Specific Heat c_p ($J/kg\ K$)	1006.43	1900	3323
Thermal Conductivity k ($W/m\ K$)	0.0242	0.13	0.3892
Kinematic Viscosity ν (m^2/s)	1.461e-5	5.6e-5	2.582e-6

Figure 2-15, Typical coolant properties [8]

2.5.2 Liquid Cooling Direct Contact

Air cooling on its own does not seem to be a viable option for vehicles that can't rely on their internal combustion engine to power the car when cells are outside operational temperatures. Therefore either an additional safety system might be added to offer protection, or an alternative coolant should be used. Liquid cooling through either direct or indirect contact is able to provide significantly better heat rejection. Both types of liquid cooling however come with their own unique obstacles. Direct cooling employs a dielectric fluid such as a mineral oil which has a fairly high viscosity. In order to maximize the cooling effort the fluid should touch as many of the cell surfaces within the battery as possible. This creates a large channel size and takes considerable pumping effort to circulate the fluid. It is however an effective way to maximize the amount of cell area that the coolant touches. **Error! Reference source not found.** Figure 2-15 lists coolant types that are typical choices for battery thermal management. Mineral oil offers multiple advantages over air cooling. It has both a higher thermal conductivity and a higher heat capacity. Liquid coolants can also achieve a higher mass flow rate in a smaller channel then air due to their higher densities. This means that for a similar size module the pumping loses will actually be greater for air at a comparable cooling rate due to the larger coolant channel [8].

While there is less pumping loss for a comparable mass flow rate using a dielectric fluid in direct contact with cells, there are other losses which need be accounted for. Manifold friction and static pressure can be significant sources of pumping loss in liquid cooling systems [8]. Air cooling systems do not suffer as significant a loss from these sources. Other factors must be considered. Module serviceability, leaks, added weight, and the combustible nature of oil are real drawbacks in practice.

2.5.3 Indirect cooling water/glycol mixture

Using a water glycol mixture through indirect contact may pose the best combination of cooling effort and simplicity. Here a heat exchanger driven by the vehicle's A/C passenger system or a heat pump provides the battery water/glycol loop with temperature control. At the cell a heat exchanger plate provides conductive heat transfer.

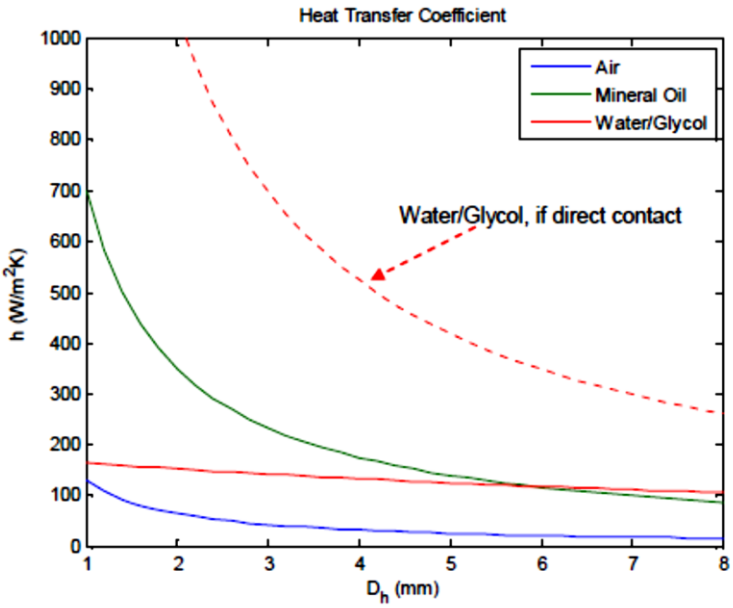

Figure 2-16, Coolant heat transfer ability comparison [8]

One study using indirect liquid cooling on a PHEV battery pack suggests that a liquid cooling system using conductive plates to transfer heat from cells into the coolant can achieve up to 10 W (5 W avg.) of heat rejection per cell using a 10 l/min flow rate (7.4 l/min avg.) through a 288 cell 16 kWh pack. The same pack is shown to create on average just over 600 W of heat on an aggressive USO6 cycle, and peaking at 1 kW [32]. If a secondary passive system could be designed to absorb peak heat energy, the main system could be downsized considerably.

2.5.4 Passive Cooling Through Thermal Isolation and PCM

Protecting from ambient extremes can be done somewhat through insulating the pack. While reducing the BTMS load created by the ambient environment, it has the drawback of trapping heat created within the pack. This can be a concern in the case of thermal runaway (fires).

One way to protect against these peak heating loads is to increase the power of the thermal management system, however it also increases the cost and mass of the system. Alternatively phase change material (PCM) can be integrated into cell modules in such a way that it can absorb heat under peak conditions. PCMs can be used to accept large amounts of heat without requiring any power input. These materials can provide cooling or heating through phase change at a desired temperature for the cells. For instance a PCM designed for battery cooling could have a melting temperature of 40 °C. Therefore as the batteries begin to heat past 40 °C the PCM would start to melt. The phase change occurring requires a large amount of heat energy that would then maintain the cell temperature. The drawback being the finite amount of energy the material can absorb during phase change. Once sufficient heat has been transferred to complete the phase change, temperatures will again begin to rise. An additional complication is PCM materials tend to have a large thermal resistance. Benefits include a large amount of heat capacity per unit mass, and it requires no excess power to provide a high temporary cooling effort [31].

An experiment was conducted by a group of researchers using an electric scooter with a phase change material that melted at around 40 °C and it was able to draw heat from the pack under peak heating situations [33]. Similar experiments have been performed with liquid cooling, comparing abilities of liquid flowing through lines indirectly cooling the cells, an oil bath directly cooling (via immersion) and air cooling. Such results showed that direct liquid cooling allowed for the most heat to be shed, however it was also the most costly [8]. Liquid cooling through a jacket or line is still a more expensive option then air cooling however it does allow for far superior heat rejection. Combining liquid cooling through a jacket, good insulation and a PCM material might optimize a cooling system to handle normal loading, with the PCM picking up any heat spikes. The liquid or air cooling system could therefore be made much smaller.

Research by the aforementioned group has also been done comparing PCM passive cooling to active air cooling in situations where a cell experiences an event which causes it to heat rapidly. The idea behind the study was to present PCM materials as a safer alternative for battery thermal management because of their ability to prevent a thermal run-away in battery abuse situations. There can always be faults in BMSs or shorts within cells that could

lead to a thermal event. The nature of Li-ion batteries is that they have high power and energy densities, and when heated beyond a point will self-ignite and quickly burn up an entire pack. To prevent such an event, the cooling system needs to be able to accept large amounts of heat at a high rate. Thus preventing the culprit cell and its neighbors from reaching temperatures at which the cell would begin breaking down.

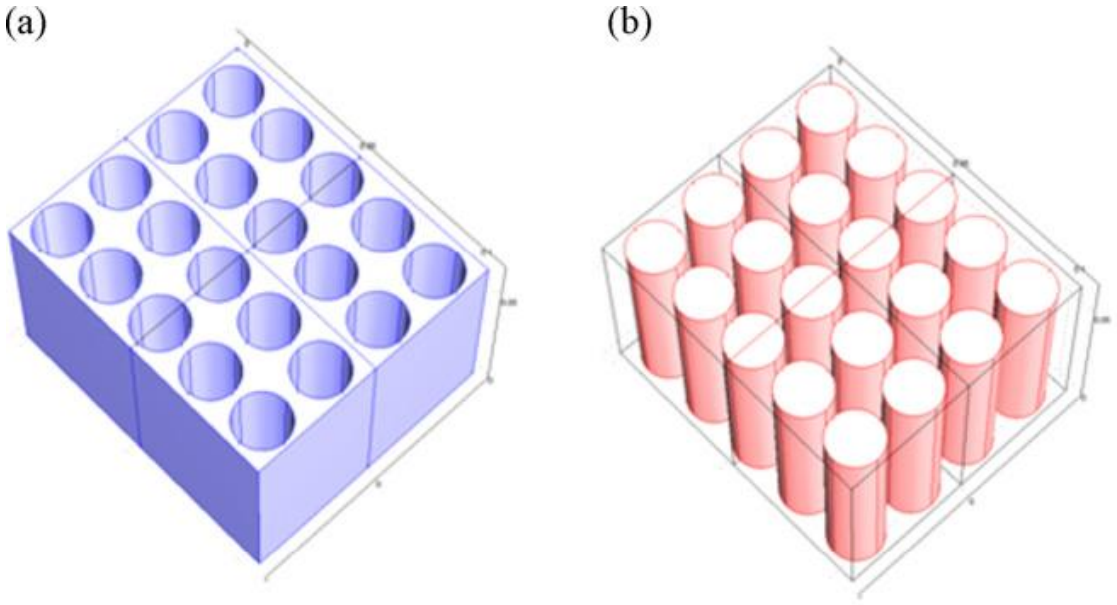

Figure 2-17, PCM cooling example: Blue = PCM, Pink = Cells [31]

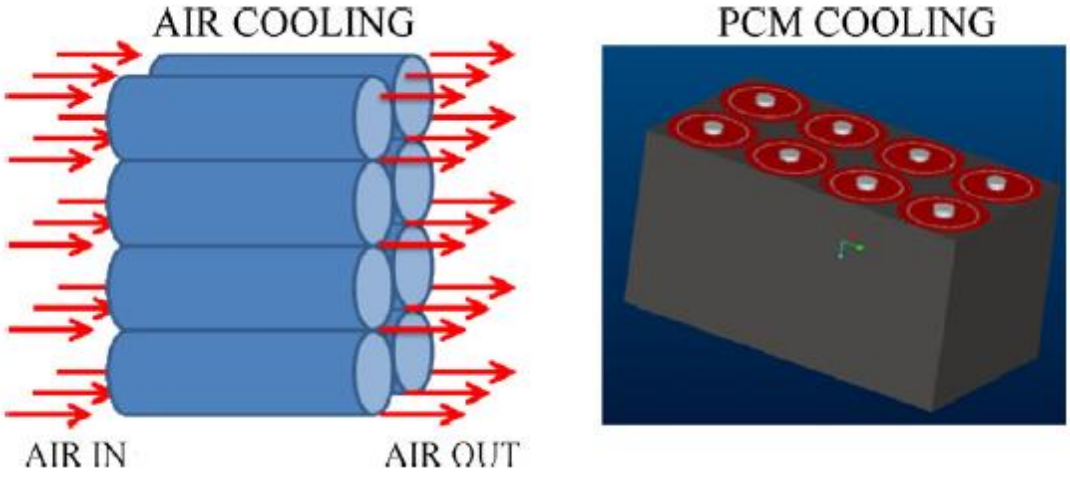

Figure 2-18, Coolant flow [31]

Property	Specification
Thermal conductivity	16.6 ($W m^{-2} K^{-1}$)
Latent heat	123 ($kJ kg^{-1}$)
PCM melting range	42–45 °C
Specific heat	1.98 ($kJ kg^{-1} K^{-1}$)
Bulk density of composite	789 ($kg m^{-3}$)
Bulk density of graphite	210 ($kg m^{-3}$)

Figure 2-19, PCM/graphite composite material properties [31]

A prototype pack was constructed by a related group of researchers using a graphite composite matrix material in which the cells were placed [31]. In figure 2-17**Error! Reference source not found.** the blue material represents the PCM and the orange represents the Li-ion cells. An air cooled pack is constructed in a similar fashion except that the space the PCM occupies is left open for airflow. Simulations were then run where batteries were cycled at extremely high rates and the ability of each type of cooling system was modeled for its effectiveness at preventing a thermal event. The PCM material was specifically designed to melt between 42-45 °C with the purpose of keeping the cell's internal temperatures below 50 °C during rapid cycling. It is also important to note the temperature uniformity inside the cells with PCM cooling remained within half of a degree centigrade as opposed to two degrees using the air cooled method. The air was ducted through the pack as shown in figure 2-18**Error! Reference source not found.**. Both packs were placed in ambient temperature of 40 °C, the cells in the air cooled pack were constrained by nylon separators. The PCM was in direct contact with the cells and the air cooled module exterior. Results showed that air cooling did not have the ability to keep the cells at a desirable temperature and the cells reached up to 60 °C at a 6.6 C discharge rate. The PCM on the other hand was able to maintain the pack under 50 °C for one cycle, with the caveat that it eventually hindered cooling on subsequent cycles [31].

An important aspect of thermal management in batteries is temperature uniformity. Even though a coolant is able to maintain a desirable average temperature throughout the battery pack it may not necessarily be able to handle extreme heating of a single cell. In order for a coolant to prevent thermal runaway in the case where a single cell is experiencing rapid heating, the heat must be absorbed or distributed broadly within the pack. This means the

PCM needs to have a good enough thermal conductivity to give the pack temperature uniformity. The PCM approach can achieve this uniformity in particular cases where there is enough of it present. **Error! Reference source not found.** Figure 2-20 compares heat dissipation from a hot cell in a PCM matrix (bottom) to thermal run away in the same situation with air cooling (top).

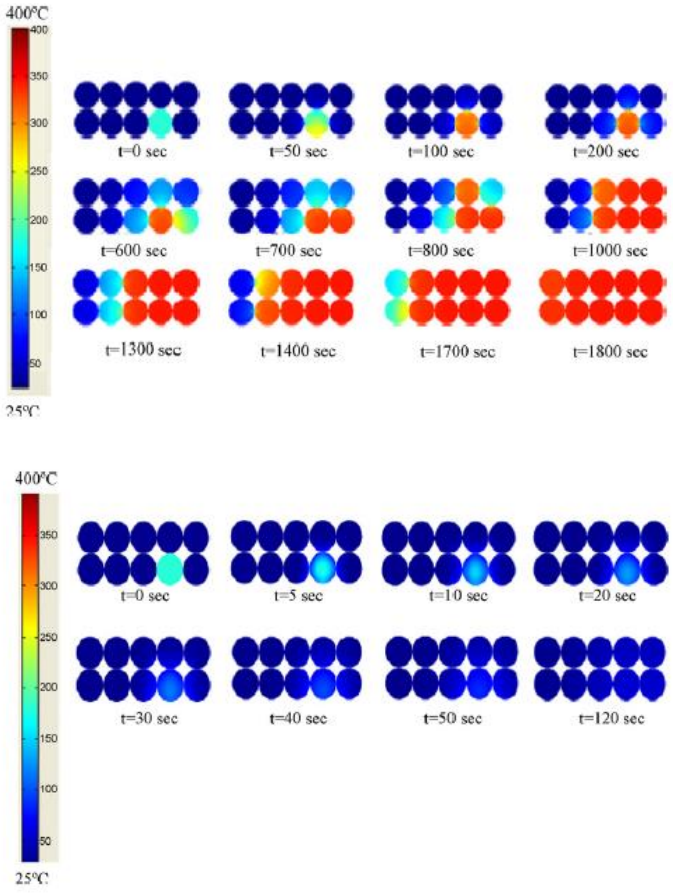

Figure 2-20, Thermal runaway propagation, Top: Air cooled, Bottom: PCM [31]

2.5.5 Optimizing Efficiency of BTMS with Thermoelectric Units

All of the cooling systems discussed have advantages and drawbacks. The most suited for a production vehicle is a combination that meets the requirements for the chosen application. For instance air cooling and heating is the simplest and cheapest to integrate into a vehicle because air conditioning and heating systems must already be in place for the cabin. Liquid cooling offers much higher cooling power per unit volume, and PCM materials might offer protection against thermal runaway. By combining a PCM with air cooling, energy that is transferred from the cells into the PCM would then be rejected to a forced air system. However this creates issues as both the air and the PCM need to contact the cell at the same time. For this reason liquid thermal management via indirect contact in conjunction with a PCM might be a better approach.

As it is costly to provide mechanical refrigeration; miniature systems (<1500-2500 W) suitable for a battery pack are cost prohibitive on the basis of cooling power vs cost. By lowering the cooling requirements of the active cooling system through passive methods such as thermal isolation and addition of PCM instead of using miniaturized mechanical heat pumps, thermoelectric units (TE) might be considered. Thermoelectric units are reasonably efficient when operated below 30% of their peak cooling capacity. They do however become very inefficient when operated near peak output. Since BTMSs use part of the ESS's capacity to provide it with temperature control, reducing the amount of parasitic loss due to heating and cooling becomes of utmost importance.

A way that a system could operate using PCM in conjunction with a liquid cooling system is that one side of the cell would be touching the PCM material and the other side of the cell would be pressed against a heat sink. Prismatic pouch cells with a large surface area and relatively small thickness would be ideal for temperature uniformity. The sizing of the system would be such that the liquid cooling and heating portion is able to handle average loads. Good ESS thermal isolation can reduce the load from the environment making such heat influx secondary. The liquid cooling system would therefore be able to handle the

internally generated heat flux at an average current draw including the thermal load emanating from the environment. During times of high power operation like acceleration or hill climbing the melting PCM material would be able to temporarily store the excess heat generated.

A standard size TE unit can achieve about 25 W of heat removal at a high efficiency. The TE unit depicted in figure 2-21**Error! Reference source not found.** is able to remove up to 80 W, however efficiency is very low at such a rate. To efficiently handle the nominal cooling load about 12 TE chips would be needed for an ESS requiring a 300 Watt nominal cooling capacity. Packaging such a system however is quite feasible as each chip has a surface area of only 1600 mm^2 [34]. Such systems could be central or distributed within cell modules depending on the required modularity. Combining such a device with a secondary PCM absorption to constrain the TE units to never leave their desired (high efficiency) operating range (see COP curve in figure 2-21**Error! Reference source not found.**) could help to further reduce parasitic loses created by the cooling requirements of the cells. A hidden benefit to the approach is the ability of TE's to act as a heat pump (by reversing polarity) and to concentrate heat generated from the vehicle's power electronics cooling loop to warm a battery to optimal conditions in cold environments. A TE's ability to provide both heating and cooling eliminates the need for separate heating and cooling devices, reducing parts count.

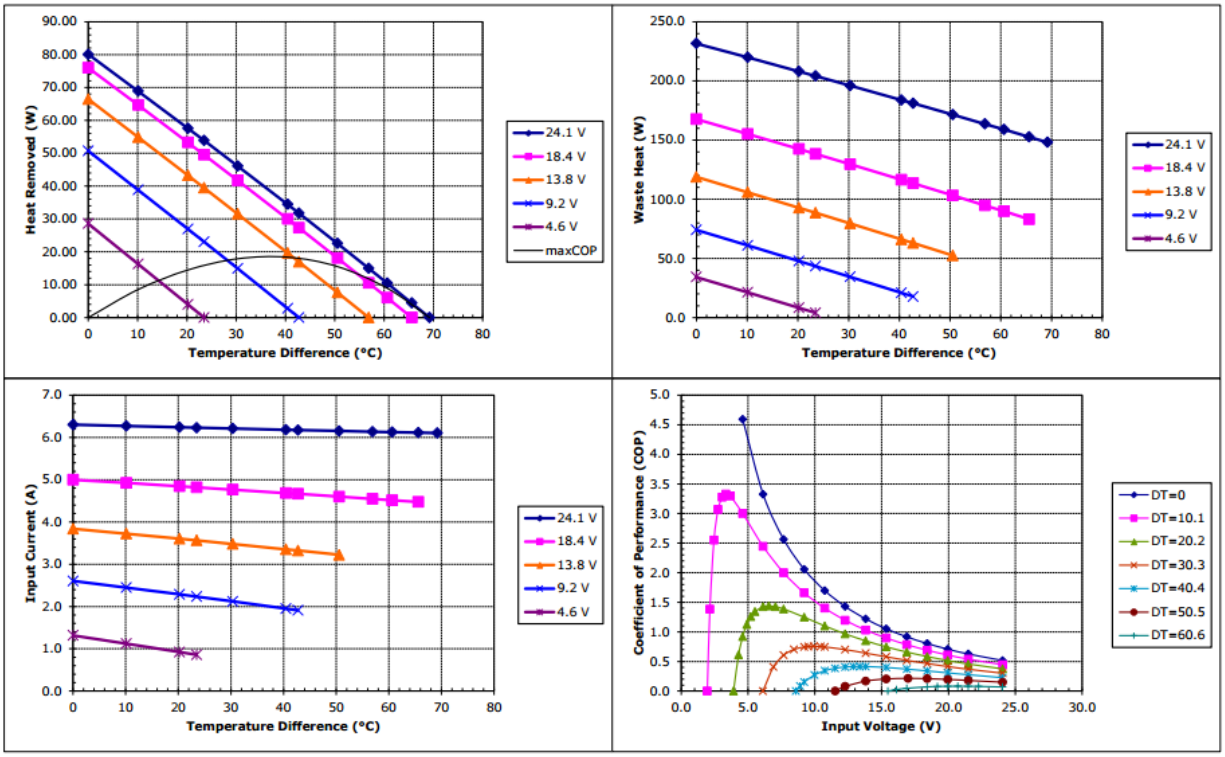

Unpotted HP-199-1.4-1.5 at a hot-side temperature of 30 °C

Figure 2-21, Thermoelectric performance, with maximum efficiency curve [34]

2.7 Construction Optimization

Optimizing ESS construction for thermal isolation is a low cost opportunity to decrease BTMS power requirements. Cost and packaging space are two of the largest contributing factors when the decision is made to add or take away components from a final production

vehicle's bill of materials. Active BTMS and PCMs represent an addition of both cost and weight. However a changes in pack construction for thermal isolation may be cost and weight neutral and therefore should be considered prior to the addition of any parts.

Figure 2-22**Error! Reference source not found.** demonstrates some experimentally found heat generation rates for different battery chemistries over changing temperature and discharge rates. The information presented measured the heat output of the cells while being subjected to both high and average discharge rates. For EV and PHEV purposes a discharge rate of around 2 C would be reasonable. This assumes that the vehicle's pack discharges in approximately 1/2 hour of use. This is a good continuous rate estimate for a PHEV and a high one for an EV. A more typical rate for an EV would be from 1C or lower depending on the vehicle range. Looking more at the specific cells examined, if they are discharged at around 25 °C, the optimal operating temperature for the Lithium chemistries, heat generation can be estimated. Using the lithium ion power cell for example, given a 40 kWh battery pack discharging at 1 C on the highway over an aggressive drive cycle, the pack would only dissipate about 72 watts of heat according to the given data using the following calculation;

$$6\ Ah \times 3.7\ V\ (nominal) = 22\ W.hr$$

$$\frac{40\ 000\ Wh}{22\ \frac{Wh}{cell}} \times .04\ W/cell = 72\ W\ for\ the\ pack$$

		Heat Generation (W)/Cell		
Battery Type	**Cycle**	**0°C**	**22-25°C**	**40-50°C**
VRLA, 16.5 Ah	C/1 Discharge, 100% to 0% State of Charge	1.21	1.28	0.4
VRLA, 16.5 Ah	5C Discharge, 100% to 0% State of Charge	16.07	14.02	11.17
NiMH, 20 Ah	C/1 Discharge, 70% to 35% State of Charge	-	1.19	1.11
NiMH, 20 Ah	5C Discharge, 70% to 35% State of Charge	-	22.79	25.27
Li-Ion, 6 Ah	C/1 Discharge, 80% to 50% State of Charge	0.6	0.04	-0.18
Li-Ion, 6 Ah	5C Discharge, 80% to 50% State of Charge	12.07	3.50	1.22

Figure 2-22, Experimental heat generations of various battery chemistries [30]

If the physical pack has a high thermal conductivity, the amount of heat let into the pack on a hot summer day could far outweigh the internal heat produced by the pack while driving. The cell's internal resistance being a secondary heat source is especially apparent in a PHEV or EREV where the battery is housed next to hot exhaust systems. **Error! Reference source not found.** Figure 2-23 for instance shows an EREV (Chevrolet Volt) with the ESS cycling power while the IC engine is running to generate additional electricity. By contrast an electric vehicle with a 250 mile range provided by an 80 kWh battery pack driving down the highway will be discharging the cells at a rate of roughly 1/3 C. This means that almost no heat is being produced by the battery and very little cooling effort is required. At such low rates of discharge the cells can even exhibit endothermic traits over certain states of charge and temperature (see figure 2-23**Error! Reference source not found.**). Therefore steps should be taken to isolate the interior of the pack from the environment to minimize the required heating/cooling effort and maintain stable conditions.

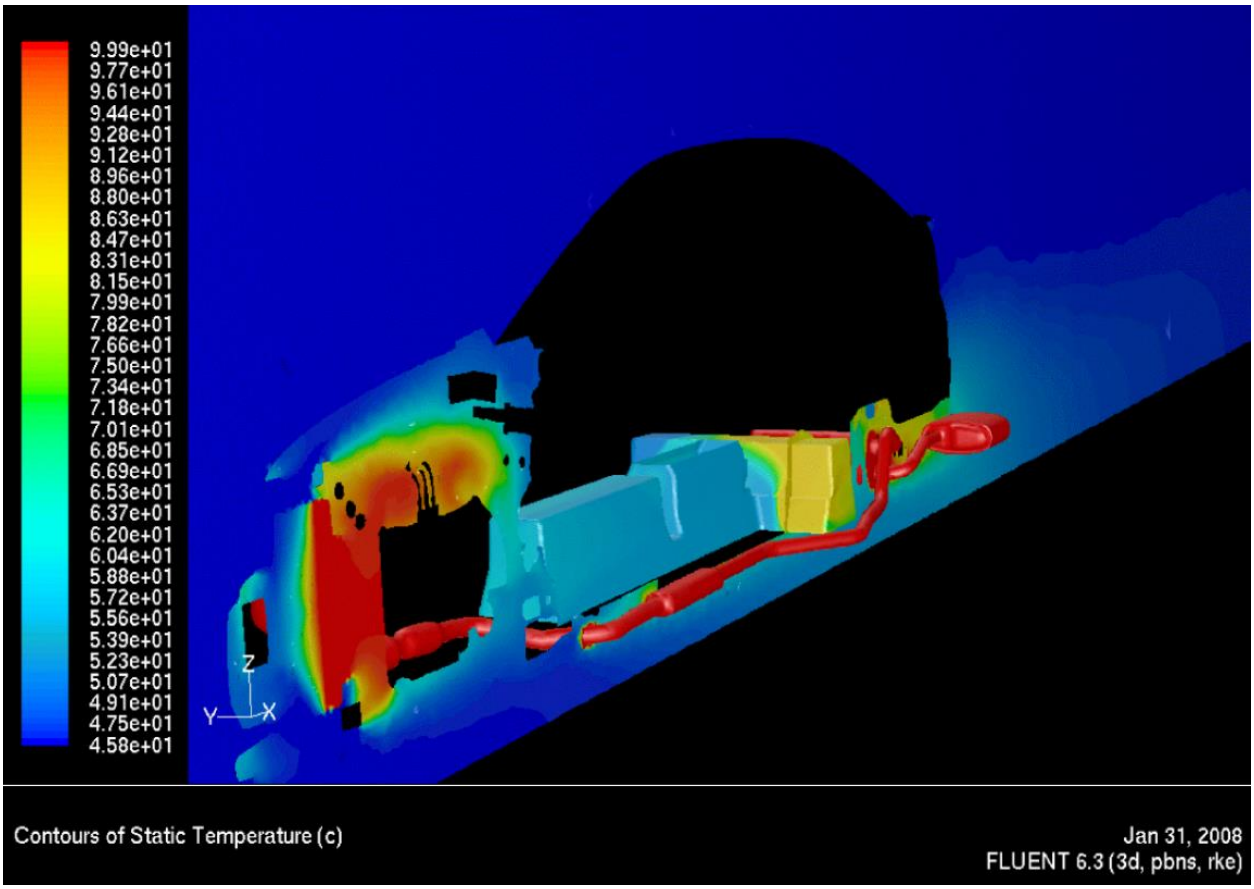

Figure 2-23, Engine and exhaust heat acting on an EREV ESS [1]

2.7.1 Optimizing Cell Parameters

Figure 2-24, Prismatic pouch Li-ion cell [35]

An important aspect of a thermal management system is cell design. Batteries carry significant thermal mass and resistance to heat flow. The outer surface of the battery may

remain cool while internally temperatures are rising. A study comparing liquid to air cooling showed that while liquid cooling provides better heat rejection, the gains become insignificant for large cell size [8]. It was also found that depending on the cell design there can be significant advantage to cooling directly within the battery. This is particularly apparent in NiMH and VRLA modules where individual cells are packaged together into larger modules.

However if a cell is designed specifically for an EV or PHEV, the arrangement can be optimized for heating and cooling. Reducing the thermal mass of the materials within the cell is one way to do this. However anode/cathode separator sheets tend to be made with polymers that have significant thermal mass. Liquid electrolytes which tend to have even more thermal mass are far more efficient at transporting Li ions through the separator sheets then solid electrolytes are. Cells that exhibit large ratios of surface area to thickness are easiest to control temperature within.

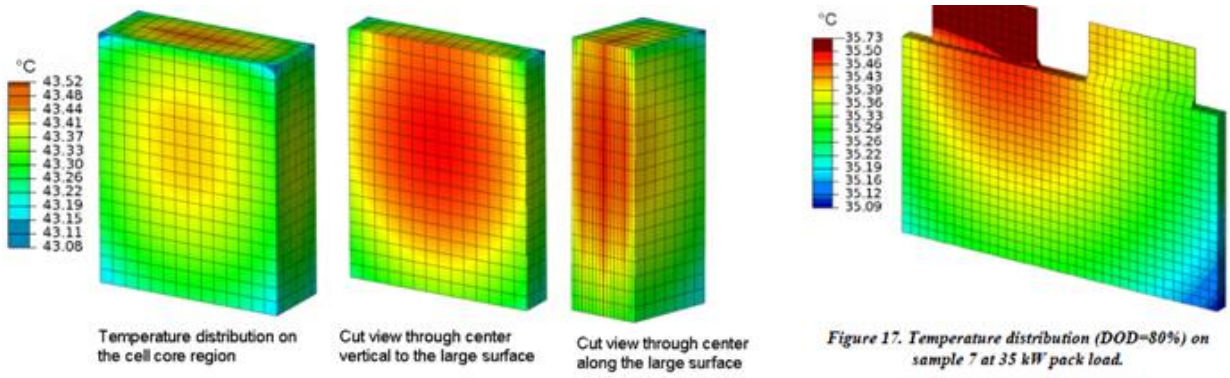

Figure 2-25, Internal heat generation prismatic vs. pouch cells [36]

As seen in Figure 2-25, the design of pouch Li-ion cells gives them excellent characteristics for employing liquid thermal management. Prismatic cells have a thick hard casing around the cell internals which make them structurally superior but difficult to cool. Cylindrical cells usually have a metal casing helping the outer surface heat transfer but the jellyroll like construction makes it difficult to remove heat from the center as the diameter increases. If modules are built up so that pouch cells are sandwiched with a cooling plate in between, modules can be packed quite tight without worrying about temperatures rising in the center of the pack. This is the cell type and construction assembly method which will be the main

focus of this thesis. The main drawback of pouch construction is the need for additional mechanical support of the cells. They also have a high potential for causing ground faults if not fastened properly as their casing constitutes only a thin layer of aluminum foil laminated to a sheet of non-conductive polymer.

2.7.2 Insulation and Pack Construction Improvements

The physical construction of the pack is extremely important. It needs to be as strong and light as possible, while minimizing its electrical and thermal conductivity. Composite materials offer benefits over metals for pack construction. They can achieve better strength to weight ratios with low thermal conductivity and no electrical conductivity. For instance aluminum has a thermal conductivity of 250 W/m K, compared to a fiberglass which is 0.288 W/m K (G10/11 fiber reinforced composite). Combining this advantage with an insulation blanket, one can achieve a high thermal resistance to minimize the amount of heat energy transferred into and out of the pack from the ambient environment. It is also important to fasten the battery modules in such a way that thermal bridges are not created between the ambient and the pack interior. Thermal bridging between ambient and the pack interior with materials that have a high thermal conductivity should be avoided when possible. To minimize the amount of cooling/heating the pack requires is paramount since such systems will use the ESS's own power to maintain itself.

To attain overall vehicle efficiency it is essential for the ESS casing to be as light, strong, and thermally isolative as possible. Material costs are also a consideration, PHEV and EV vehicles already come at a price premium to a traditional IC powered vehicle. Metals should not be integrated any more than necessary to minimize the electrical and thermal conductivity of the pack. Composite materials present a good alternative, and many are available on the markets today that don't incur a cost differential.

It is important to use good insulation materials especially in places where thermal bridging to the chassis occurs. The most common form of insulation is matted fiberglass or expanded foam which typically achieves thermal conductivity as low as 0.03 W/m K. Using an

insulation material within the pack can further help to decrease heat transfer from the environment. Materials such as Aerogel insulation blankets are advantageous, exhibiting approximately half the thermal conductivity of foam or fiberglass. A cost benefit analysis would evaluate if such added measures achieved a payback via further downsizing of the battery HVAC system components and/or provide a calendar life extension of the battery pack. However, the economic concern aside, the second half of this thesis and the key research contribution is centered on first quantifying the improvements possible in terms of designing a battery pack for maximum environmental thermal isolation yet retaining proper structural integrity.

Mean Temp.	°C	-200	-150	-100	-50	0	50	100
	°F	-328	-238	-148	-58	32	122	212
k	mW/m-K	9.8	11.4	12.3	12.9	13.8	15.5	18.6
	BTU-in/hr-ft²-°F	0.0681	0.0793	0.0852	0.0894	0.0956	0.1076	0.1291

Figure 2-26, Aerogel blanket thermal properties [37]

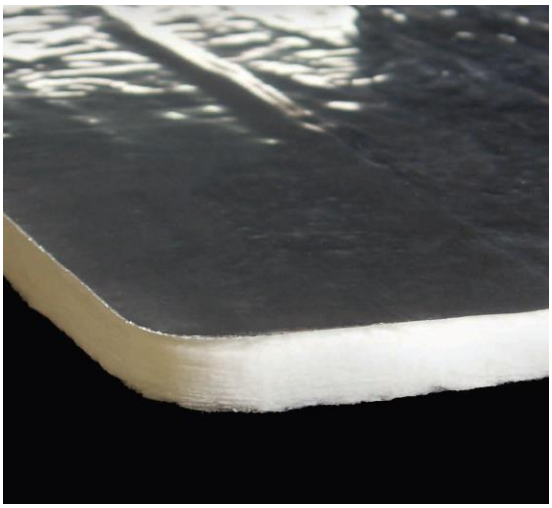

Figure 2-27, Aerogel insulation blanket [37]

2.8 Total System Integration

To provide both efficient cooling and heating a heat pump can be used. However their limitations in terms of heating become apparent near freezing where it may become as efficient to use resistive heating. If a PCM material is being utilized to handle the high thermal load situations and the exterior of the ESS is well insulated, the cooling system may be sized much smaller. When insulation and PCM are used together the HVAC system need only be able to remove/add heat at a rate that combats the average heat flux from ambient plus the cell's own heat generation.

To identify the requirements for the ESS, one must consider the rate that heat enters or leaves the pack from the ambient environment. This includes vehicle engine heat if applicable. The other sources of heat that must be considered come from electrical inefficiencies within the ESS. A full understanding of how heat is generated is important, however when designing on a system level what needs to be known are primarily the sources of heat and their amount. A lumped capacitance model is a good way to estimate cooling requirements for an ESS. Modeling this for various environment and cell loading conditions can enable estimation of average/peak heat production. Using such information the cooling system can be decided upon and sized for the application. This method works well for system level design; to better understand the cooling needs on a component level a CAE model will show in detail where heat is generated and transported.

Chapter three and onwards in this thesis explores pack level construction and the heat transfer associated. Through both CAE and practical experimentation, the goal is to understand where thermal efficiencies can be gained by altering the construction of an ESS. Ultimately reducing energy requirements of BTMSs and improving electrified vehicle range is the objective.

Chapter 3. ESS Design

Building on the research from the initial two chapters a cell type, BTMS strategy, and potential construction materials can be selected given the use case identified. As discussed previously, the two main sources of heat are from the local ambient environment, and from electrical inefficiencies within an ESS. In order to reduce cooling requirements these heat sources should be minimized. It is difficult to improve electrical efficiency within an ESS, therefore the primary area of design focus becomes excluding the ambient environment. This is especially true for PHEVs, and EREV, where thermal loads are present due to the vehicle's IC powertrain components (figure 2-23**Error! Reference source not found.**). To design an optimized system, the sources of heat must be understood. A relatively simple and effective way to comprehend the thermal loads within the system is to make use of a lumped capacitance model.

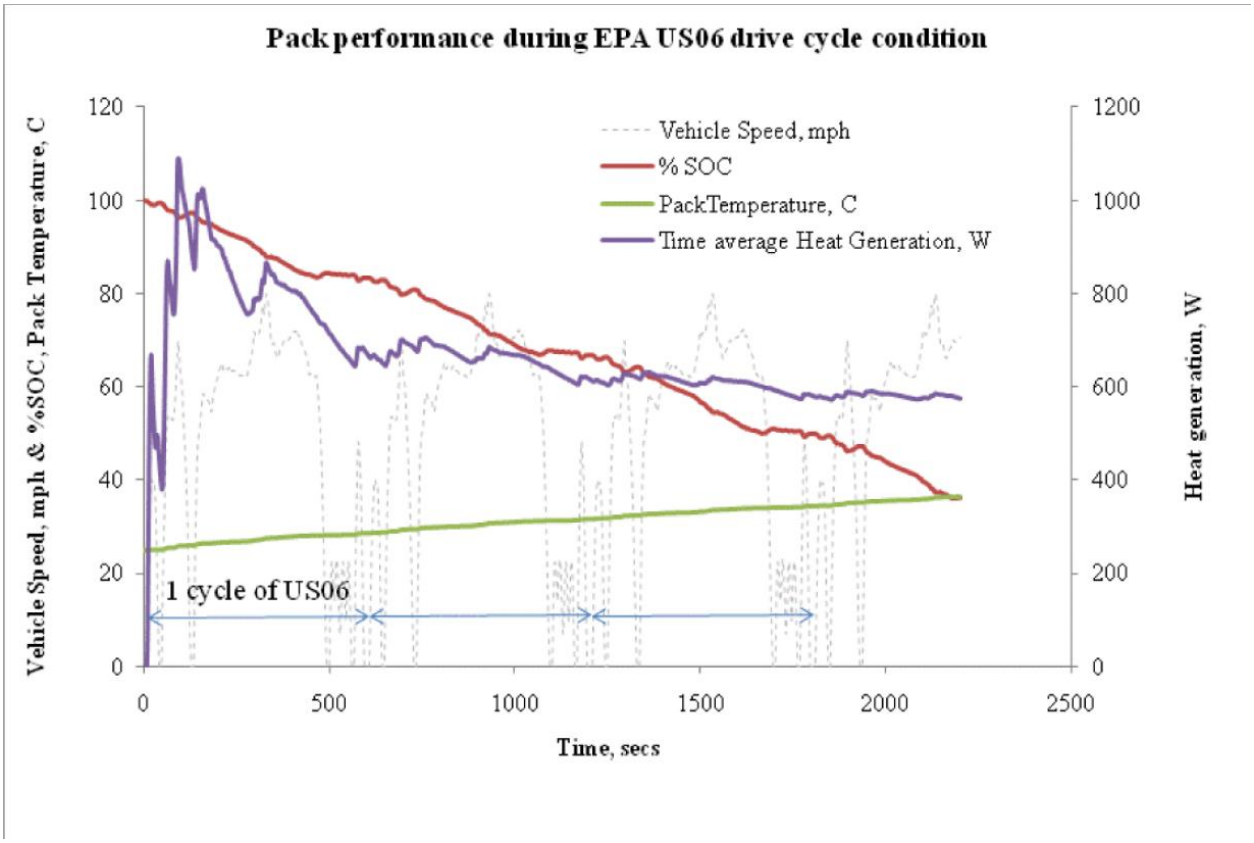

Figure 3-1, Heat generation of an EREV pack during multiple US06 cycles [32]

Figure 3-2 is representative of a battery system that has not been optimized for thermal management, nor with thermal isolation in mind. Hence a more powerful liquid cooling system is required, taxing the vehicle's electric range in order to keep the cells at the temperature set point. By refining construction methods such that the pack is more thermally isolated and adding insulation materials to the exterior of the cell packaging, the loads can be reduced significantly, possibly allowing for alternative cooling methods to be used.

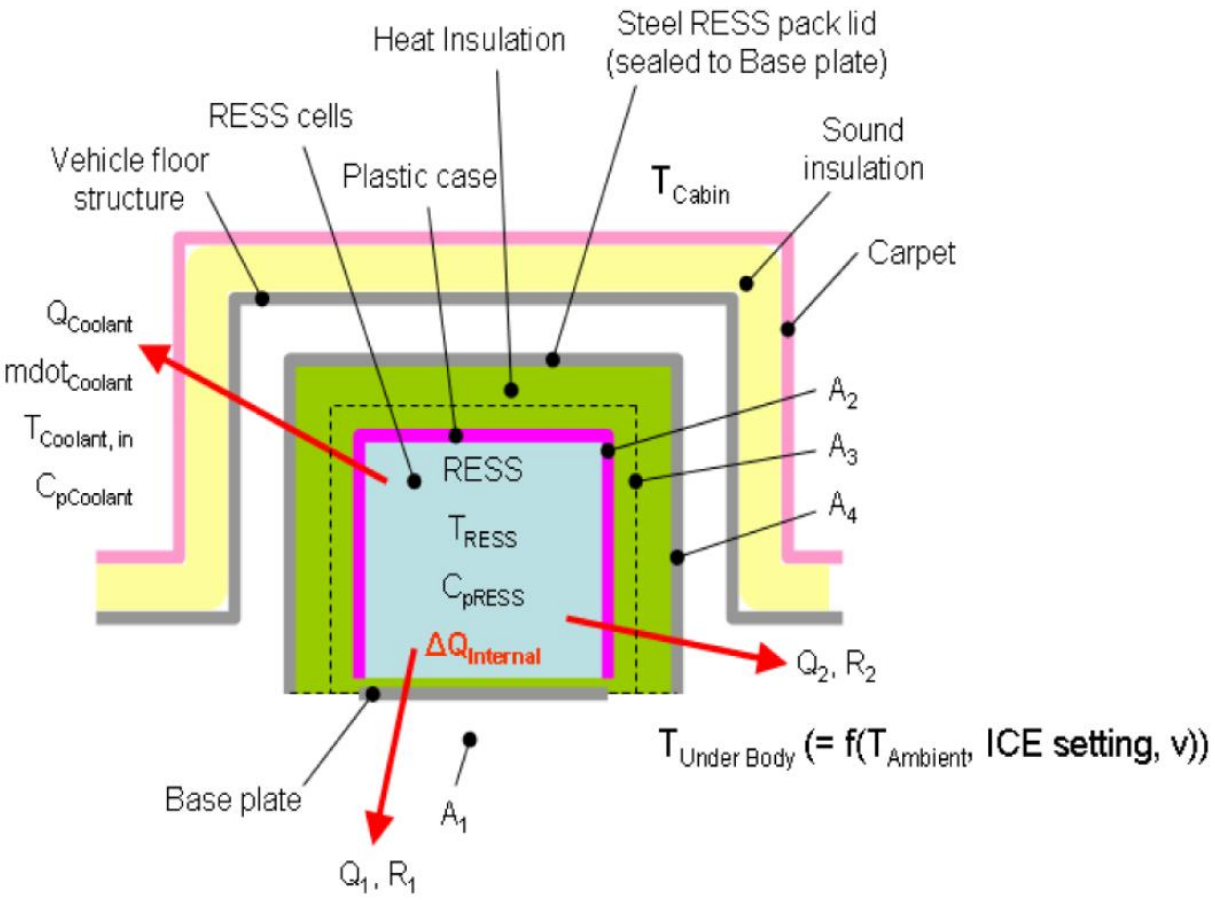

Figure 3-2, Lumped thermal model of an EREV ESS [32]

3.1 Framing the Problem

The production test case that was used as a starting point for design development improvements is an underbody mounted ESS used to power an EREV (Chevrolet Volt). The total capacity of the pack is ~16 kWh. The pack was evaluated both physically and through FEA analysis. Construction materials and insulation were then deployed as variables to quantify the amount of improvement that could be achieved. A much larger pack constructed

out of composite materials featuring thermal insulation, and a liquid cooling system was also initially designed as a proof of concept. This earlier research and practical application represented a high level analysis, looking for large efficiency gains over what remained on the road at the time (ZEV era vehicles), as yet no current era vehicles had been released aside the Tesla Roadster prototype.

Pouch type Li-ion cells were chosen; their large surface area and lack of protective casing lends them to have superior heat rejection characteristics compared to their cylindrical, and prismatic counterparts. Material selection for pack construction was based on optimizing both physical strength and thermal resistance. Also considered in selection of materials was cost, and electrical isolation.

3.2 Initial Testing

The concept vehicle for focusing on the development of a passive thermal management system approach for shaving peak heat loads was originated from a 500 km range EV designed and built by UOIT's EcoCAR team. In order to propel the vehicle 500 km on a single charge the ESS had to have ~85 kWh of capacity. Creating a pack this size presented many packaging challenges. The learnings from its creation have influenced much of the research presented. The initial concept was to build a structurally robust pack made with composite materials for thermal and electrical isolation. The pack was to be insulated and liquid cooled with a system that minimized parasitic losses without compromising the cell integrity.

Figure 3-3 shows the component layout. This was conceptualized in 2007, designed in 2008-2009 and built in 2010-11 to compete as UOIT's entry in the "EcoCAR: The Next Challenge" competition [39]. This vehicle was designed around the vehicle competition guidelines which required the design to maintain production intent. UOIT chose to build a full function EV for this competition, designing the ESS from the ground up. Battery thermal management was considered to be important based on the size and expense of an ESS capable of propelling the vehicle 500 km on a single charge. It was also a rules requirement.

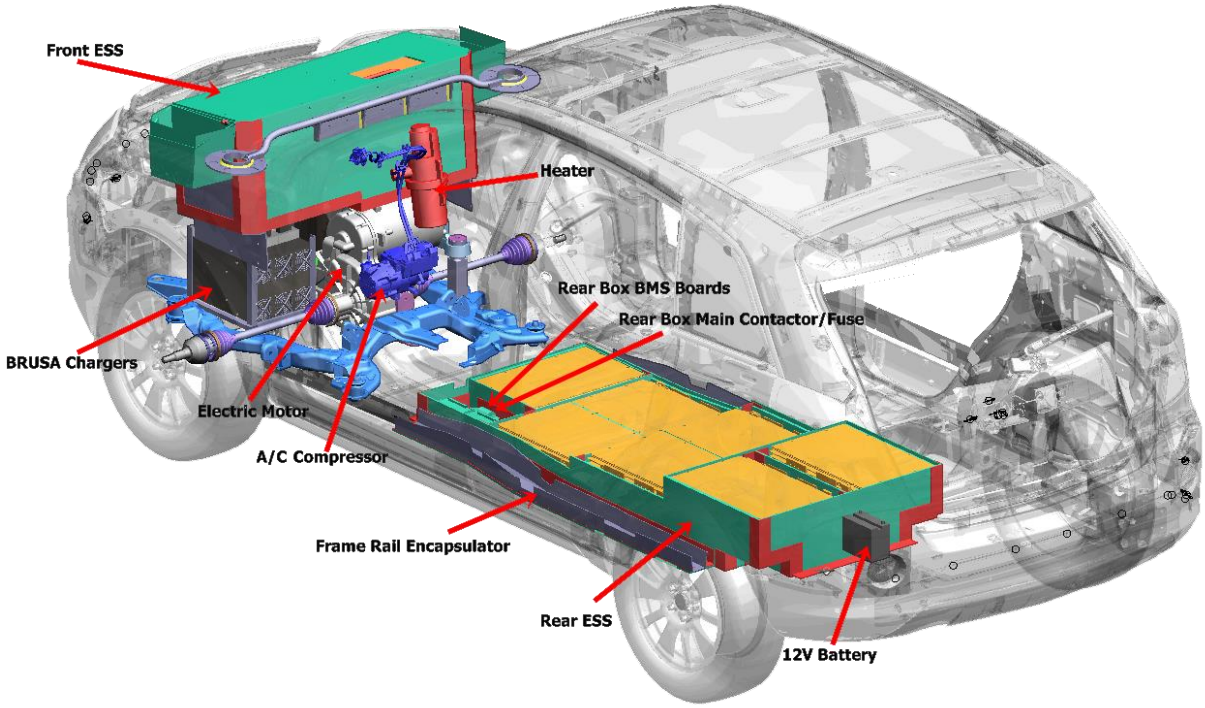

Figure 3-3, UOIT EcoCAR schematic [38]

When the task of improving the BTMS on a production Chevrolet Volt ESS was instigated as a thesis objective, concepts initially deployed during the EcoCAR design competition became more directly linked to the BTMS improvement goals for the Chevrolet Volt. Figure 3-4 shows the ESS layout within a production Volt. Comparing Figure 3-3 and Figure 3-4 it is apparent they employ similar ESS packaging. This allowed the EcoCAR design to serve as a prototype toward the implementation of increased pack thermal resistance.

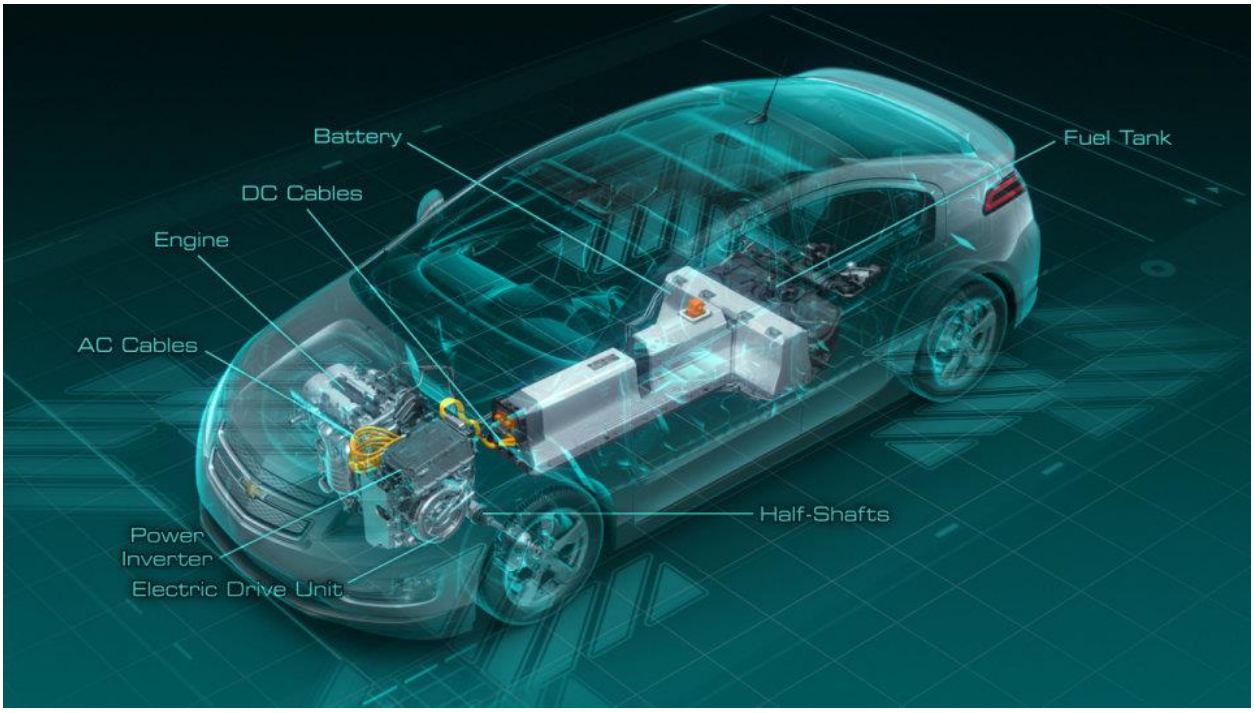

FIGURE 3-4, GENERAL MOTORS VOLT ESS LOCATION [40]

3.2.2 EcoCAR Prototype

The initial EcoCAR design consisted of an underbody ESS containing all of the cells. As the design progressed it was deemed necessary to split the ESS into two separate packs due to rules constraints. One situated under the vehicle's hood, and the other remained underneath the vehicle (Figure 3-3). Arranging the cells in series gave a total system voltage of just under 400 V at full charge. All cell modules were wrapped in a blanket of insulation. Liquid cooling was integrated through aluminum plates sandwiched between each cell. A coolant tube was soldered onto each cell retaining frame around its edges. The concept entails that the cells conduct heat onto the plate which would then be rejected through the coolant tubes. Each module of cells was plumbed parallel to the manifold line which ran the perimeter of the pack. The original concept was to have very thin coolant lines running between each cell rather than at the perimeter, but due to the manufacturing limitations of a student project, this was not possible and the alternative described was invoked.

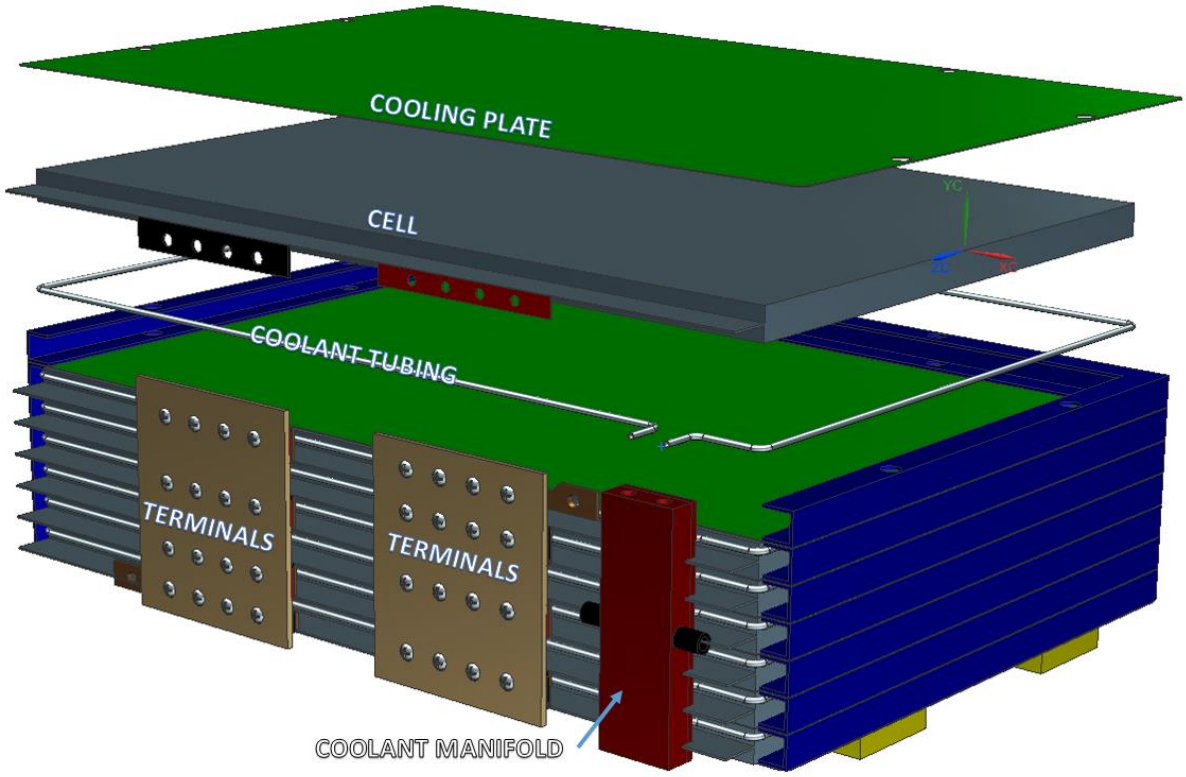

Figure 3-5, Single module from EcoCAR ESS

The pack did however act as a proof of concept for composite material use and insulation packaging methods. The team was able to show that it was indeed possible to retrofit a conventional vehicle with an ESS capable of providing 500 km of range per charge, and acceptable performance without removing any interior space. Next steps were to take the learnings from this prototype and apply them to a commercially manufactured ESS. Understanding where both improvements can be made through retrofitting the existing pack, and through redesign. An ESS out of a newly mass produced EREV (Chevrolet Volt) was used as the basis of further development.

Figure 3-6 through Figure 3-8 show the evolution of the physical pack build for the original prototype. The base plate for the pack was constructed from a single sheet of SP-1002 composite. Walls were constructed of G11 composite and these were bonded to the plate and GPO-3 fiberglass angle side reinforcements. Cells were compartmentalized into modules (Figure 3-7), and then surrounded with 10 mm of Aerogel thermal insulation (Figure 3-8).

Figure 3-6, Base plate of EcoCAR prototype ESS with frame rail attachments

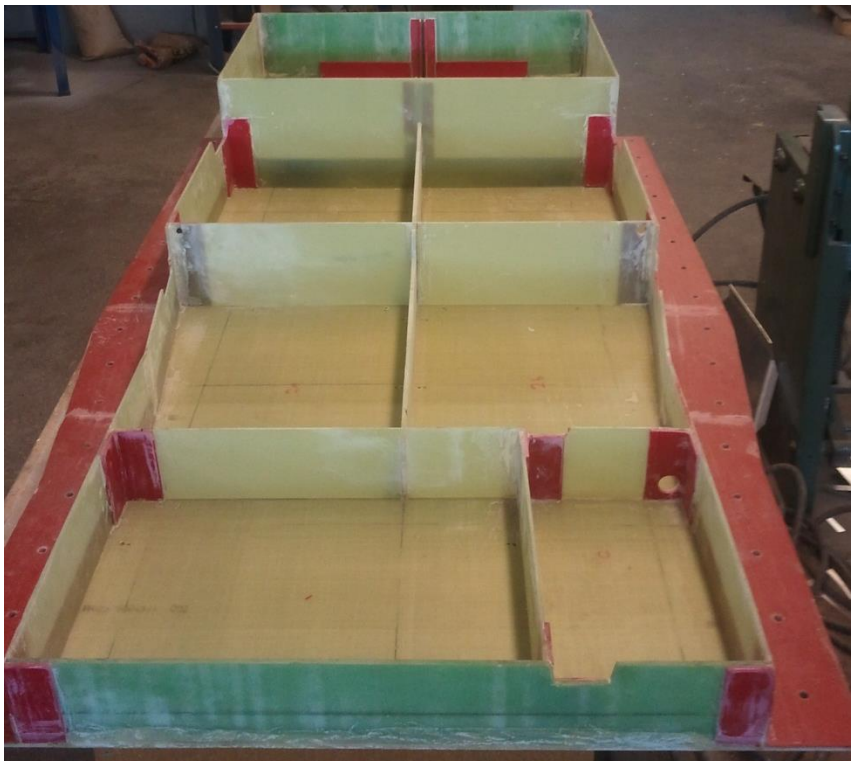

Figure 3-7, EcoCAR prototype ESS composite structure

Figure 3-8, Cell module places in EcoCAR pack with cooling and electrical lines

3.2.3 Quantification of Prototype Concepts

While structural FEA was conducted in the design of the EcoCAR prototype. No thermal FEA or thermal testing was conducted to quantify the effects of increasing thermal isolation though pack construction techniques. There simply was not enough time, only theoretical design calculations were relied upon. During this period a unique ESS design using modules of Li-ion polymer cells with a liquid BTMS distributing the cooling effort through indirect contact via aluminum cooling plates gathered attention. Therefore when the Volt pack design was revealed to the research group members, it naturally followed as the best means to quantify the construction methods used in UOIT's prototype on a real product.

Initial testing focused on establishing a performance baseline, and understanding where improvements could be attained without a complete pack redesign. The ambient (20 °C) pack was placed in a thermal chamber heated to 50 °C, with thermocouples placed in strategic

locations to record the temperature change. The process was repeated three times; no additional insulation was added for the first run, a 10 mm thick layer of Cryogel® Z aerogel insulation was added to the exterior of the pack for the second run, this was then removed and a 5 mm thick layer of Cryogel® Z was added internal to the pack casing for run #3.

Figure 3-9, Ess with 10 mm aerogel wrap in thermal-chamber

The objective of this test was to discover how much thermal cooling load could be removed from the system through pack insulation. Temperatures were recorded using 13 thermocouples both internal and external to the pack (See Appendix A for placement). The data obtained was used to estimate a thermal time constant (τ) for the three cases. The thermal time constant of the system is an effective way to quantify gains. It is used in a lumped capacitance thermal model, where τ is the amount of time it takes the system to reach 63.2% of its asymptotic value. This represents the characteristic time of a 1st order lumped system model whereby the environment is at a steady temperature. As the battery temperature approaches its steady state, the rate of heat transfer slows asymptotically to zero.

Building on the physical testing, CAE models were created that allowed for varying the pack's physical parameters. The pack was 3D modeled to study packaging constraints within the vehicle. Insulation and alternate cooling sources were looked at. The complexity of the model

was subsequently reduced for CAE analysis. Portions of the pack were meshed and imported into a CFD solver. Multiple models were created with different physical solutions. The cell and its attachment scheme was eventually modeled separately due to computing limitations. This cell level model was then deployed as an input to the larger CAE model. The end result has helped to prove many of the concepts employed in UOIT's EcoCAR project, and led to refinement and quantification of variables affecting a commercial design, as represented by the VOLTEC platform.

3.3 ESS Pack Design

The initial step when creating an ESS design is evaluating the packaging space. The assumption is that manufacturers will generally fit an ESS within an existing vehicle architectural platform until such time that EVs have gained a large enough market share. Even in a unique architecture, the same occupant and interior constraints exist. This will dictate the ESS be packaged either under the vehicle, behind the occupants removing cargo space, or under hood. Under hood space tends to be limited for larger packs, and placing it behind the occupants removes reportable cargo volume. Placing it under the vehicle lowers the center of gravity, centers the weight distribution and generally provides more packaging space then under hood. This makes it a common ESS location for EVs and front wheel drive (FWD) EREVs. This space is more limited in the case of a rear wheel drive (RWD) with a forward mounted tractive motor or IC engine as in pickup trucks or sports sedans. Disadvantages of mounting underbody include: Exposure to environment, and being one of the vehicle's lowest points hence susceptible to physical damage from road obstructions.

Available packaging space will often dictate a cell type and size. Pouch cells are a common choice, and the one that was studied in this work. These cells are both volumetrically, and thermally efficient. The main drawback being that the cells rely on the module they are contained within for structure. Module configuration can also impact cell sizing. It is a common practice to configure an ESS into multiple modules; this eases manufacturing, and helps downstream if at some point part of the pack needs to be repaired. Within these modules the cells are arranged in series and parallel. The number of cells in series will

determine nominal voltage. The more cells in series, the higher the nominal pack voltage, the lower the current required to achieve the desired power output. Since electrical power is the product of the voltage and current applied (P=V*I), and voltage is defined by the chemistry and SOC of the pack, increasing current is the only way to generate additional power output once a voltage limit is set for the design. Most variants of Li-ion cells have a nominal voltage somewhere between 3.3-4.2V, and most EVs operate at a system voltage between 300-400 V at 100% SOC. Commonly 90-100 cells in series are required. For added safety and to increase the ampere hour count, cells are usually arranged in a series-parallel configuration. The number of cells in series is generally consistent, but the number in parallel can change depending on the cell size and current requirement.

Using CAD software allows cell/module configurations to be created and uncovering the most efficient packaging solution. It is important that the package be as compact as possible without sacrificing structural and thermal efficiency. The electric motor will dictate the peak power output requirements for the ESS assuming the motor is to be operated up to rated power, the RMS (root mean square) power rating will be at a specified amperage which should not be exceeded except for bursts. This will allow an optimal pack voltage to be derived and then determine the number of cells that should be placed in series within the pack. Assuming 90-100 cells are placed in series to attain a 100% SOC voltage of ~400 V, the only way to increase capacity is to increase the amp-hour count of each cell in series. This can be done by either increasing cell size or placing cells in parallel groupings. The disadvantages of increasing cell size are: packaging is more restricted and the vehicle is unable to operate if a single cell drops out. Larger cells contain more chemistry which will make them more volatile in thermal runaway situations. The disadvantages of increasing cell count in parallel groupings are; the inability to balance individual cells, (which can accelerate capacity loss) and increased packaging volume and wiring mass is required since individual cells need to be connected and constrained.

Constraining the cells within modules provides many challenges. Pouch cells will expand with age, and when at high SOCs. The cells need to be able to expand without the internal pressure increasing to a point where the cells burst. There also needs to be a cooling surface on each cell to extract heat and large cells are at a disadvantage because they lack surface

area per unit volume. Exposure to conductive materials should be limited, as any leakage current can find its way to ground and create shorts within the pack. Choosing a modular design for cell constraints and cooling allows for increased flexibility and decreased manufacturing costs. Present technological limitations considering the above factors usually lead to battery modules constituting two or more cells in parallel with capacities of 15-30 Ah each. Series strings inside modules tend to remain under 60 V peak for safe handling considerations (typically around 48 V nominal).

3.3.1 ESS Module Design

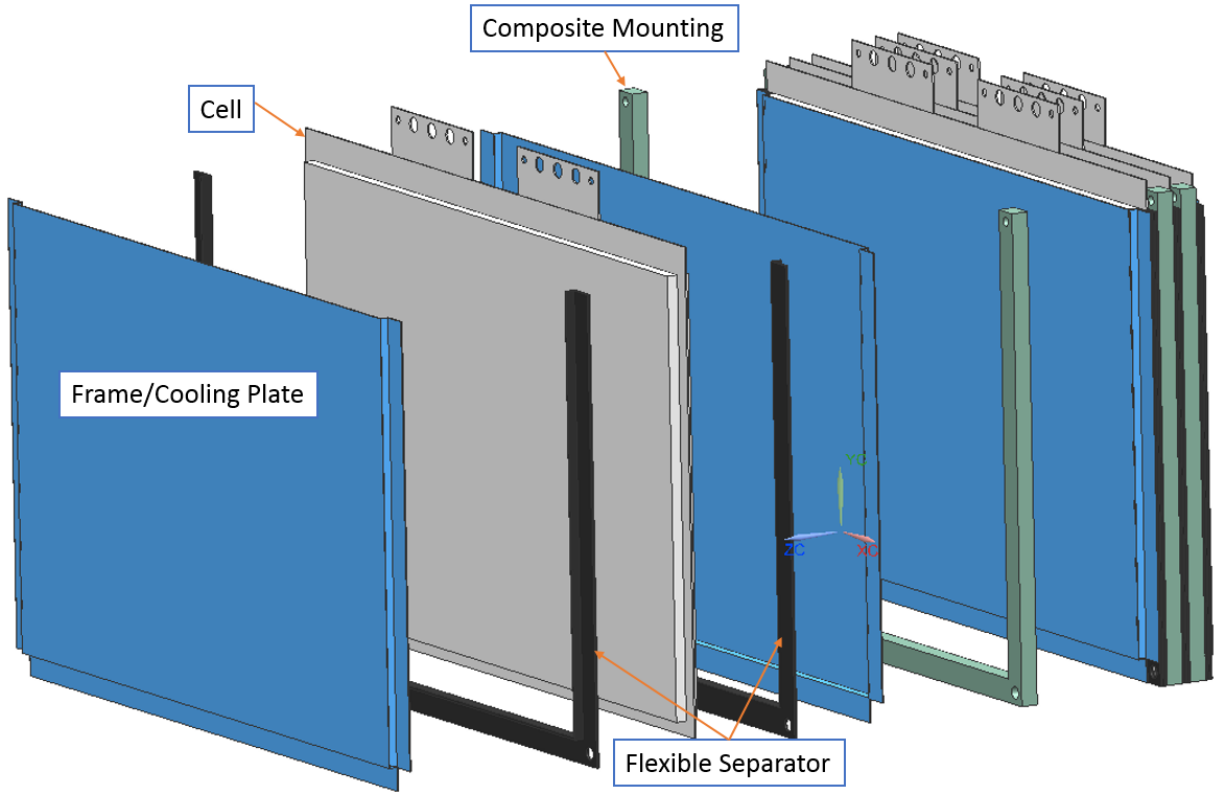

Figure 3-10, Modular construction example #1

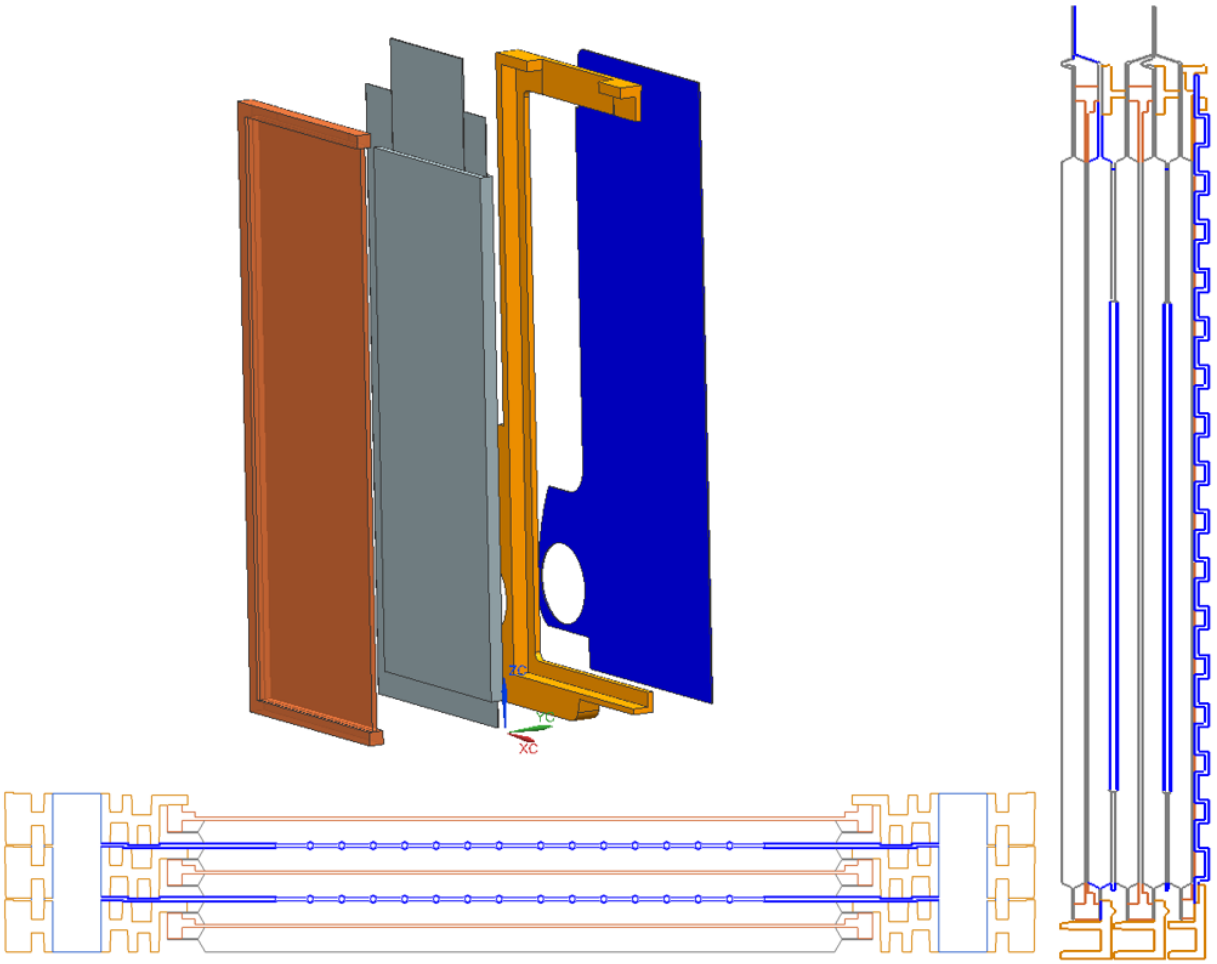

Figure 3-11, Modular construction example #2

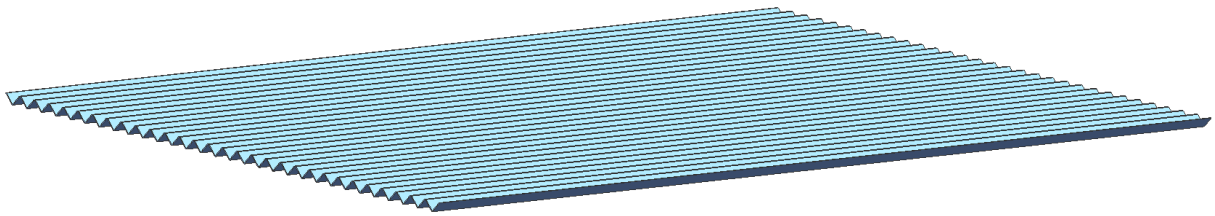

Figure 3-12, Air cooling plate

Above, Figure 3-10 and Figure 3-11 show some modular strategies for ESS cell packaging of Li-ion pouch type cells. Ideally each cell face touches both a cooling surface, and an expansion surface. It is important that each cell be in contact with a large area cooling surface as lithium ion cells have poor conductivity in the normal (through thickness) direction. The cells are

composed of a positive and a negative electrode, separated by porous polymer sheets soaked in electrolyte and the whole cell is wrapped in a foil laminate pouch. Table 3-1 shows some of the thermos-physical properties of an EiG Corporation ePLB C020 Li-ion polymer cell. Given the cells described are Li-ion polymer with a pouch type construction, they provide little too no mechanical resistance of their own and require a support structure to be packaged into cell modules. The other notable property is that each stacked layer is separated by a polymer sheet with a high heat capacity and low thermal conductivity. Typical conductivities of a pouch type cell would be as low as 1.2 W/(m K) in the normal direction while in plane conductivity would be closer to 30 W/(m K) [41].

Table 3-1, Thermophysical battery component properties [42]

Material/layer	**Thickness [µm]**	**Number of layers**	**Density [kg*m^{-3}]**	**Heat capacity [J/(kg K)]**	**Thermal conductivity [W/(m-K)]**
Aluminum Foil	21	17	2702	903	238
Copper foil	12	18	8933	385	398
Separator sheet	25	36	1017 (wet)	1978 (wet)	0.34 (wet)
Pos. Electrode	70	34	2895 (wet)	1270 (wet)	1.58 (wet)
Neg. Electrode	79	36	1555 (wet)	1437 (wet)	1.04 (wet)

The pouch containing the cell is minimally thick and not resistant to chaffing, it is made from a polymer laminated foil with minimal thickness (generally aluminum foil laminated in polypropylene). Frame materials need to be chosen wisely to retain cells without adding additional stresses to the cell packaging. Generally excess bagging material that is not used to seal the cell is cut off. This can lead to potential leakage currents in improperly manufactured cells as there is exposed conductive foil surrounding the cell's edge. The concept in Figure 3-10 uses a non-conductive flexible material between the cooling plate and

the edges of the cell for retention. In Figure 3-11, the coolant plate and cell are attached to the frame at independent locations. The frame is constructed of nylon and in direct contact with the cell edge.

Figure 3-13, 20 Ah A123 batery systems cell [43]

Pouch cells have a tendency to expand both with age and during cycling. Expansion estimates range from 0.5% to 4% during charging [56]. This is largely due to the expansion of active material on the negative electrode as the concentration of Li-ions increase at high SOC. There is also expansion that occurs with age as SEI layers build up over time. Allowance for this expansion should be built into cell modules. Both module examples in Figure 3-10, and

Figure 3-11 offer different approaches to deal with cell expansion. In both cases the rigid frame is built such that it is larger than the nominal cell width. Example #2 (Figure 3-11) uses a semi rigid foam to hold the cell in place, and a less rigid foam along the face of the cell to allow for expansion. In this construction opposite faces of each cell are in contact with foam for expansion, and a cooling plate on the other side while being rigidly held along the edge by a non-conductive frame. This strategy leads to a robust design which was used for thermal analysis. Each coolant plate is plumbed in parallel to the main coolant loop which delivers coolant to each module.

It is important the modules be retained to the main body of the ESS in such a way that there is electrical isolation from the cells. Two different strategies are employed to retain the modules, examples are demonstrated in Figure 3-10 and Figure 3-11. Figure 3-14 depicts the module from Figure 3-10 mounted to a composite bottom plate. Here the cell frames are constrained using rods threaded into a composite block around the edges. The block is also mounted to the base plate in a separate location. This keeps the module both thermally and electrically isolated from the base plate.

In the case demonstrated the pack's base plate is also a composite material, which provides further isolation. Figure 3-15 shows the mounting strategy associated with the commercial module shown in Figure 3-11 wherein the composite frame within the module creates isolation. In this case the module is clamped onto a metal base plate. In this design the cell frame is providing all of the retention for the cell.

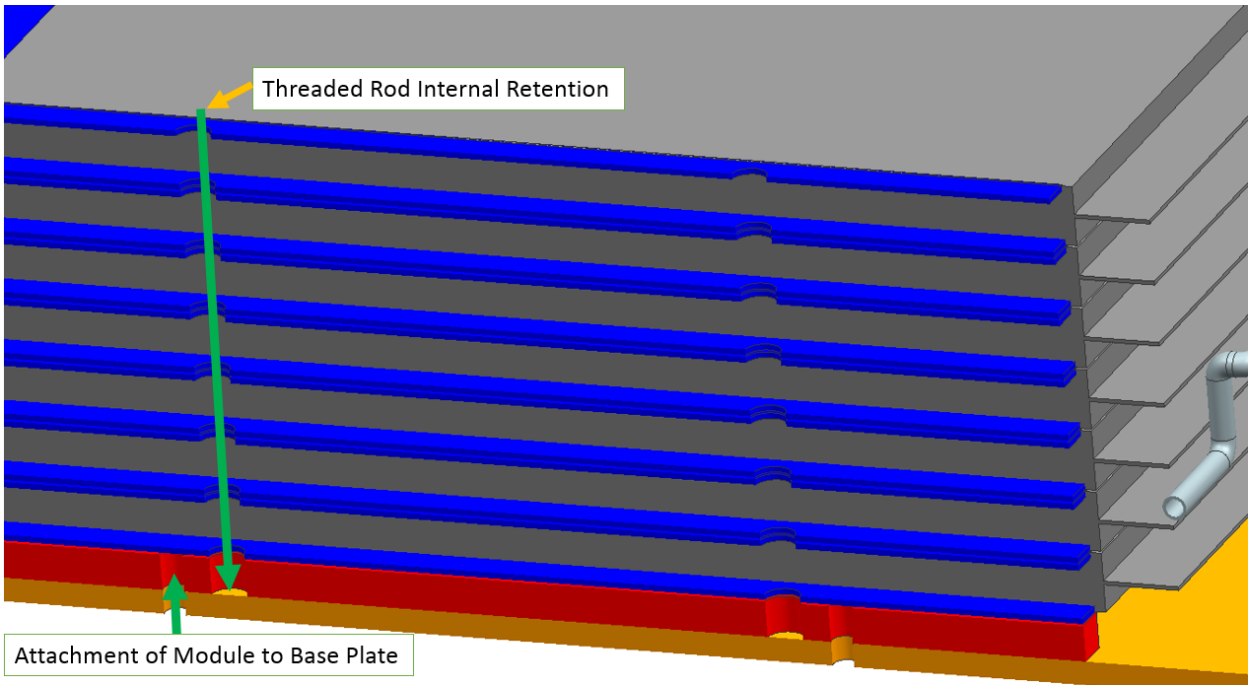

Figure 3-14, Retention strategy, construction #1 (flexible separator removed for clarity)

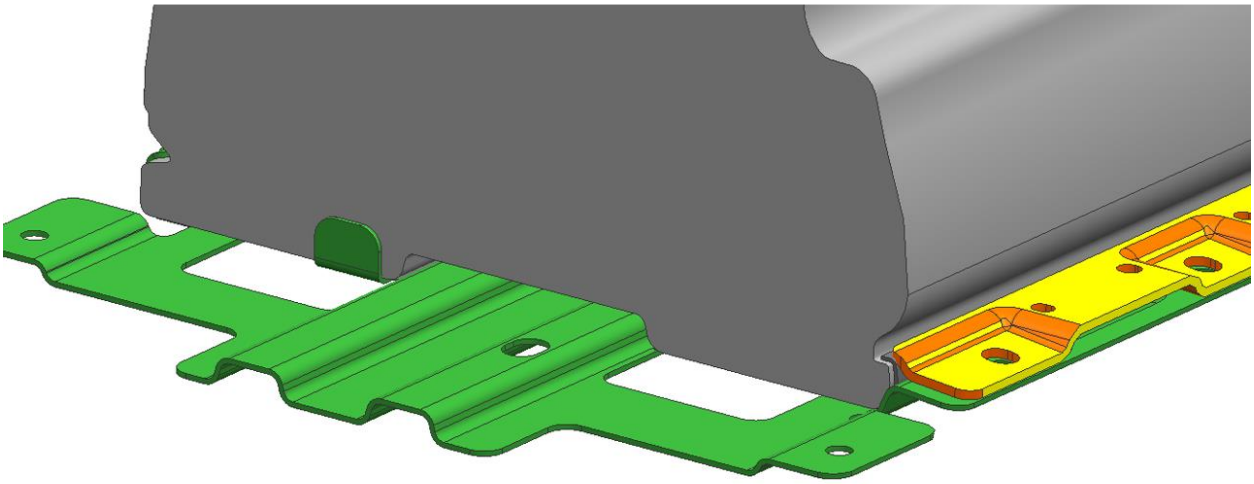

Figure 3-15, Cell frame retention strategy, construction #2

3.3.2 Pack Cover and Base Plate Design

Typically battery packs mounted underbody are constructed with a protective composite cover made minimally thick to protect the modules from the environment. The cell frames attach to the base plate structure which is generally reinforced steel or aluminum. This strategy is cost effective and adequately protects the ESS from mechanical shock. Thermally it offers little resistance. The strategy relies heavily on the cooling/heating system internal to the pack to protect it from ambient exposure. Optimization of this structure to increase the thermal resistance of the pack can help to decrease the amount of energy which needs to be removed or added to the ESS to maintain temperature. Consequently such energies are not being used to create tractive power and thereby decreases the overall vehicle efficiency. The pack would also be able to maintain itself at safe temperatures for a longer period of time in the case where the ESS is let to soak in extreme ambient without an external power source to operate its cooling/heating system.

A simple way to decrease the pack's thermal conductivity without requiring redesign is to insulate the ESS. In a new design, or where redesign is deemed feasible, replacing the metallic base plate with a high thermal resistance composite can improve thermal performance. Since the ambient environment is deemed the largest heat source, increasing the thermal resistance between the interior and exterior of the pack should be the goal. Table 3-2, and Table 3-3 show some property differences between metal alloys, and composite materials in the mechanical and thermal sense respectively.

Table 3-2, Comparison of mechanical properties

Material:	Young's Modulus (GPa)	Flexural Strength (MPa)	Tensile Strength (MPa)	Poisson's Ratio
Aluminum (6061-T6) Alloy	69	275	310	0.33
Steel AISI 4340 (normalized)	200	860	1310	0.29
Steel AISI 1018 (cold drawn)	200	370	440	0.29
GPO-3 (pultruded fiberglass shape)	6.9	165	62	0.17
G11 (compression molded fiberglass panel)	11	517	310	0.17
SP-1002 (autoclaved FG panel)	38.6	1151	965	0.26

Table 3-3, Comparison of thermal properties

Material:	Thermal Conductivity k (w/m-K)	Density ρ (g/cc)	Specific Heat Cp (J/g-K)	Thermal Expansion Coefficient (10^{-6}/°C)
Hand layup fiberglass 35 Vol%	0.300	1.45	0.967	23.6
SP-1002 Crossply (Autoclaved Fiberglass)	0.334	1.85	0.879	11.7
Cryogel® Z Aerogel Insulation	0.015	0.13	1.05	11.7
Sheet molding compound 30% FRP	0.300	1.45	0.967	20.0
Steel AISI 4340	54	7.85	0.49	9.0
Aluminum (6061-T6) Alloy	167	2.70	0.896	8.6

The strength of the SP-1002 composite is similar to that of 4340 Steel, while its thermal conductivity is two orders of magnitude lower. Structurally there is less flexural resistance, but this can be overcome by designing the ESS cover itself to be a structural component. This concept was demonstrated through UOIT's EcoCAR build. The underbody pack was constructed using a SP-1002 composite sheet with biaxial reinforcing ply. The vertical walls of the ESS were built out of the G11 composite shown in Table 3-2. FEA was conducted on the pack, to verify the design. A loaded ESS constrained along its vehicle mounts was subjected to a simulated 8g vertical load, a concentrated (10 cm diameter) 2g load, and a 4g high centering simulated load. In all three instances the base plate was not stressed beyond its manufacturer's specifications.

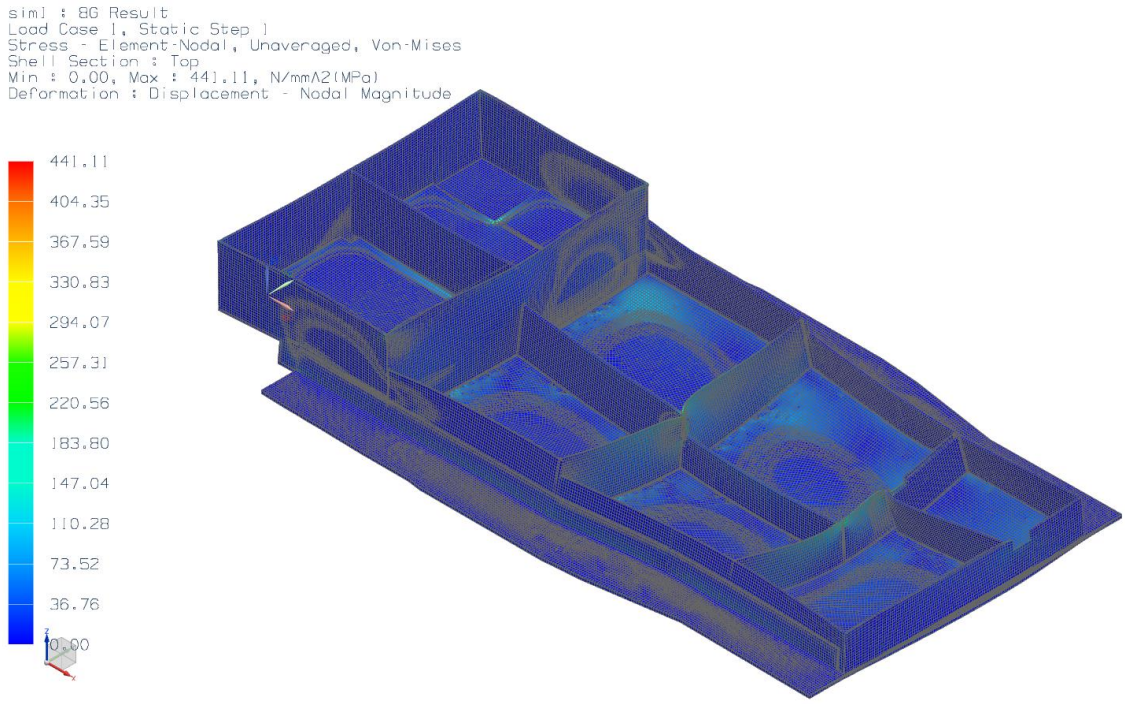

Figure 3-16, EcoCAR pack stresses with 8g distributed load [38]

The top of the pack only needs to protect the ESS from water and debris. Each "tray" within the EcoCAR ESS was built to accept a modular cell structure containing an appropriate number of cells to the height of the tray. 10 mm of extra space was left on every surface in contact with an outer wall of the pack. Aerogel insulating material was then added to further

decouple the interior of the pack from the environment. Cooling lines were plumbed through the vertical walls of the ESS creating a main loop. This loop is connected to a universal manifold at each cell module which creates internal parallel flow through the cooling plates.

The system was designed to be modular. Repeating cell frames were stacked to create various sized cell groupings. Coolant manifolds have a standard connection, so the main coolant loop is independent from the size of the cell groupings within each module. Coolant plates and expansion surfaces are also standardized and placed on opposite sides of each cell, both of which are shared with the neighboring cell. The modularity of the design allows for many ESS configurations and capacities to be constructed out of the same components. The concept can be scaled to different cell sizes and is adaptable to series/parallel cell arrangements.

Chapter 4. FEA Modeling

The full ESS CAD model needs to be simplified in order to conduct FEA analysis. Each component is represented by elements. One, two and three dimensional elements create the sections, surfaces, solids and in the case of computational fluid dynamics (CFD) the gasses/liquids with the model. This is done to limit the computational power needed, and memory required to model how components will behave in a dynamic environment. Therefore without resorting to exceptional computing power it is impractical to represent an entire system in a finite element (FE) model. The ESS needs to be reduced into a series of models which are used to represent the system at various scales.

In this case a series of three dimensional solid meshes and two dimensional section meshes were created to model the ESS on a component level, and system level. Within each model material changes and environmental changes could be made to represent a variety of conditions. The primary objective of the two dimensional models was to parameterize the cell module internals so that they could be represented by a single solid within the full thermal three dimensional system model. This treats the cell module internals as a lumped capacitance. Figure 4-1 outlines the method of integration between the FEA models. The results from the 2D cell module level FEA are transmitted to the 3D battery pack system model as inputs. 3D CAD models are iterated based on the final results to optimize both the module and the pack construction.

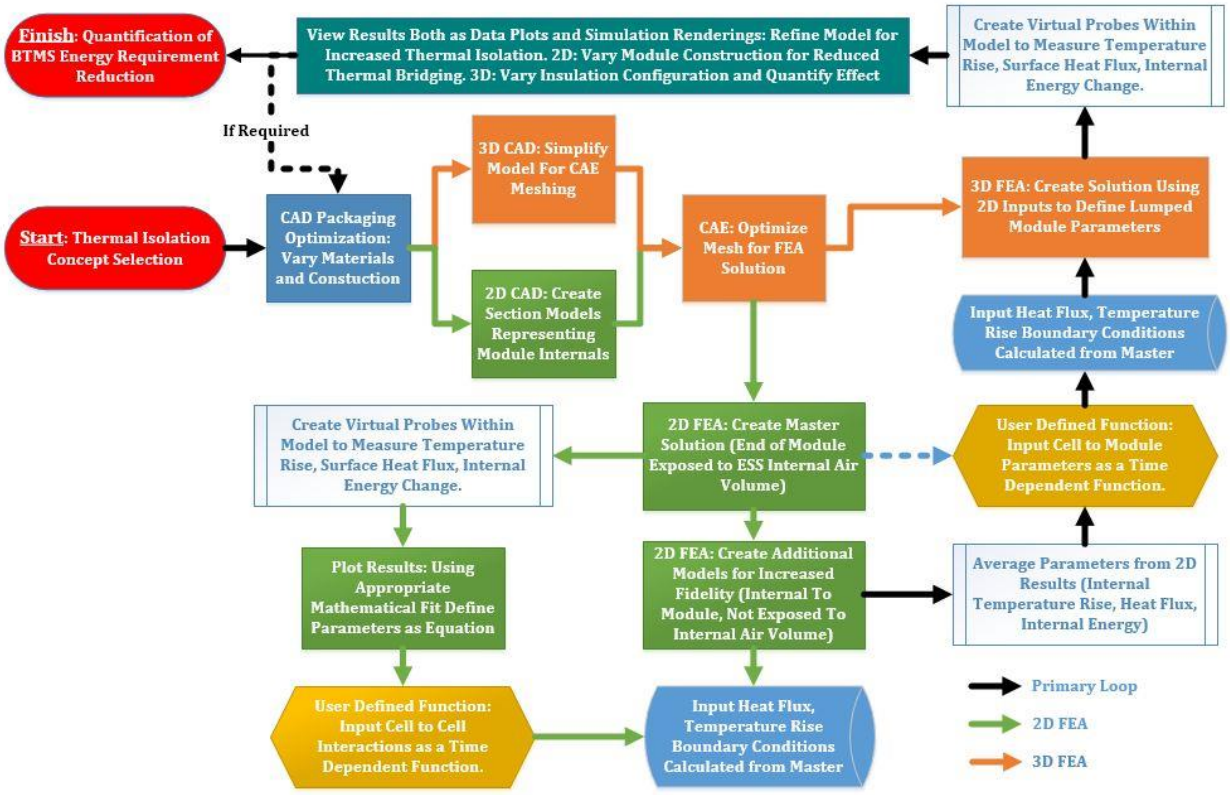

Figure 4-1, FEA process flow

4.1 Two Dimensional Model

Within the cell module there are many small components relative to the size of the pack. In order to create a simulation with good fidelity these need be accounted for, hence three different sectional two dimensional models were created. The purpose here was to parameterize the module internals in order to feed the system level model. Out of scope however was fully parameterizing a cell level model. Modeling heat transfer within Li-ion cells is a whole topic onto itself. Average properties of the cells were assumed based on data from others researchers. In scope for the two dimensional model were the cells, coolant plates, retaining foam, and cell frame. This model dictates that only generalized internal thermal parameters need to be understood.

To discover the rate of energy transfer into and out of the cell module, a three dimensional CAD model was created consisting of grouping of five cells, three frames, two cooling plates,

and three foam pieces allowing for cell expansion. Very similar assemblies are undergoing physical testing that is being carried out by another graduate student in a parallel work endeavor. Sections were then cut through the center of the main coolant line which feeds the individual channels in parallel and runs through the coolant plates in contact with each cell. An additional horizontal section was cut through the upper third of cells, and a final section was cut vertically which can be seen in Figure 4-2.

The geometry of each section was then meshed in separate software (Altair Hyperworks). In order to complete CFD analysis all fluid volumes must be meshed. Such meshes were created to represent coolant, air trapped within the module, open volume, and all solid components in the models. The results of such are demonstrated in Figure 4-3 through Figure 4-8. When creating a mesh for components that interact with one another, nodes need to align at the interface to create a couple within the solver.

The initial phase of two dimensional model testing was conducted with the models shown in Figure 4-3, Figure 4-5, and Figure 4-7. These represented the “stock” module where the only modification made to the module structure was to simplify the geometry to allow it to be meshed for CFD analysis. The models in Figure 4-4, Figure 4-6, and Figure 4-8 represent the second iteration or “optimized” module construction. The most significant design difference being that the cells are no longer in direct contact with the module frames reducing thermal bridging. Other improvements were also made to these models to improve the accuracy of the simulations. Additional cells were added to the vertical section model (Figure 4-8) to more realistically simulate the effect the end plate has on heat transfer into the cells within. These models also removed the air surrounding the cells in the normal direction as in a full assembly these surfaces would not be exposed to air volumes. A further explanation of the optimized models can be found in section 5.2.2.

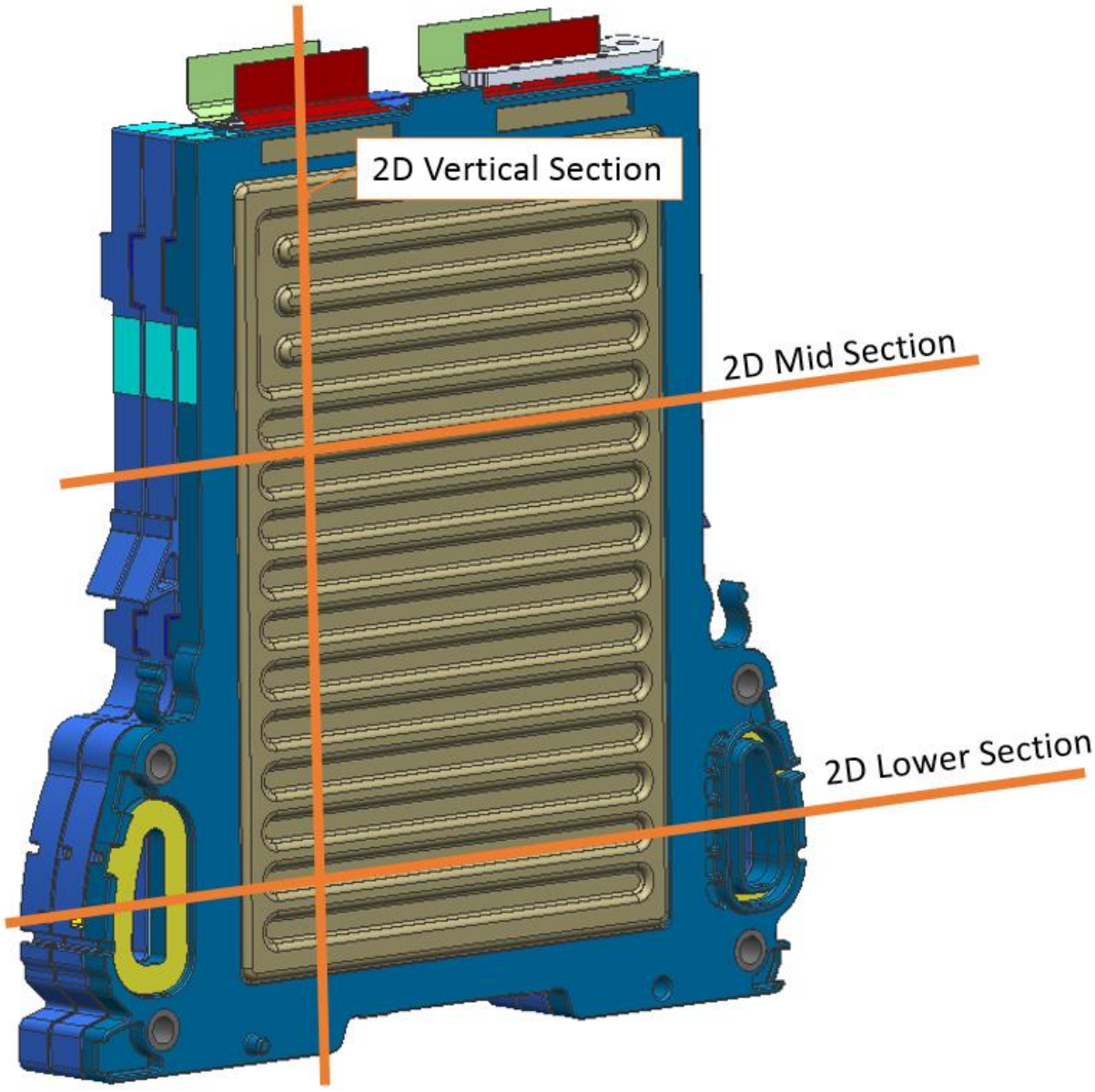

Figure 4-2, Two dimensional section locations

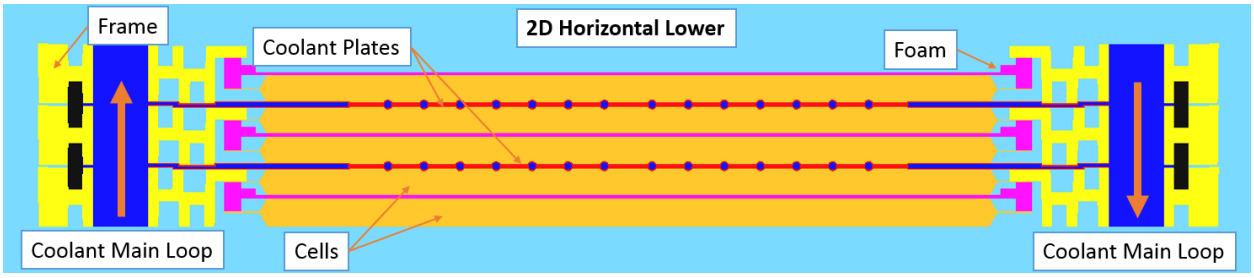

Figure 4-3, 2D lower horizontal section non-optimized: used in section 5.2.1

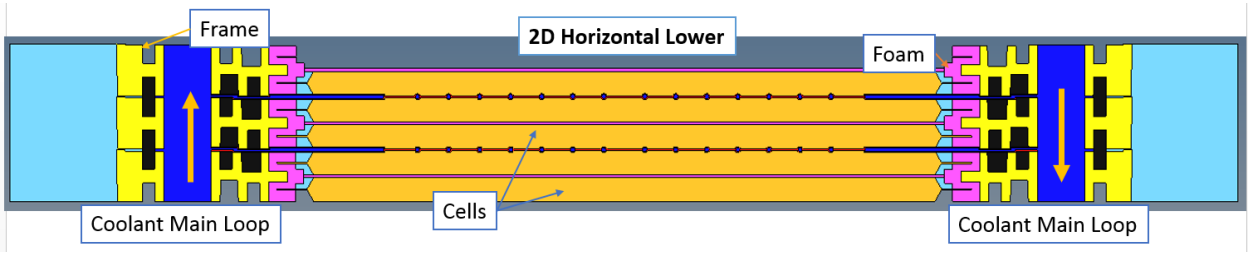

Figure 4-4, Two dimensional lower horizontal section optimized: used in section 5.2.2

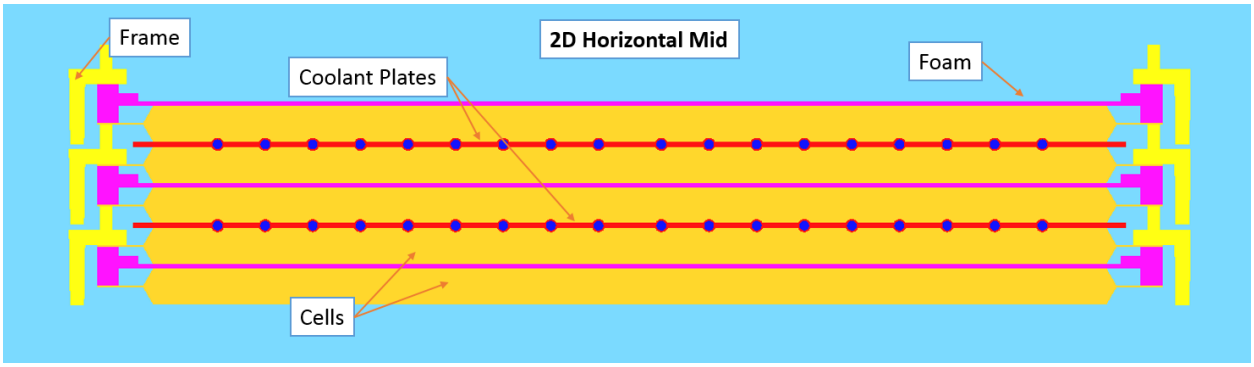

Figure 4-5, Two dimensional cell mid horizontal section non-optimized: used in section 5.2.1

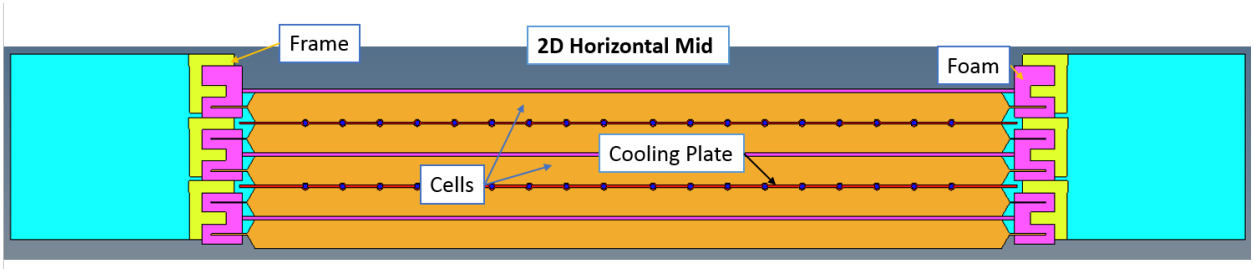

Figure 4-6, Two dimensional cell mid horizontal section optimized: used in section 5.2.2

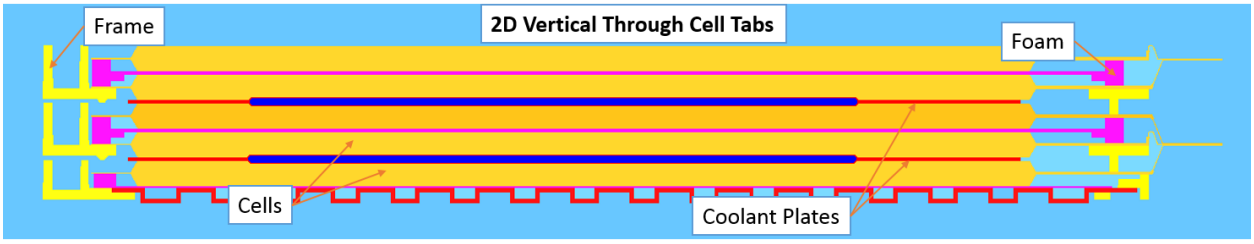

Figure 4-7, 2D cell vertical section with end plate non-optimized: used in section 5.2.1

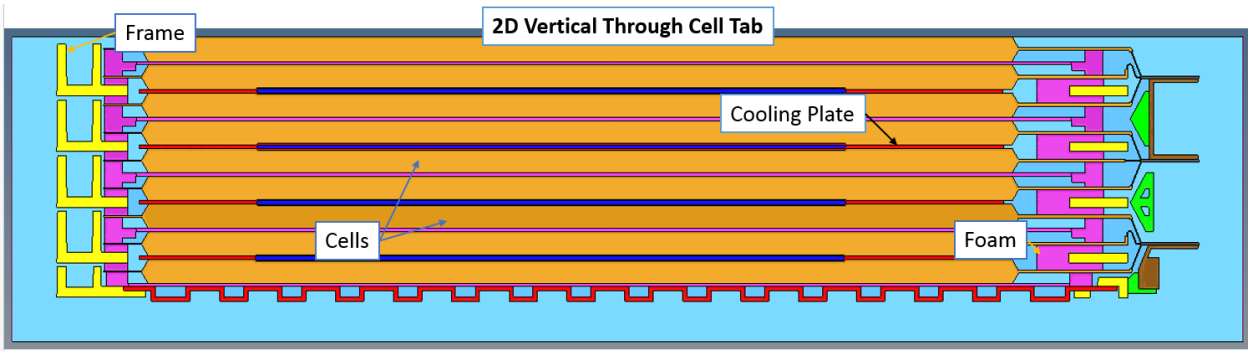

Figure 4-8, 2D cell vertical section with end plate optimized: used in section 5.2.2

Fluids in the mesh are treated differently than solids. Fluid interactions with solid and porous surfaces require a large number of elements to model accurately. For this reason it is good practice to model boundary layers into all fluid volumes. This allows higher fidelity velocity profiles to be created. Using boundary layers also allows more accurate modeling of wall friction at fluid-solid interfaces without adding significant computational weight to the model as the main volume mesh can remain larger. In order to accurately calculate flow, boundary layers should be sized such that they encompass all of the fluid not traveling at free stream velocity. Boundary layer thickness may be tuned by mapping velocity profiles. For a general guide line boundary layer total thickness can be calculated by the following equations.

$$\delta \sim 4.91 \sqrt{\frac{vx}{u_o}} \qquad \text{(Equation 4-1)}$$

For laminar flow and

$$\delta \sim 0.382x/{Re_x}^{1/5} \qquad \text{(Equation 4-2)}$$

for turbulent flow where.

Re_x = Reynold Number and

$$Re_x = \rho u_o x/\mu \qquad \text{(Equation 4-3)}$$

δ = boundary layer recommended thickness

u_o = Free stream velocity

x = Distance downstream from the start of the boundary layer

v = Kinematic viscosity

ρ = Density

μ = Dynamic viscosity

Equations 4-1, and 4-2 were used to calculate optimal boundary layer thickness. The fluid volumes were modeled using the resultant boundary layer thickness in all areas possible. It was necessary to reduce boundary layer thickness in areas where the depth of the fluid volume did not allow sufficient core mesh between boundary layers of the calculated thickness. Hypermesh is able to dynamically calculate where boundary layer reductions are necessary and create the mesh accordingly.

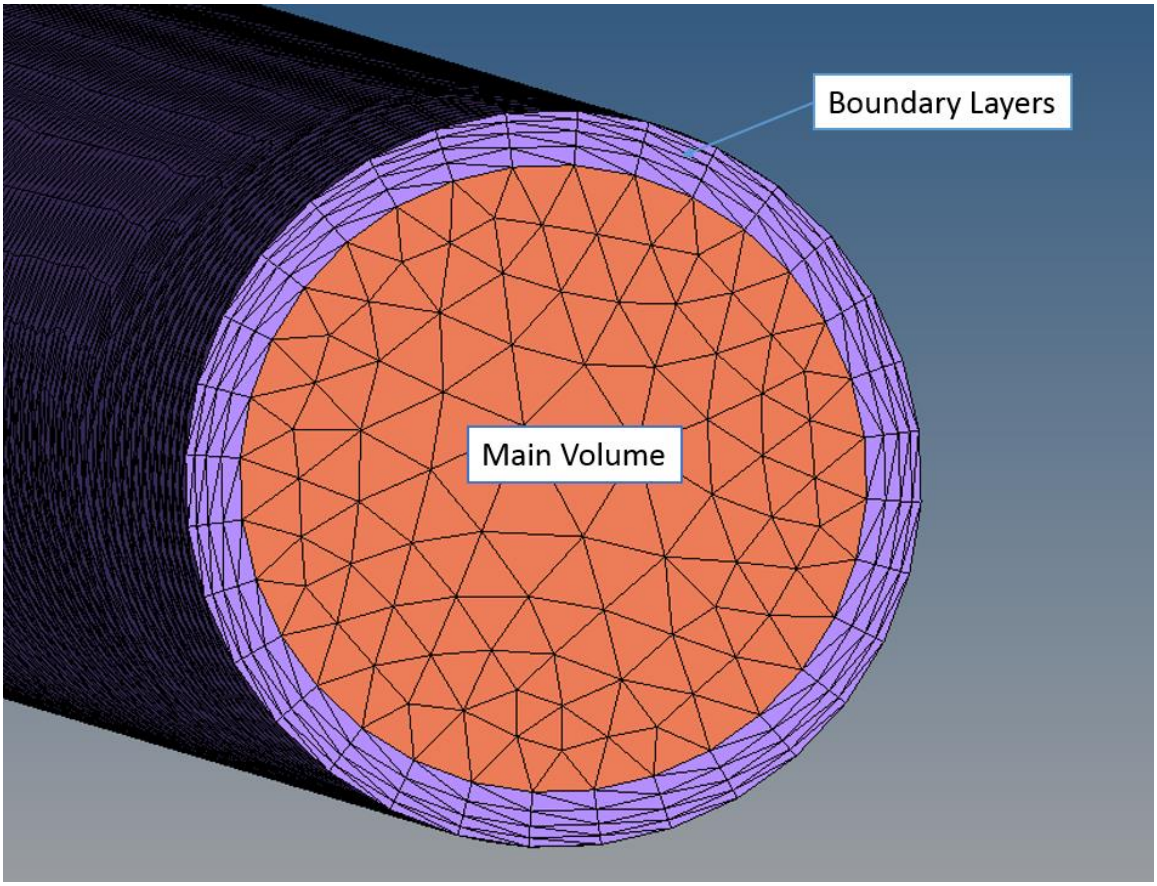

Figure 4-9, Fluid boundary layer and core mesh (exhaust tube)

Once the mesh was set up and checked for consistency, it was imported to the CFD solver to create a solution. Within the solution, materials and interfaces are defined. ANSYS FLUENT

was the CFD solver used for this modeling. The software is quite versatile, allowing the user to select between a number of solution methods and strategies. For this model the energy equation was used with laminar flow. Temperature and internal energies of the components were monitored/recorded and later employed to create properties for the lumped three dimensional battery model.

4.2 Three Dimensional Model

The three dimensional model is also limited in size due to available computing resources. Therefore only a section of the complete ESS was used. Parameters for the cell internals are derived from the two dimensional model. The cell assembly is thus modeled as a solid. The focus of this model is to quantify the effects of construction techniques and material selection on the thermal loads within the pack. Along with the cell module, the fluid volume inside the pack, as well as all attachments and cover housing needs to be modeled. Fasteners are omitted due to their complexity. External to the pack, the fluid volume is equally modeled as a part of the system.

In the fluid volume outside of the ESS, there are surfaces to represent the various heat sources. A surface that represents the underside of the vehicle, components within the engine compartment, the road, and the exhaust system in the case of an EREV. Modeling these heat sources allows data to be collected that will uncover how large a cooling system is necessary in order to maintain safe cell temperatures in extreme conditions. This should also lead to a potential for downsizing the cooling system components in conjunction with improved thermal isolation of the cells from ambient.

Throughout the CAD model development, the three dimensional version underwent many iterations both to improve quality, and to enable a solution to run in CFD. The model began with a full three dimensional representation of the same production pack used for the two dimensional model. This included the vehicle environment in which the pack is placed. The initial step was to repackage the pack internals to increase the thermal insulation of the cell modules within.

For this the cell assemblies were left untouched. The exterior of the pack and the module attachments were redesigned. The original design made use of a structural steel base plate upon which the cell modules were clamped. Both the base plate and the clamping mechanism were metallic. The stock cover is a relatively thin molded reinforced plastic. It functions as a protective cover and not a structural member of the ESS. The stock configuration, as well as a better thermally insulating initial design concept, can be seen in Figure 4-10 and Figure 4-11 respectively. Both the base plate and the pack cover underwent a material change. Employing the learnings from building the EcoCAR pack, the bottom plate was redesigned using a similar glass reinforced composite.

The cell modules in the redesign are retained by composite rails with end caps to prevent the modules from sliding fore-aft. The rails are grooved to accept the lower portion of the cell module. Once placed, the battery module with rails is lowered onto the insulated bottom plate and rigidly fastened. In this construction no metal fasteners transgress both internal and external boundaries. This serves to better thermally and electrically isolate the pack internals.

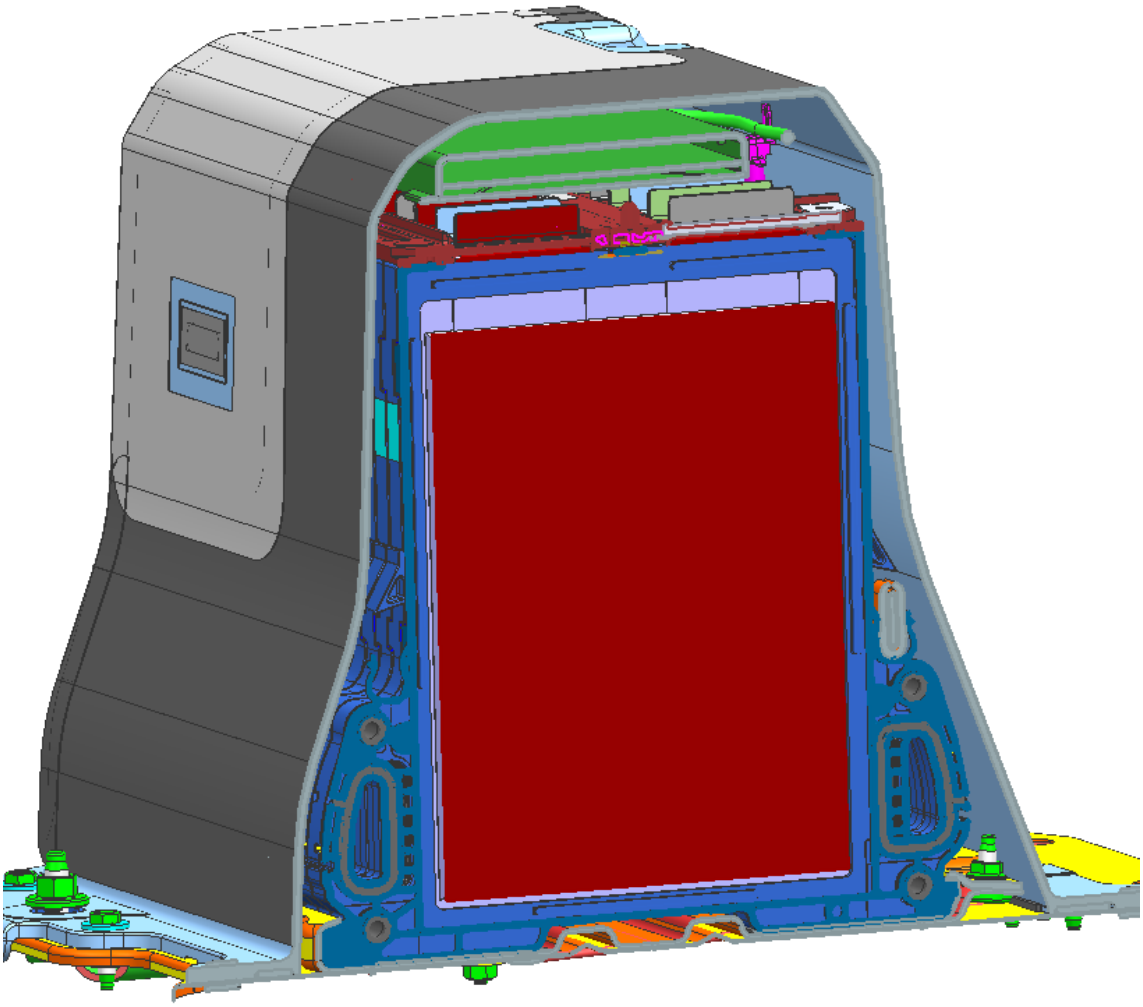

Figure 4-10, Stock pack structure and module mounting

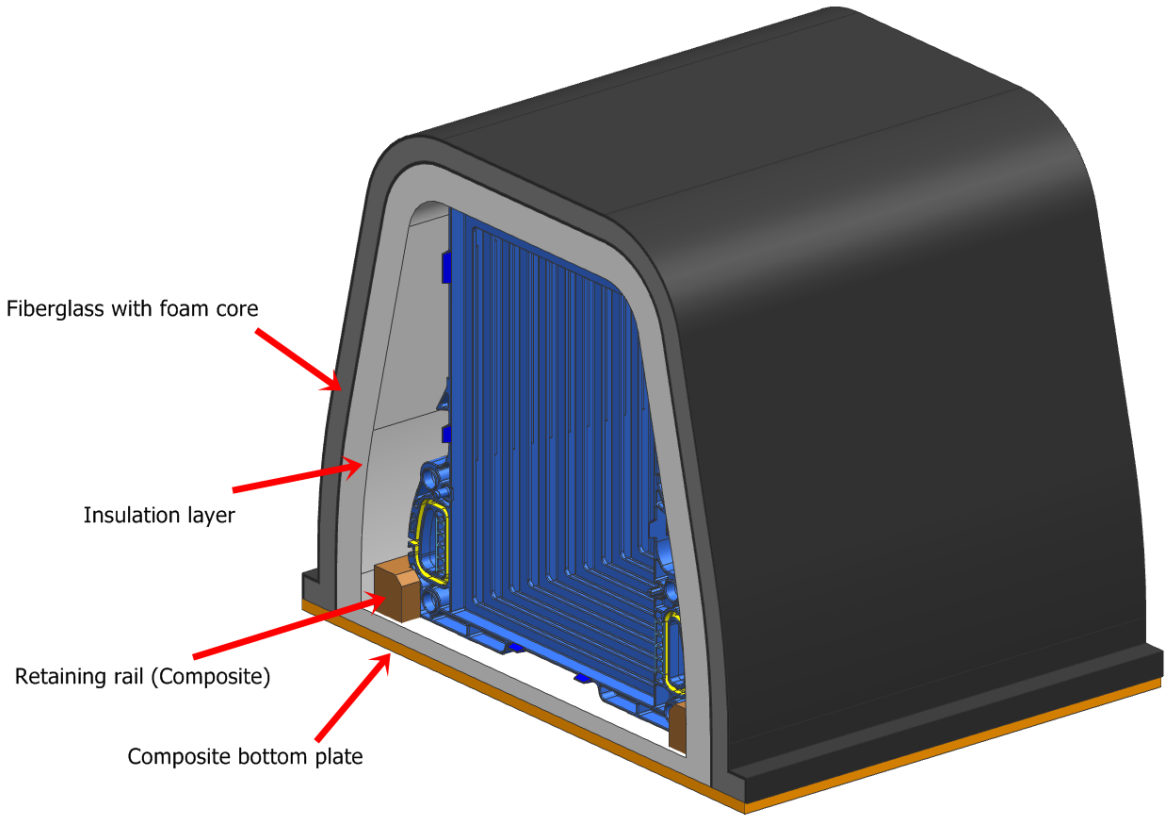

Figure 4-11, New construction proposed with retrofit module

The interior of the redesigned pack is lined with Cryogel® Z Aerogel insulation on all surfaces able to be lined with insulation. Only the module attachment rails, high voltage pos/neg leads, and coolant inlet/outlet are not insulated. Both 5 mm, and 10 mm insulation thicknesses were modeled. The exterior of the pack underwent design iterations. Both foam core fiberglass and sheet molding compound constructions were investigated. In order to better match the physical tests, it was decided to use the sheet molding compound (SMC) for the simulations (Figure 4-13 shows final design).

Once the packaging has been constrained to fit within the available physical space of the stock chassis the model needed to be simplified in order to mesh for thermal analysis. The model was first reduced so that only the forward portion of the ESS was being modeled. The forward portion is selected so that airflow can be better simulated. This allows for heat source effects such as the radiator, IC engine, and exhaust system to be simulated.

Beginning with the trimmed portion of the ESS, and corresponding vehicle sheet metal, a simplified version of the model was created with the bottom side insulation switched to be underneath the base plate as opposed to the original proposal where it was placed within the casing. Figure 4-11 shows the module prior to this modification, where there would now be no insulation between the module and the base plate but with the retaining rails still present. Since the main concern is modeling heat transfer, and not airflow, complex shapes were simplified into geometry that can be meshed more consistently. The cell assembly was thus modeled as a single solid with variable properties over time. Air within the pack, insulation, cover, base plate, and mounting rails were included. An exterior volume of air was also created using the underside of the vehicle, and road surface as bounds. A void was placed within this air to represent the under hood components, and the exhaust pipe coming from the engine compartment. Inlets were created to represent the airflow entering through the radiator and the free stream airflow under the vehicle. The various external surfaces were modeled at their representative temperatures.

Figure 4-12 and Figure 4-13 show the final iteration of the fully insulated model prior to the meshing process. Here we see some differences from the initial CAD of the production model (Figure 4-10) and the initial insulated concept (Figure 4-11). Mainly the geometry is simplified from the production CAD due to computational limitations. The foam core fiberglass in the proposed retrofit is replaced with a molded SMC fiberglass cover and the retaining rails have been altered. The primary reason for the change in the cover design is space constraint. 10 mm of insulation along with the foam core fiberglass cover did not leave an appropriate amount of space for manufacturing tolerances and requisite clearance to the chassis. To ensure that there is no rubbing or chaffing of the cover against the underside of the chassis or with the internal insulation of the cell module, a simple molded cover was used in the final model. The alteration on the module retention strategy was done to provide additional stability and mounting surface area between the cell module and baseplate. Currently these are separate parts, but the cell retention frames could be molded in such a way that the retention rail would be integrated into the frames.

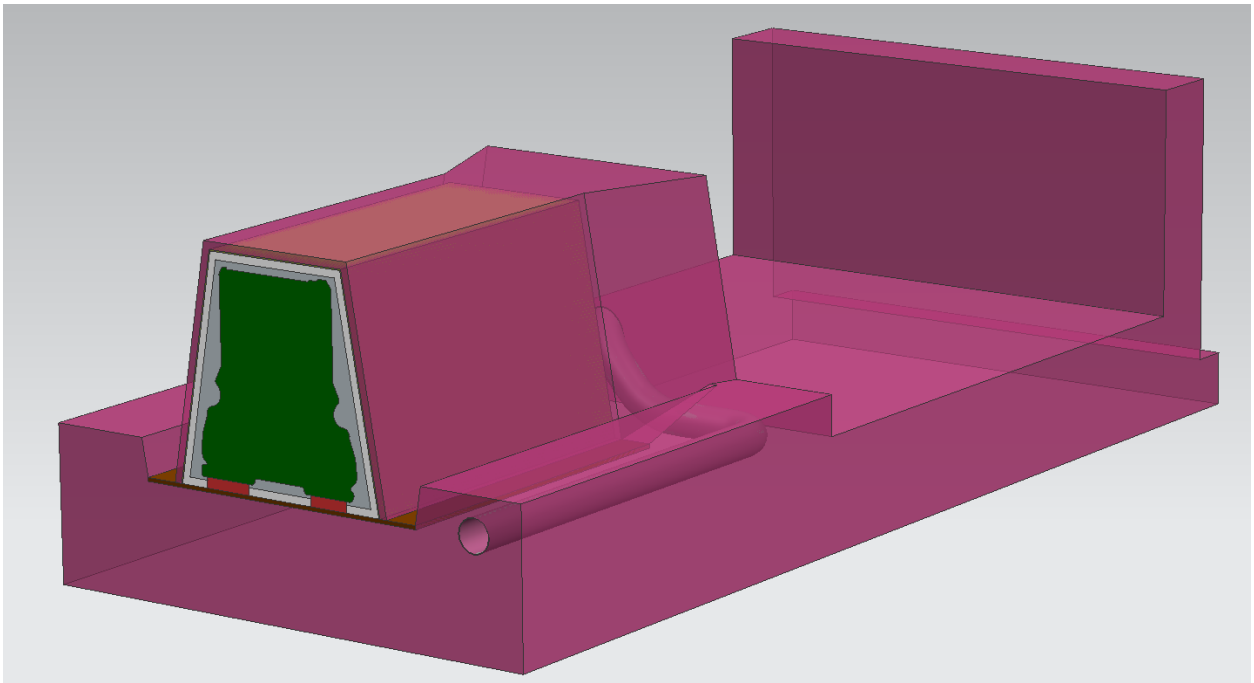

Figure 4-12, Final model (fully insulated) prior to meshing

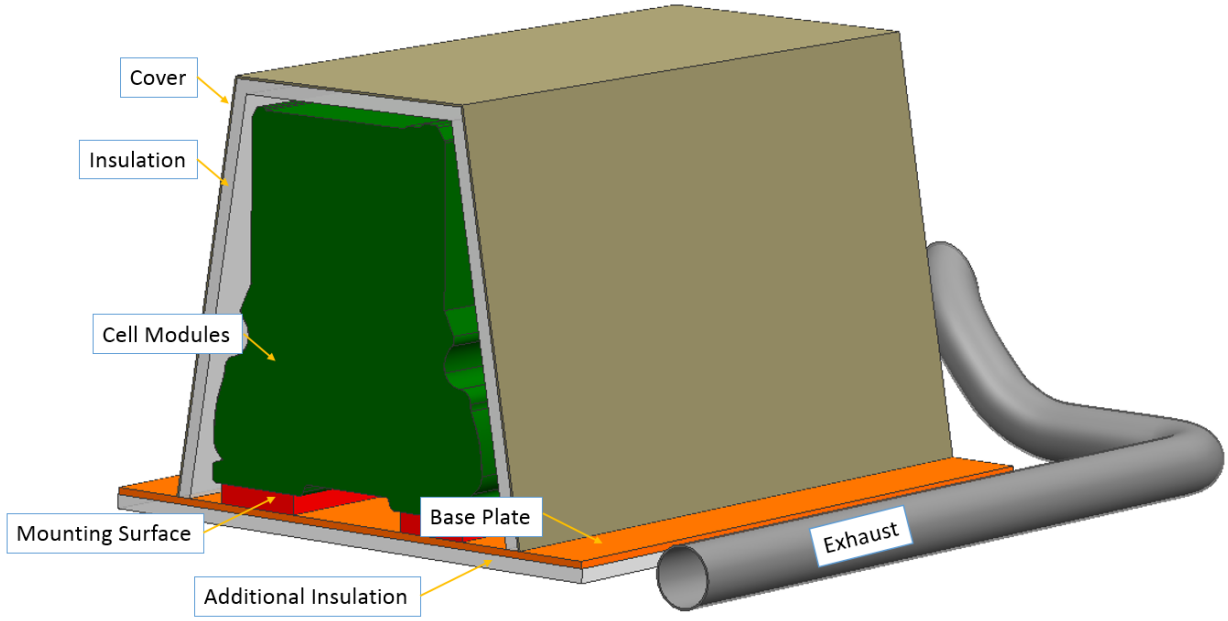

Figure 4-13, Final model (fully insulated) prior to meshing with fluid volumes removed

Meshing the model proved to be difficult. In order to create a stable solution in the CFD solver the mesh must meet certain quality standards. A model with inferior quality mesh will lead to unstable results when a solution is computed. Many iterations of meshing and model simplification were required to build a model capable of producing stable results.

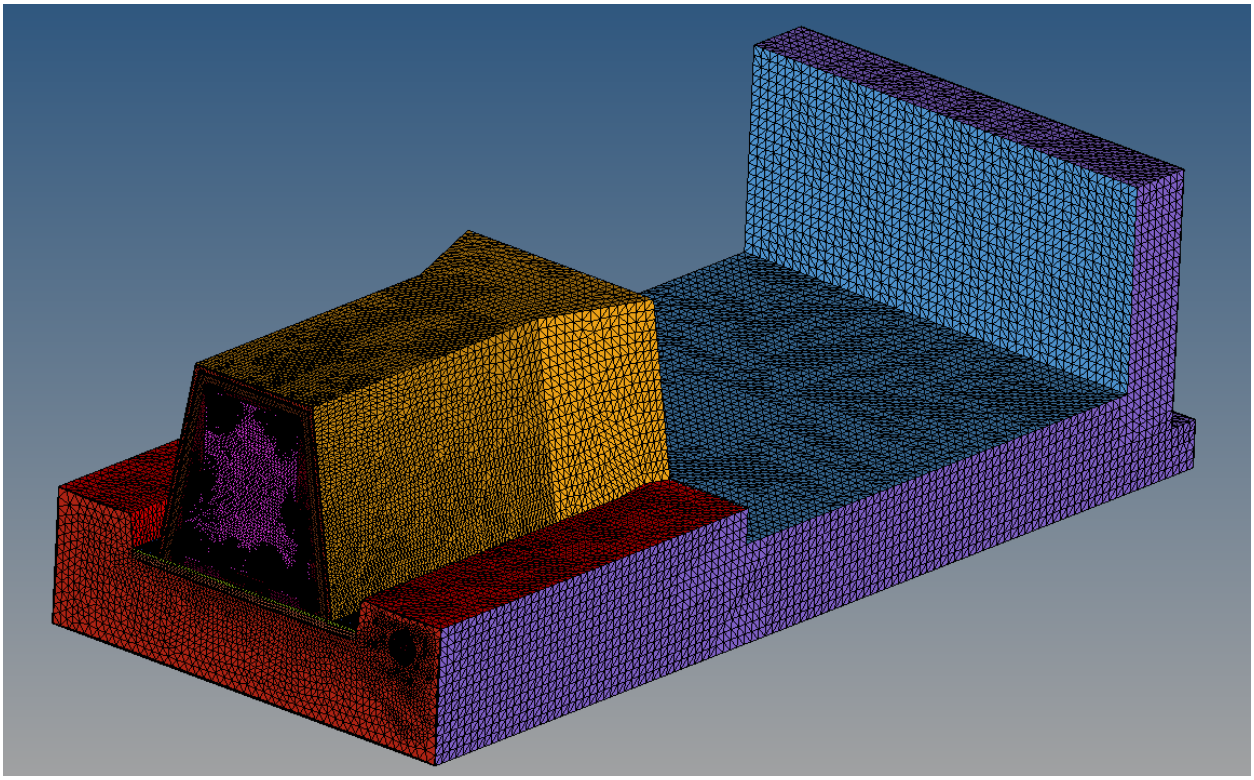

Figure 4-14, Completed model meshed (fully insulated version)

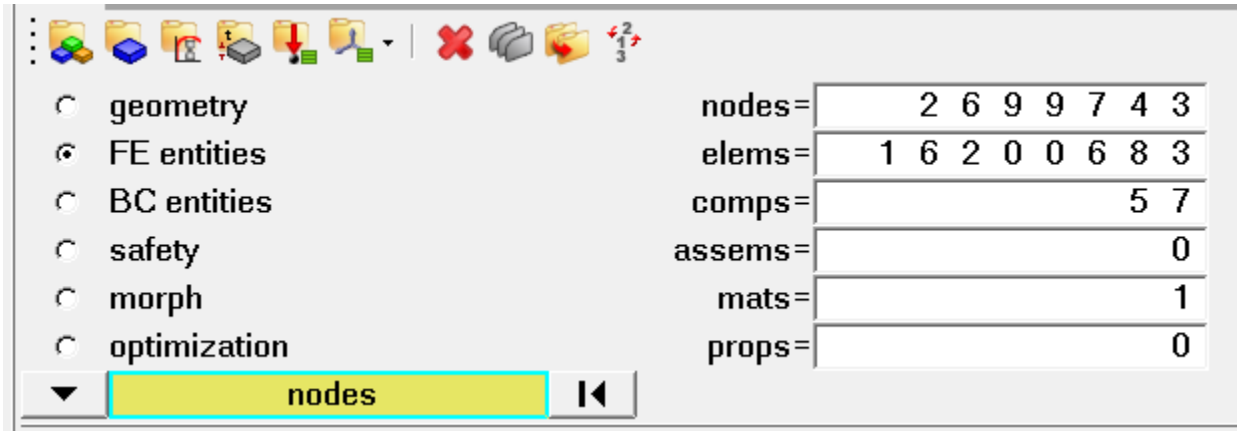

Figure 4-15, Completed mesh element information

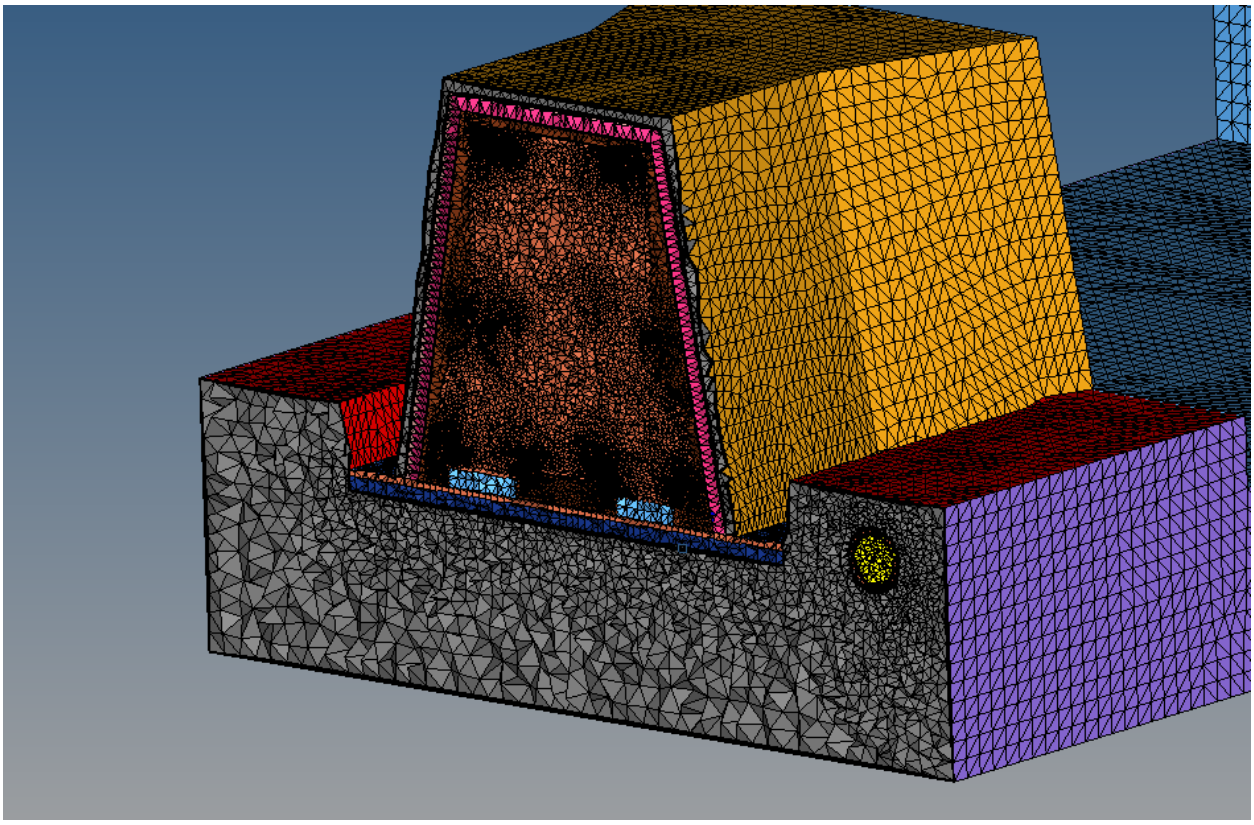

Figure 4-16, Cutaway showing 3D tetrahedral elements

Figure 4-14 - Figure 4-16 show some mesh information for the final model used in simulations. Including component interfaces, the final model contains over sixteen million finite elements. In order to properly define boundaries between components two dimensional interface meshes were created. The two dimensional interface and each of the three dimensional components do share common nodes at the interface. This allows each of the components within the model to be easily coupled to one another. Solid components use a tetrahedral mesh connected to a triangular two dimensional interface. Fluid meshes are similar with the exception that the boundary layers are designed to better model flow around these boundaries.

4.3 CFD Solution

Setting up the CFD simulation properly is critical to obtaining accurate results. The mesh input must be of an appropriate quality or the solution will be unstable, yielding inaccurate results. Once the mesh has been sufficiently refined, and interface nodes connected, the solution can be defined.

Each of the two dimensional meshes were imported separately to create the FLUENT solution. A solver method must be selected, and the default pressure based solver was used. This method remained for all cases. The density based solution is typically used for high-speed compressible flows. For purposes of these models, the pressure based solver more accurately estimates the flows. Even modeling the flow while a vehicle is moving at speed would be considered "low-speed". Therefore the pressure based solver where pressure is obtained through a correction function based on continuity and momentum is applied. Gasses within the model are considered incompressible. As the model's purpose is to measure heat transfer in an open environment there is no need to consider the compressibility. Within this solver, the coupled algorithm is used. Pressure and velocity can be calculated in a segregated or coupled scheme [44]. Since these models are assuming a steady state incompressible flow, the coupling of momentum and pressure yields results more efficiently.

The two dimensional models focus on heat transfer within the cell module. The entirety of the model only considers components local to the inside of the ESS. For this case all flow is considered to be laminar and at atmospheric pressure. The battery is in a semi sealed environment where air is allowed to enter and exit through small vents. There is no forced air current, and pressure is able to stabilize to ambient. Therefore the velocity of the fluid within the model is minimal (< 0.5 m/s). The intent of the two dimensional models is to evaluate how the subsystems within a cell module interact thermally and to develop equivalent thermal properties to be used in the three dimensional macro model. Therefore for simplification it was assumed that the coolant within the plates remains at a constant 20 °C when cooling is active.

Boundaries between components may be modeled either with unique properties derived from their neighboring components, or they can be treated as coupled. Coupled boundaries are used where both sides of the boundary are connected to a solid. This allows the heat to transfer between components based on the material properties of the connected solids. Where a solid component interfaces with a fluid volume, the interface was defined using a heat flux. Heat from the solid is being released into the surrounding volume as a function of the exposed surface area.

The three dimensional model or the macro model in this case is aimed at predicting the influence of the ambient environment on the cell module. Similar to the two dimensional model, walls between solids are coupled, while walls interfacing to fluid volumes transfer heat at a given rate. This model contains three independently flowing fluid volumes: the outer volume represents ambient, the inner volume represents air convection within the ESS, and an exhaust volume exists that flows when the IC engine is running. The model is setup such that it considers the airflow under the vehicle. Including a representation of the exhaust and portions of the vehicle allow a broader scope of scenarios to be modeled. It can be ran with the vehicle propelled in EV mode, powered with the IC engine running, and in combination.

To model the heat transfer while the vehicle is moving, flow needs to be represented. The airflow around a moving vehicle is more complex than that which was modeled for the pack internals. For this effect turbulence was introduced into the solution; it allows a more accurate development of flow around the ESS and underbody components. While flow velocity impacts heat transfer, it is not the primary concern of the model. Therefore a relatively simple turbulence model was selected. More accurate flow around the underside of the vehicle allows for prediction of heat loads on the ESS that would require extensive instrumentation and testing to reproduce in the real world. Adding value to the model developed is the ability to easily alter the materials and geometry thus arriving at an optimized design much sooner.

Chapter 5. Results

Results were first collected from live thermal chamber testing. Here production packs were outfitted with thermocouples and soaked from ambient to 50 °C. The packs were configured with and without insulating material. The thickness of the insulating material when fitted was also varied. Temperature data was recorded and used as a baseline for later computer simulations. Packs were then modeled using CAD software. A simplified version was finally used to create a thermal model which included a portion of the pack and underbody vehicle components. The ESS module internals were modeled separately in a two dimensional model and CFD results were fed into the larger three dimensional model. Different scenarios were then ran, with variance in insulation, vehicle speed, and IC engine operation. The final result is a model able to predict the effects of pack construction choices on the thermal management system power requirements.

5.1 Thermal Chamber Data

Two production battery packs were heat soaked to an initial 30 °C temperature differential and placed inside a large thermal chamber (see Figure 3-9). One pack contained all the ESS battery modules and the other was an empty shell. The packs were instrumented with thermocouples to record the transient temperature change as they soaked. The process was then repeated where a 5 mm thick layer aerogel blanket was added to the inside of the pack cover and bottom (see Appendix B for Aerogel Specifications). For the final run, the 5 mm thick layer was removed from the inside of the cover and a 10 mm thick wrap of Aerogel was added to the outside covering the entire pack.

Data was collected on the outside of the cover, inside of the insulation and cover, on the outsides of the cell modules, on the baseplate, in the open air with the pack, and on the (dormant) power electronics. Without access to the harnessing and pack controls, exercising the pack and turning on the power electronics was not a possibility. Assumptions for heating within the modules were assumed in later thermal models. Additional work currently being

conducted by other MASc students includes exercising the pack while soaking at temperature and providing coolant to the cell modules. Such data will help to tune and validate results derived from the computer simulations.

Initial testing was conducted on the uninsulated pack in order to create a baseline. The metric used to measure the response of the system is its thermal time constant. The primary goal is to slow the system's response to ambient conditions. The thermal time constant in a lumped system model where a solid is being referred to is assumed to have uniform temperature distribution and can be calculated using:

$$\tau = \rho V c / hA. \qquad \text{(Equation 5-1)}$$

Where:

τ = thermal time constant (s)

ρ = density (kg/m$^{3)}$

V = the volume (m$^{3)}$

c = the specific heat (J/kg K)

h = material heat transfer coefficient (W/m^2 K)

A = surface area (m^2)

The thermal time constant can also be found by plotting the temperature change over a period of time. As the temperature reaches its asymptotic equilibrium value, the rate of heat transfer slows to approach zero. The time constant is meant to represent the nominal system reaction time to a heat input. One portion of interest is the steady state. More generically the time constant is $1 - \frac{1}{e} \cong 63.2\%$ of the asymptotic value. This method should only be used when the Biot number is sufficiently small as it implicitly assumes no temperature gradient within the solid. A complete pack will have many different time constants for the various components, however any component that has sufficient thermal conductivity relative to the surface heat transfer rate can be considered a "lump" given its Biot number is less than 0.1. In this case we are not concerned about the temperature gradients within components. The purpose of the testing is to define and minimize thermal load upon the cells.

The ESSs within the thermal chamber were outfitted with thermocouples. Each pack received thirteen thermocouples distributed on the outer cover, inside of the cover, in the pack's internal volume and on the cell modules (See Appendix A for locations). The packs were soaked at a ~30 °C ΔT from ambient and the system response time was calculated by plotting the readings received from the thermocouples over time.

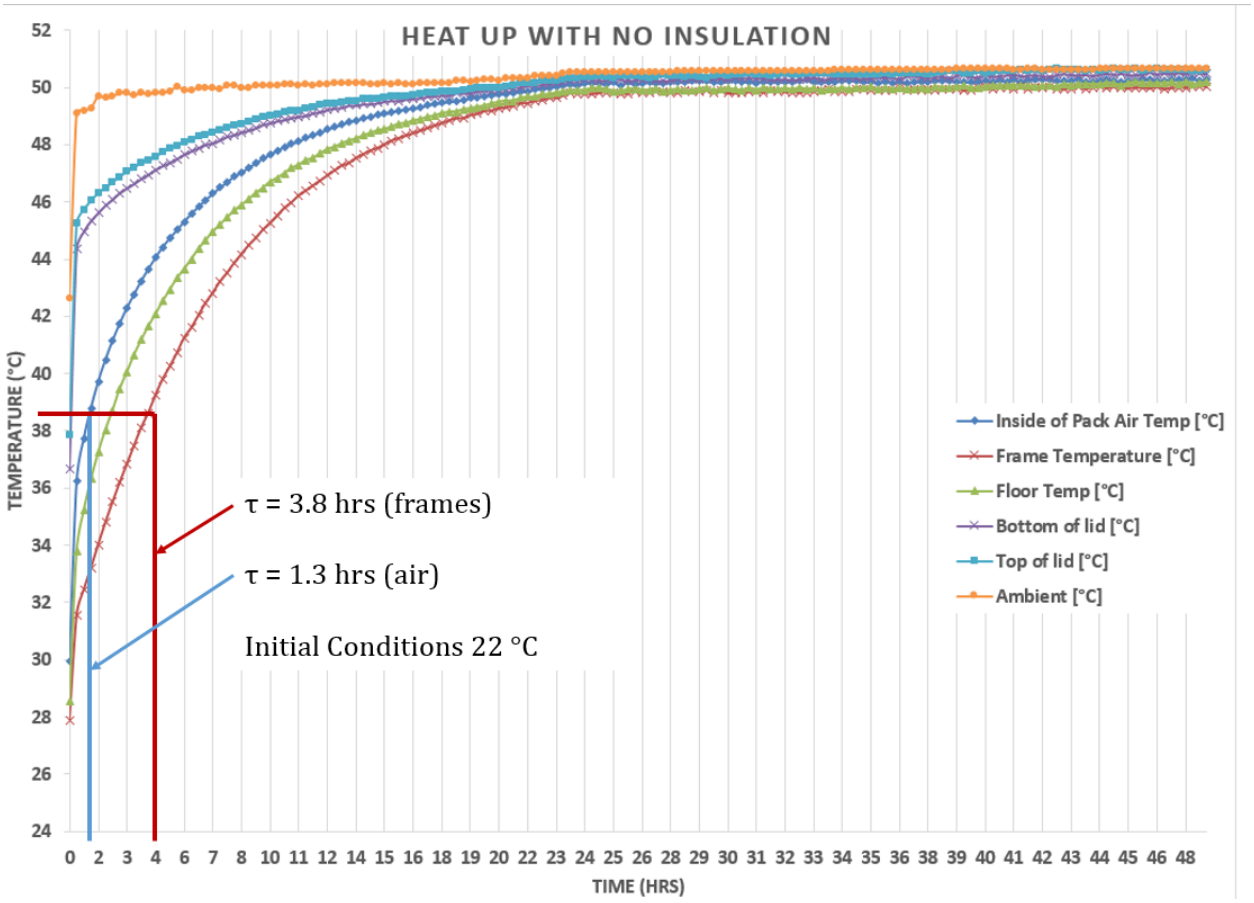

Figure 5-1, Temperature response: Stock pack (no insulation)

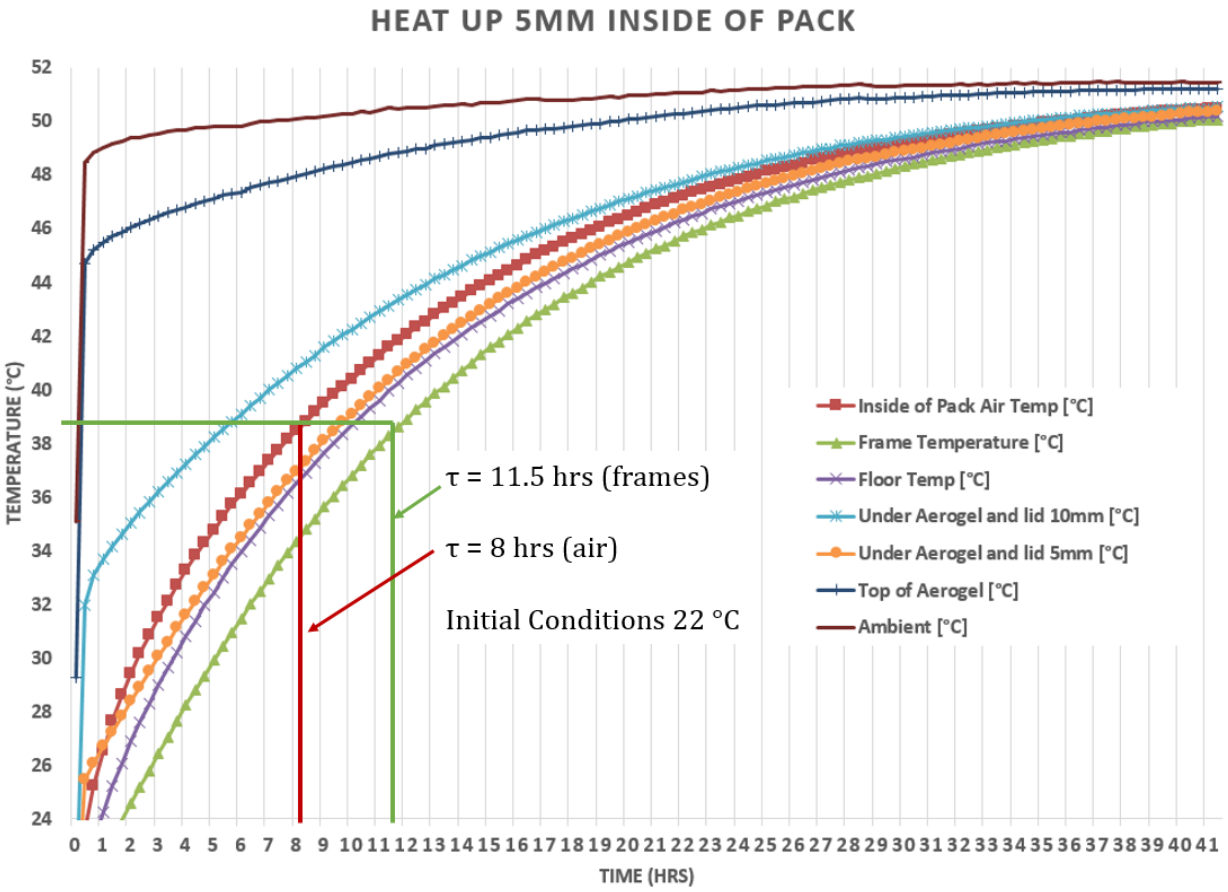

Figure 5-2, Temperature response: 5 mm insulation inside cover

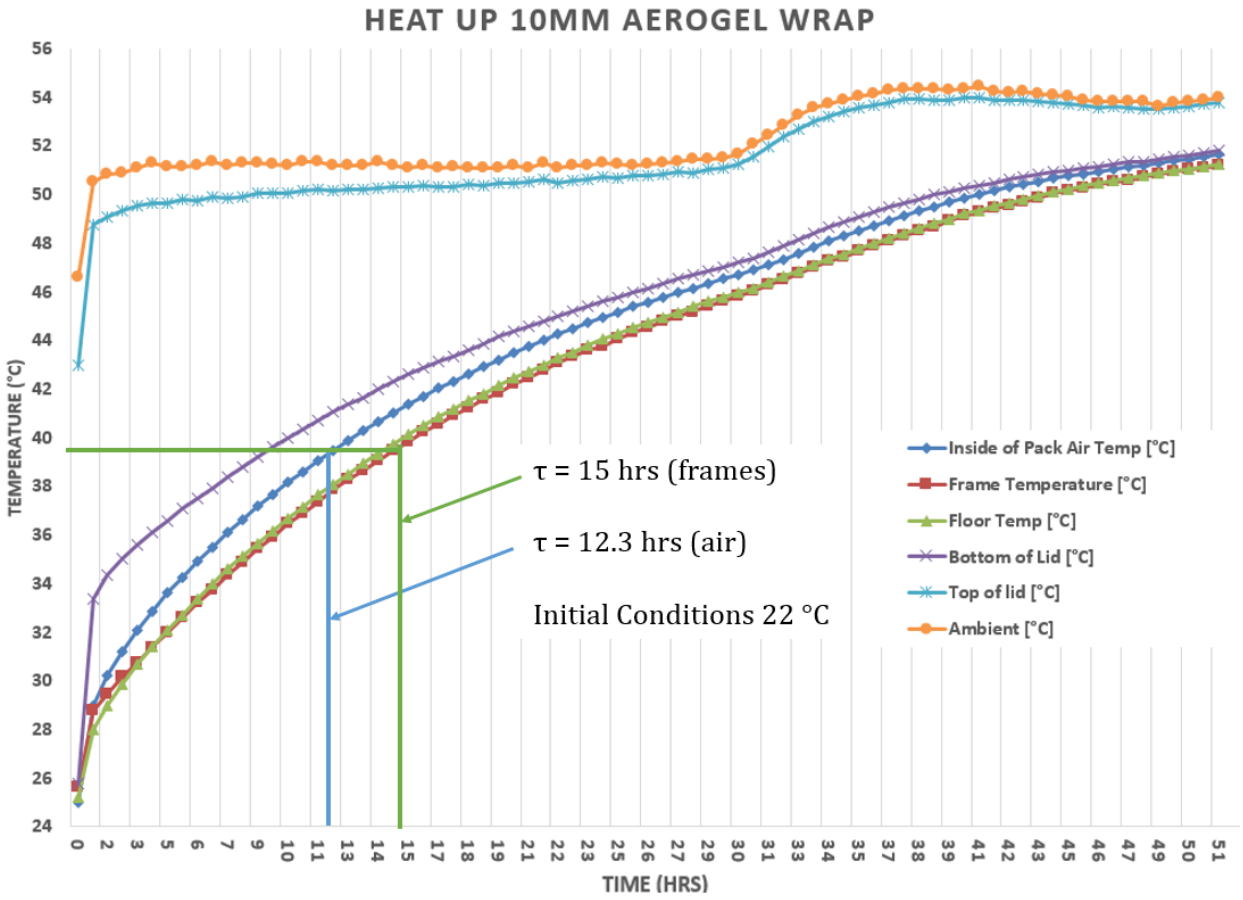

Figure 5-3, Temperature response: 10 mm insulation wrap

The images above represent the data for the three different scenarios tested on the pack which contained cell modules. Figure 5-1 being the baseline with no added insulation. This showed that with no additional heat sources the cell frames would soak to 63% of the ΔT exposure within four hours. The air volume within the pack soaked equivalently in 1.3 hours. Knowing the heat transfer coefficients for the pack cover, baseplate, and the total surface area one can calculate the rate of heat transfer. Using Newton's law of cooling the rate of heat transfer can be calculated using:

$$\dot{Q}(t) = hA_s[T(t) - T_\infty] \qquad \text{(Equation 5-2)}$$

Where,

$\dot{Q}(t)$ = rate of heat transfer (W)

h = heat transfer coefficient (W/m^2 °K)

A_s = surface area (m^2)

$[T(t) - T_\infty]$ = temperature change (°K)

Solving for rate of heat transfer yields a rate of ~650 W for the uninsulated pack. Figure 3-1 shows that the same pack while being exercised by performing a US06 drive cycle where it generates an additional 600 W of heat on average, with peaks of over 1000 W. In order to maintain a constant temperature, the cooling system must thus be able to remove a total of 1.7 kW of heat from the ESS. This is ignoring additional external heat sources such as the exhaust system or IC engine's wash of heated air over the battery pack for the case of charge sustaining vehicle operation. Figure 2-23**Error! Reference source not found.** shows a temperature profile where the IC engine is running. Temperature sources of 800 °C can be seen near the pack's outer surface closest to the exhaust system which adds significant additional loads to the system.

The addition of 5 mm insulation to the pack increased the time constant for the air within the cover to 8 hours, and the cell module frames to 11.5 hours (see Figure 5-2). This represents over 500% slowing of the pack's thermal response. Applying the same equation, the rate of peak heat transfer is reduced to 104 W from the ambient environment. Removing the 5 mm of insulation placed internal to the cover and wrapping it externally with a 10 mm thickness blanket of insulation surrounding the pack, the time constants were increased again to 12.3 hours for the air volume and 15 hours for the cell modules (see Figure 5-3). This represents an almost 850% improvement from the baseline condition, and a 50% improvement from the 5 mm thick insulation case. In Figure 5-3 there is a point roughly 30 hours into the experiment where the thermal chamber temperature control wanders from the set point. This causes a slight error in the results reported, however the effect is minimal as the bulk of the temperature rise had already occurred at this point. As later the introductory discussion already showed, response beyond 24 hours has little significance in practice.

Considering an EV only operating mode, in a 50 °C ambient extreme (example Arizona) such alterations if implemented in a practical way would reduce the peak cooling requirements

to just over 1 kW. This represents a ~ 1/3 reduction in peak heat load, opening the possibilities of considering alternative and possibly more efficient cooling systems. One may consider that during a US06 drive cycle heat is generated internally at an average of 600 W and only 50 W additional would be added from ambient using an insulated pack. This would bring the nominal cooling requirement down to 650 W for a US06 cycle and lower if "normal" driving is considered. For regular driving conditions the heat generation rate would more likely be in the range of 500 W. Thus reducing the nominal parasitic loss from maintaining ESS temperature from ~ 1150 W nominal and 1650 W peak down to 550 W nominal and 1050 W peak. Such changes represent a considerable design influence in battery thermal management particularly if coupled with other peak load shaving techniques, for example using PCM's as described earlier.

5.2 CFD Modeling: Two Dimensional Models

The three models simulated were cross sections taken at different heights and orientations through a section of five cells with frames, cooling plates, foam separators, and an end plate. The purpose was to develop bulk properties to be used in the pack level three dimensional model. The rate at which heat is gained and rejected is the primary concern. Other thermal properties were also developed using this model, such as a weighted heat capacity, surface heat flux, and thermal resistance for the module assembly. These properties were then used to define the lumped mass which represents the cell module at the pack level model.

Each of the three models was ran in an environment with conditioned air in free convection transferring heat to the modules. Inlet temperature of the air (T_{air}) was 50 °C for all "tests", then as the air passed over the module heat was transferred into the module through free convection. All internal components were initialized to T_{nom} of 20 °C. All models were ran with and without liquid cooling active. The amount of heat added or rejected from the cell module was measured through the change in internal energy within the components, and the surface heat flux. The system response was measured by collecting temperature data internal to the cell modules.

5.2.1 Stock Configuration

Initial runs utilized the module in its stock configuration. Sections consisted of a subset of five individual cells along with structural frames, cooling plates, and foam separators. The first of the three models ran was oriented along the vertical axis of the cells. It was the only one amongst the three models to include the cell tabs and the module end plate. Figure 5-4 depicts where the surface heat flux and temperature was measured at locations where solids interface to the ambient air. Volume averaged internal energy was also measured for each component. All measurements were taken at each time step as the model reached an equilibrium temperature.

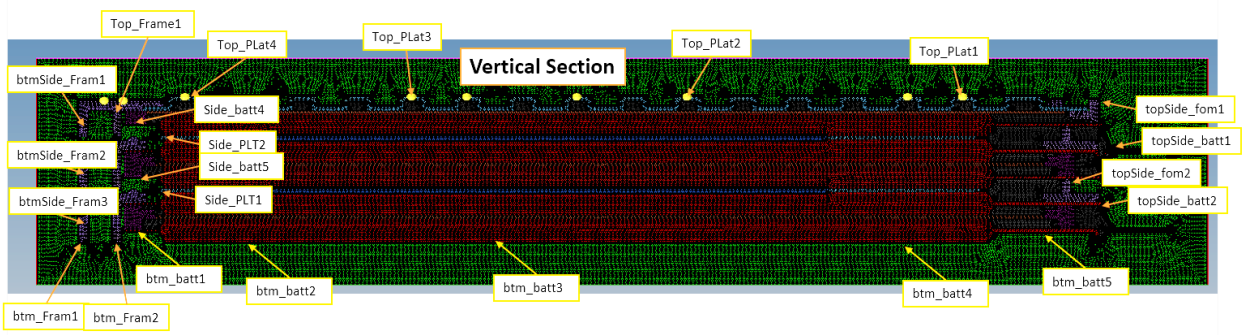

Figure 5-4, Heat flux measurement locations

Figure 5-5 through Figure 5-7 show temperature profiles of the module with coolant running. The coolant system is able to maintain T_{nom} through the bulk of the cell volume. The last cell in the group was not modeled with its coolant plate. This cell stabilized with 13 °C higher temperature than the cells that were cooled, demonstrating the effectiveness of liquid thermal management. The findings through this portion of testing were consistent with expectations. The change in internal energy, along with surface heat fluxes were also being measured during the same subtest. Figure 5-8 through Figure 5-7 show the contours of internal energy of the cooled section at temperature equilibrium.

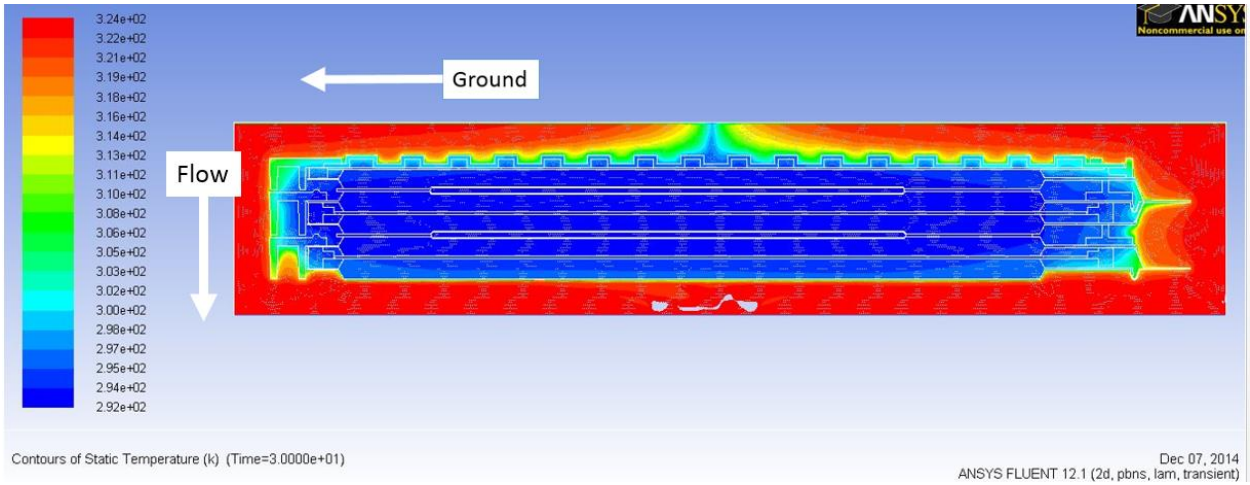

Figure 5-5, Temperature contours: Beginning of test, cooled (flow developing)

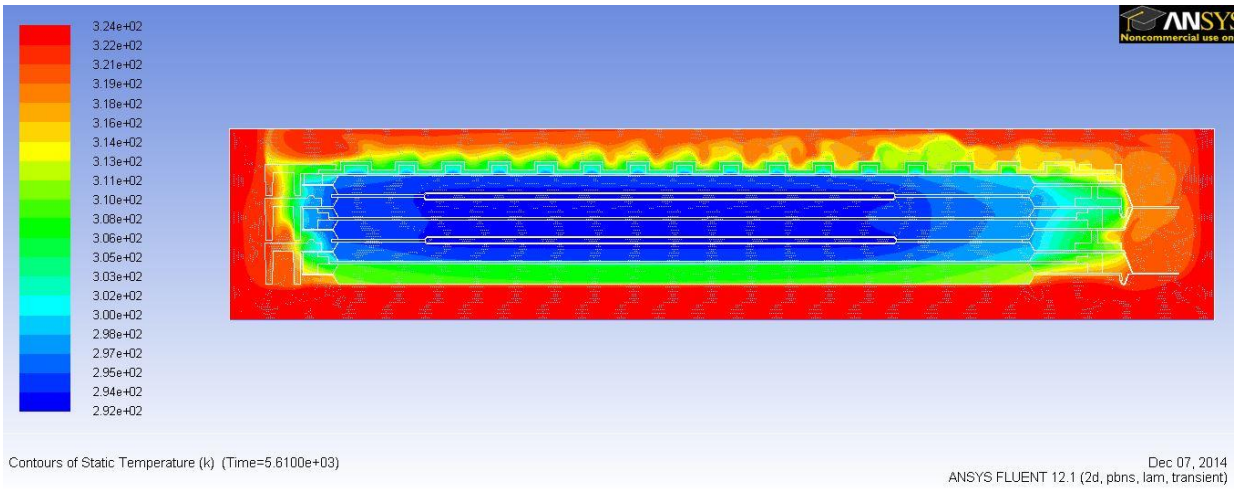

Figure 5-6, Temperature contours: 1.5 hours into test, cooled

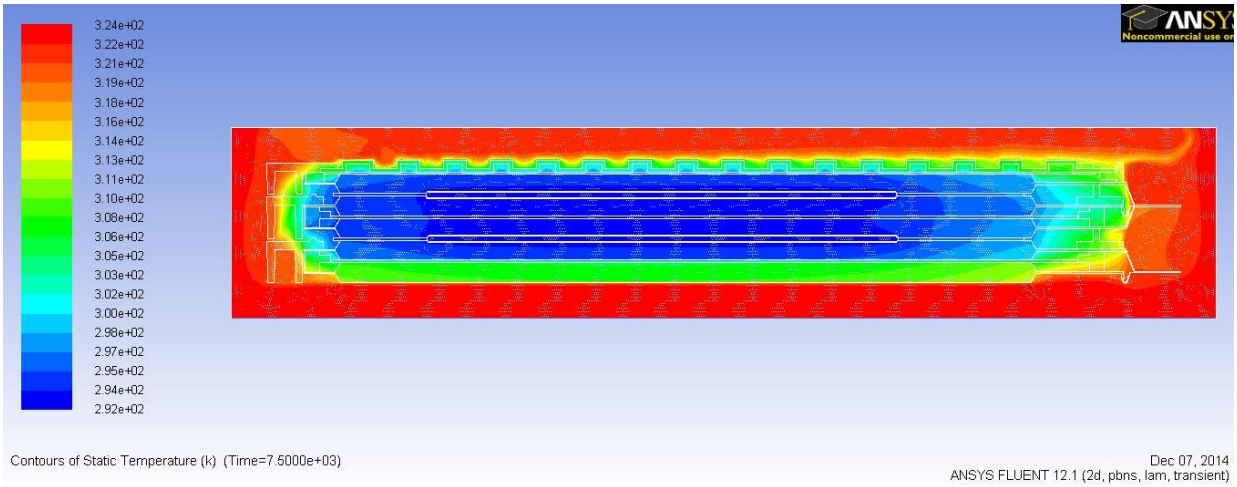

Figure 5-7, Temperature contours: end of test, cooled (2.1 hours)

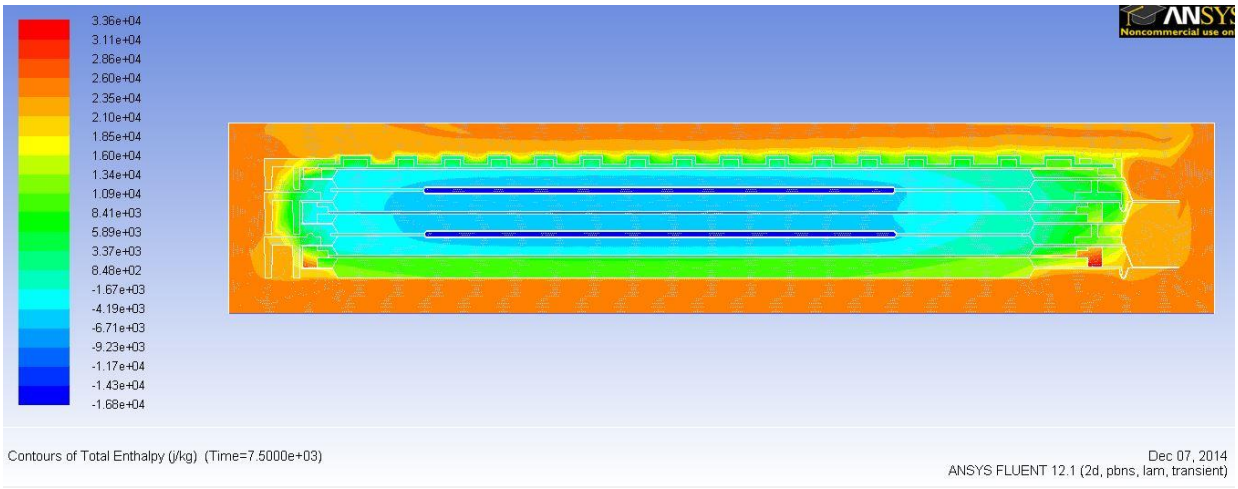

Figure 5-8, Internal energy contours: end of test (2.1 hours)

The "test" was repeated with no cooling active while the same properties were measured. Figure 5-9 shows the temperature contours 30 minutes into testing and Figure 5-10 shows the contours of internal energy after one hour. As expected the cells heat more quickly and eventually reach equilibrium with ambient conditions. By completing both simulations with all three sections the rate at which the battery module absorbs energy as a whole can be estimated. This also demonstrates the amount of heat energy that a constant temperature coolant must be able to reject in order to maintain a given temperature delta to the air inside the pack.

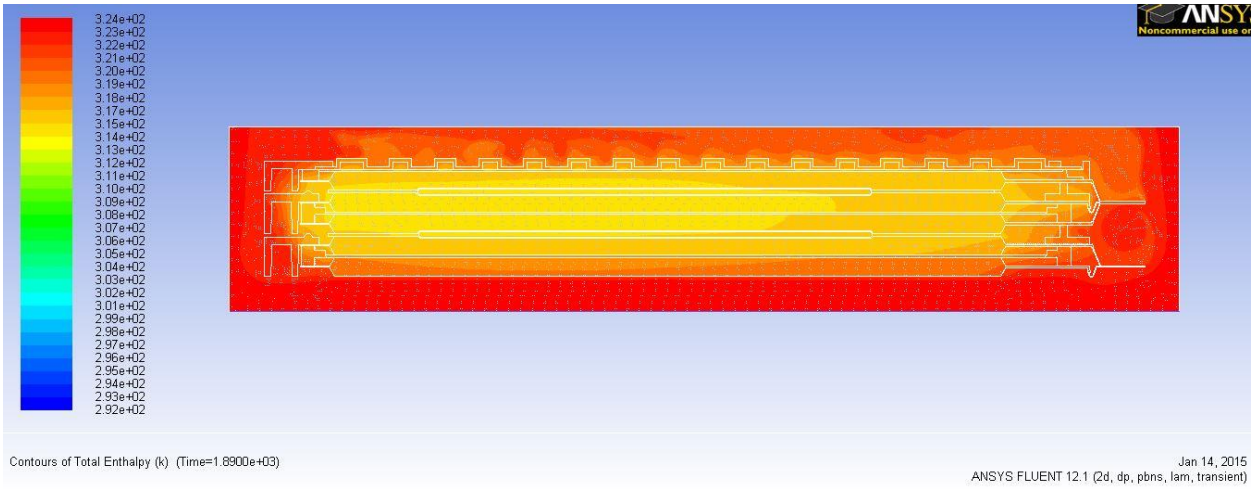

Figure 5-9, Uncooled temperature contours: 30 minutes into test

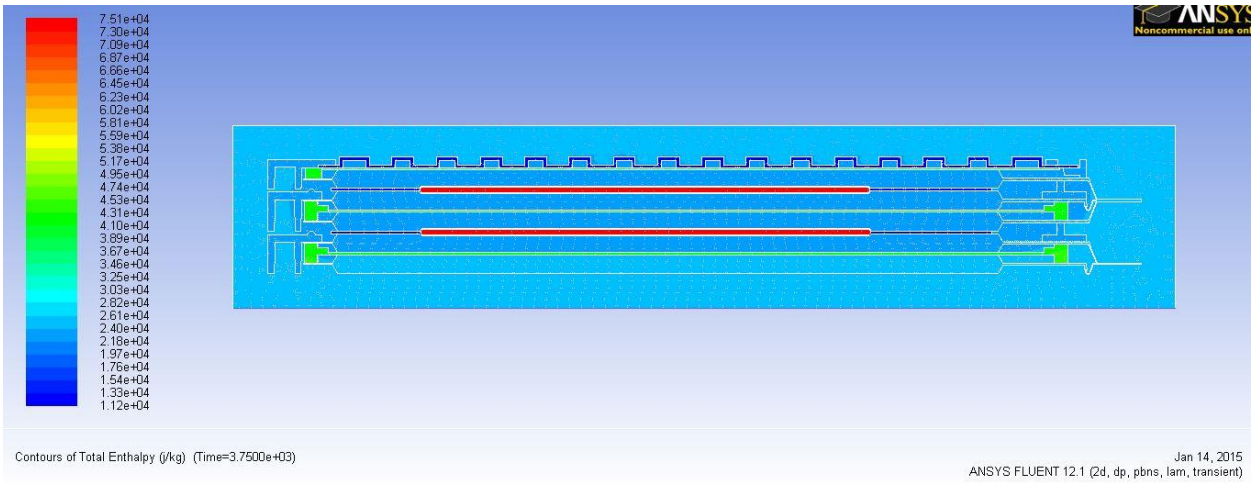

Figure 5-10, Uncooled internal energy contours: ~1 hour into test

Figure 5-11, and fFigure 5-12 show the surface heat flux for the horizontal section 2/3 of the way up the module. Heat flux is shown in both figures. The sign of the values is dependent on which volume the measurement is associated with. The figures show the rate that heat is flowing into each component from ambient in a cross-section. Heat fluxes for each of the other two cross-sections were also analyzed and the results of all three sections were compared. A combined property was input into the three dimensional model and used to define the surface heat flux of the cell module. To translate the heat flux from the 2D cross-section models to the 3D macro model the heat flux values from the top, side, and bottom of the module were averaged from the three sections for both the uncooled and cell heating cases. The averaged values were plotted as heat flux top, heat flux side, and heat flux bottom. A best fit line was drawn through each averaged flux defining the heat flux from each surface as a function of time. The equation defining the line was input into FLUENT as a user defined function to represent the surface heat rejection of each lumped module surface. In the cooled cases the heat flux was input as a constant value based on the averaged steady state flux of each side of the module.

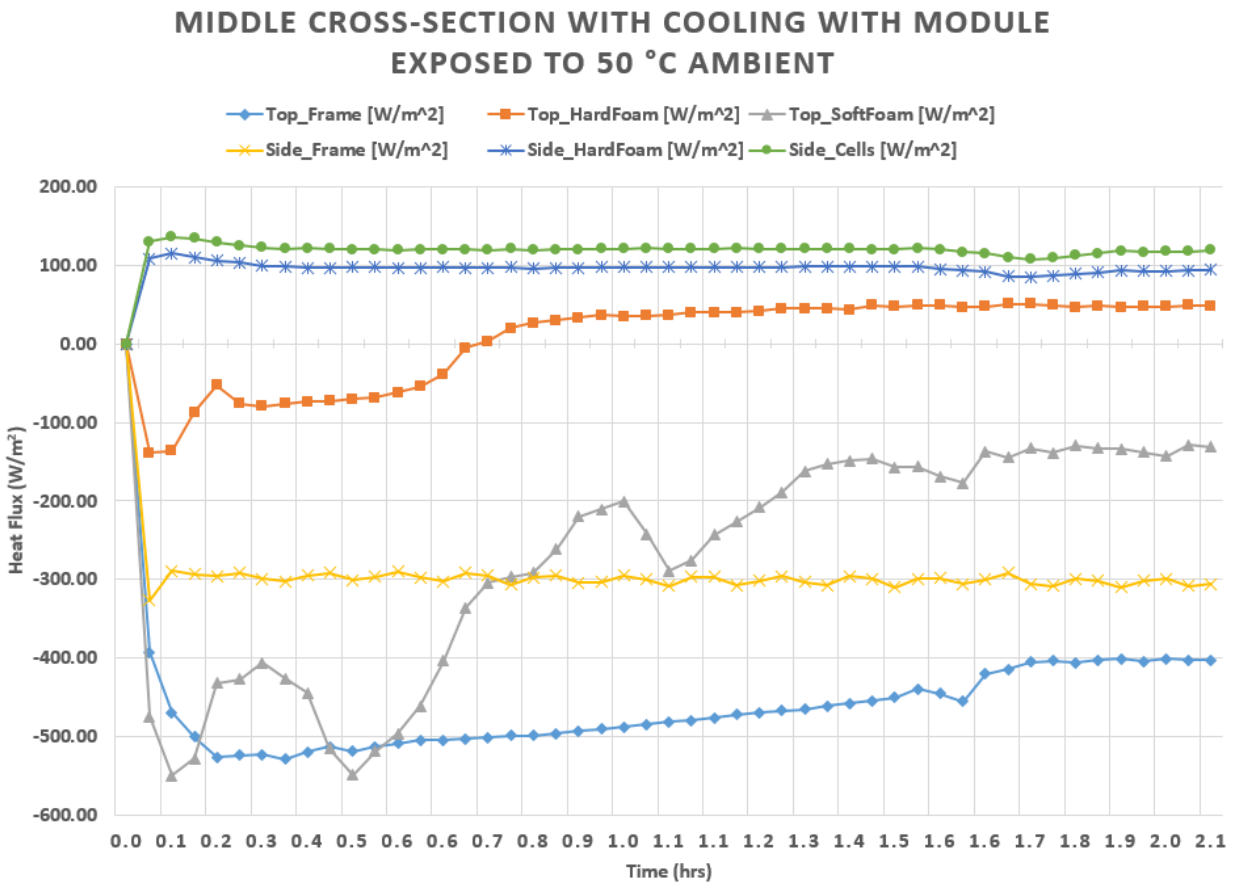

Figure 5-11, Surface heat flux: middle section, cooled

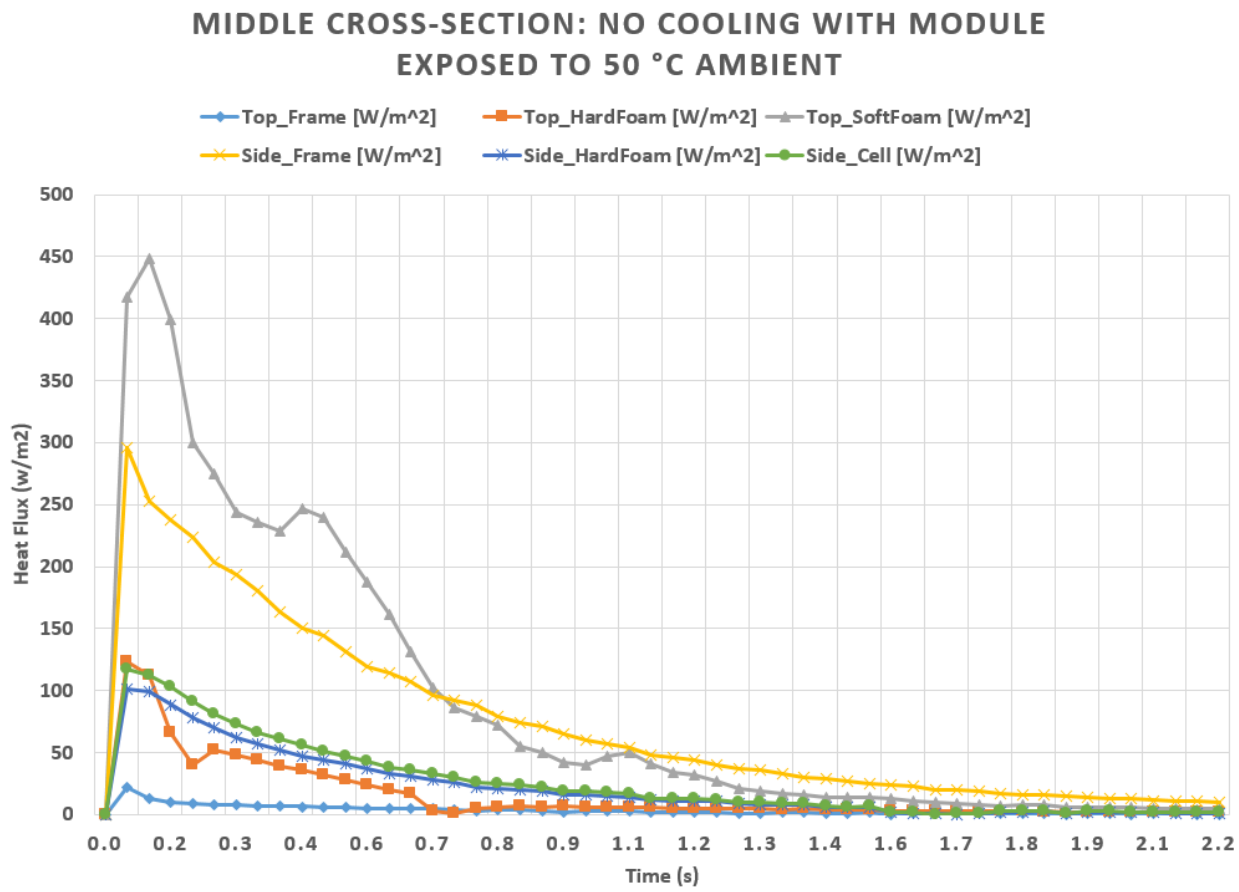

Figure 5-12, Suraface heat flux: middle section, uncooled

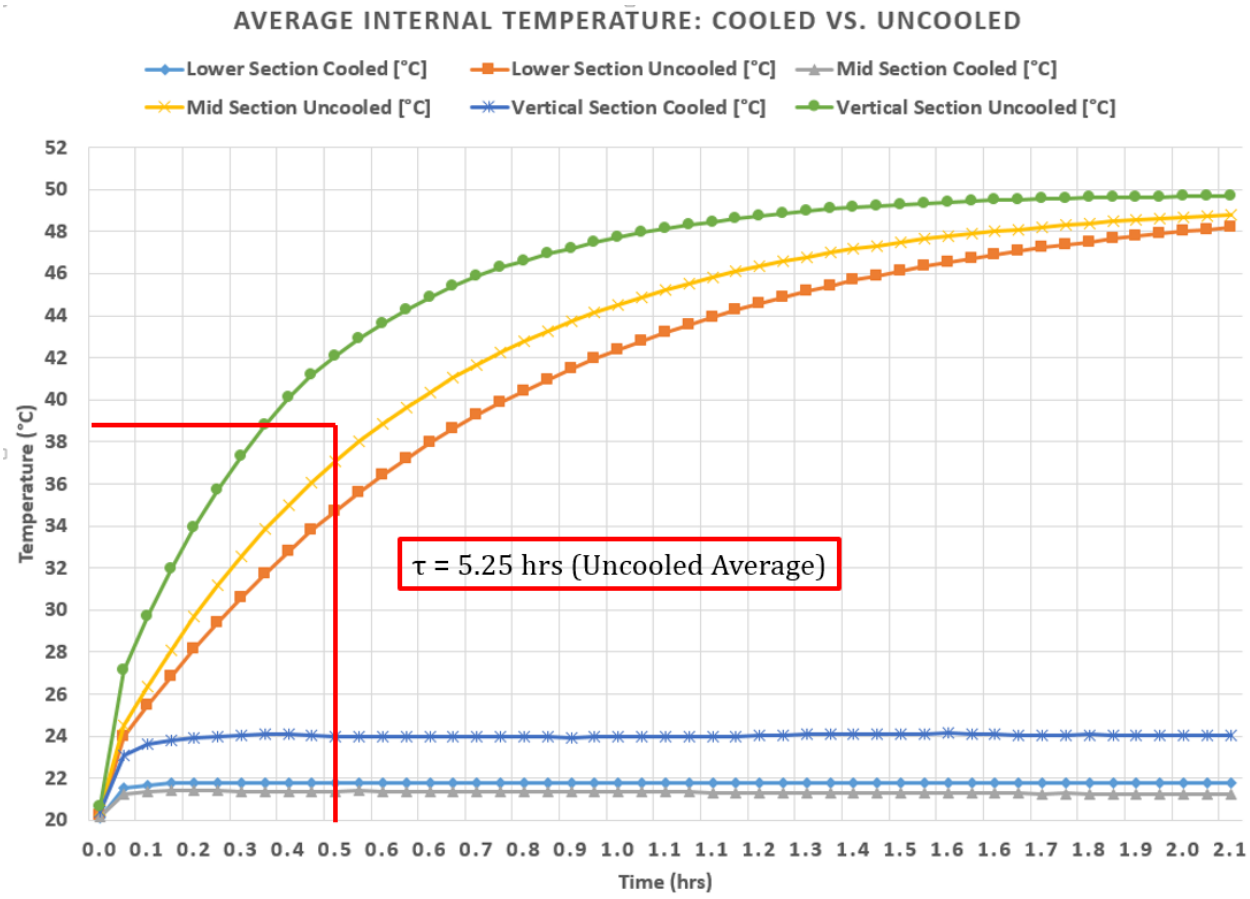

Figure 5-13, Component Temperature Averaged

Figure 5-13 shows the combined temperature profiles of all three sections, both cooled and uncooled. This allows the thermal time constants of the system components to be calculated. Figure 5-14 shows the change in internal energy for various key components within the cell module. Measuring the change in internal energy from the beginning of the simulation up to the time constant of the system allows for the rate of energy absorption to be calculated. Knowing the time constant, change in temperature, rate of energy change, along with other physical parameters allowed functional relations and constants to be defined that accurately represent the cell module as a single three dimensional solid.

The change in specific heat of each component was measured in each case and totaled allowing the specific heat to be calculated using equation 5-3. The heat transfer coefficient can be input as a function of time into the three dimensional model using equation 5-2. $\dot{Q}(t)$ is found by integrating the measured internal energy of the components with respect to time. The value of internal energy at each unit of time is being defined by the equation of a "best-

fit" line though the experimental data. The best fit line describing the simulated results is used such that the temperature rise, heat flux, and change in internal energy of each components is able to be described in a time dependent formula. 2nd and 3rd order polynomials were used to describe the change in each variable with respect to time. When a second order polynomial's regression value is sufficiently high ($R^2 > 95\%$) it is considered to describe the simulated data with enough accuracy, when the regression value is lower, a 3rd order polynomial was used to better fit the data. In the case of internal energy (Figure 5-14) the data was fitted with a logarithmic trend line as the change in internal energy follows a logarithmic shape. For the uncooled case the internal energy can be described by a logarithmic trend line developed from the simulation data as shown for the module frames of Figure 5-14. For the cooled case the value quickly settles and remains constant, and therefore internal energy is considered to be a static value. The derived values for module thermal properties are summarized in Table 5-1 in the next section under the stock module column.

$$C_p = \frac{Q}{m*\Delta T} \qquad \text{(Equation 5-3)}$$

C_p	Specific heat
Q	Heat added (J)
m	Mass (kg)
ΔT	Temperature Change (°C)

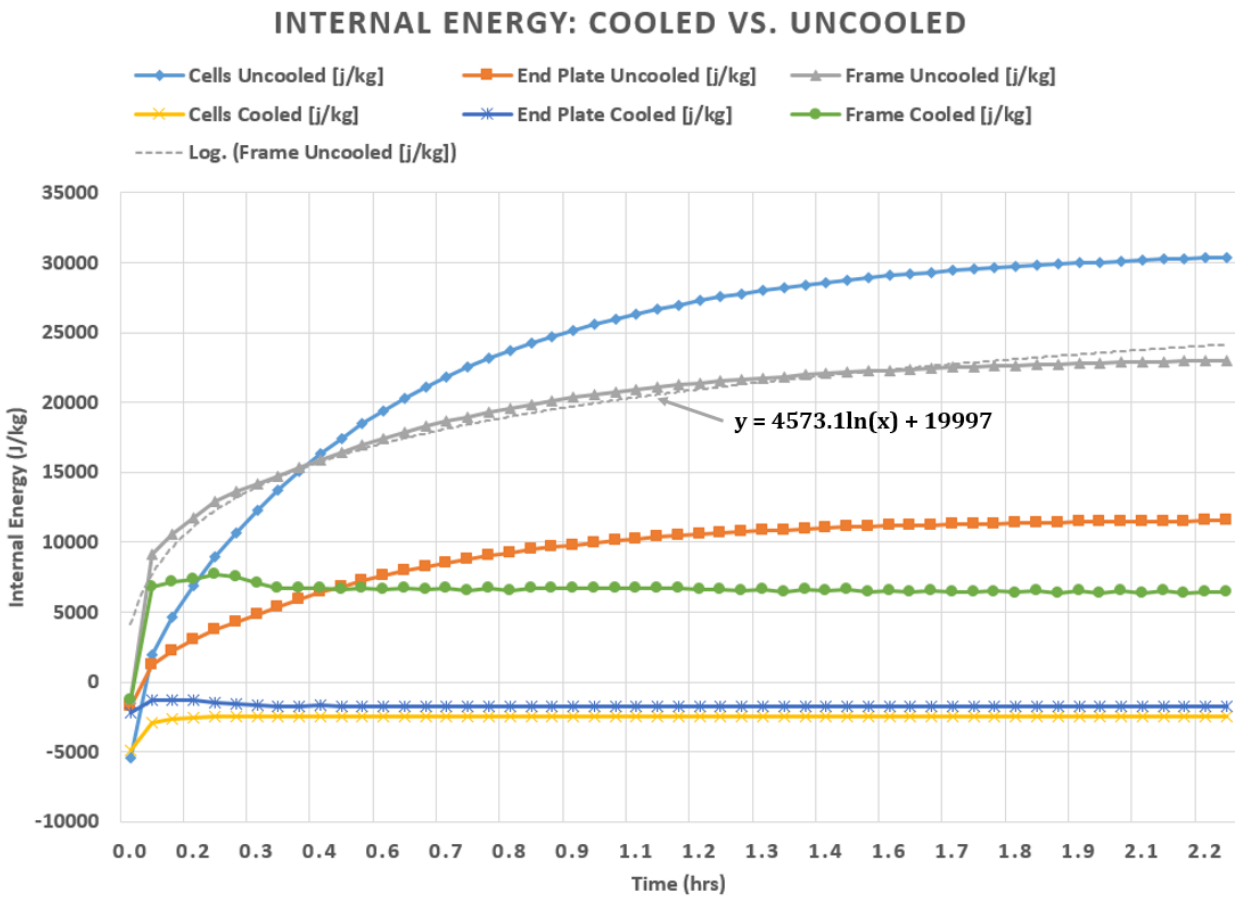

Figure 5-14, Internal energy change of key components

5.2.2 Optimized Module Configuration

A further step was to thermally optimize the design inside the module. Stock configuration testing was used as a baseline. Thermal bridging was eliminated as much as possible between the nylon frames and the cells by using additional foam material in isolating the cell edges. The same three sectional models were constructed and ran through the same subset of "tests". Additional runs were made using constant internal cell heat generation values. Cell heating values were estimated from US06 cycle data presented for the Chevrolet Volt battery [32].

Further improvements to the models were also made for this iteration of testing. During the initial tests for the stock configuration, there were too few cells thus amplifying the effects

of the module end plates in the results. To remedy this, the vertical section model gained four additional cells. Added to the vertical model were cell to cell bus bar connections, the main module electrical connection, and the top portion of the module that holds the cell tabs in place. The other two modules remained largely the same aside from receiving thermal optimization, where the cells now no longer make contact directly with the structural frames; Figure 4-4 through Figure 4-8 show the optimized design.

Further fidelity was introduced to the results from this portion of simulation by measuring the heat flux between the cells and surrounding components using the new vertical section. The results were then weighted to account for effects from the module end plate; the fluxes computed subsequently were supplied as inputs for the other two sectional models via a user defined function in FLUENT. This allowed for higher fidelity modeling of heat inputs from surrounding cells into the models without having to model additional cells.

Figure 5-15, through Figure 5-17 depict a visualization of the vertical model as it soaked from 20 °C to 50 °C both with and without volumetric cell heating. From the figures it is apparent that better insulating the cells from their frames improves the thermal resistivity of the module in a significant way.

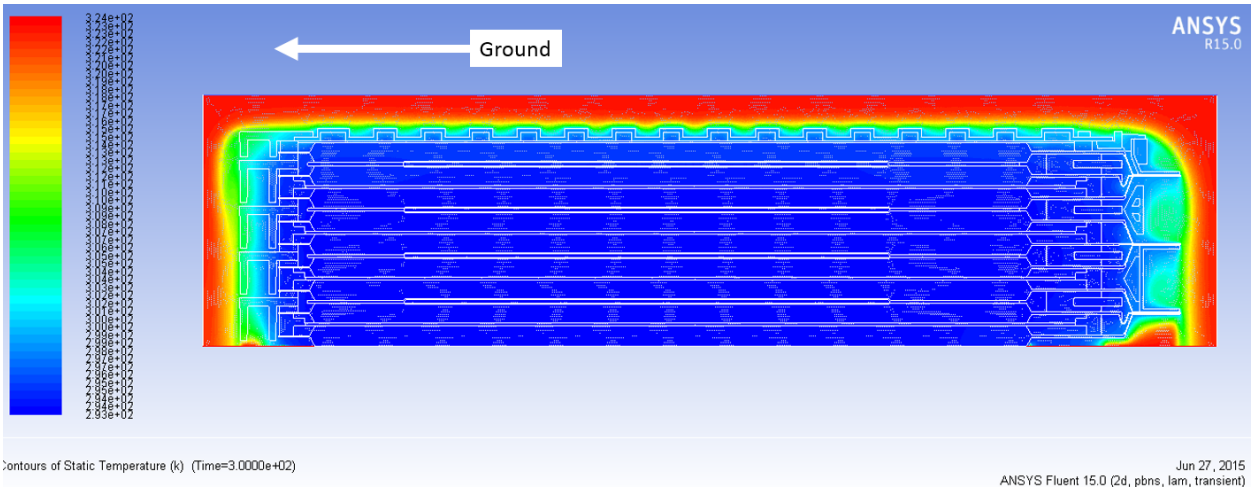

Figure 5-15, Vertical section: no cell heating or cooling, initial time step

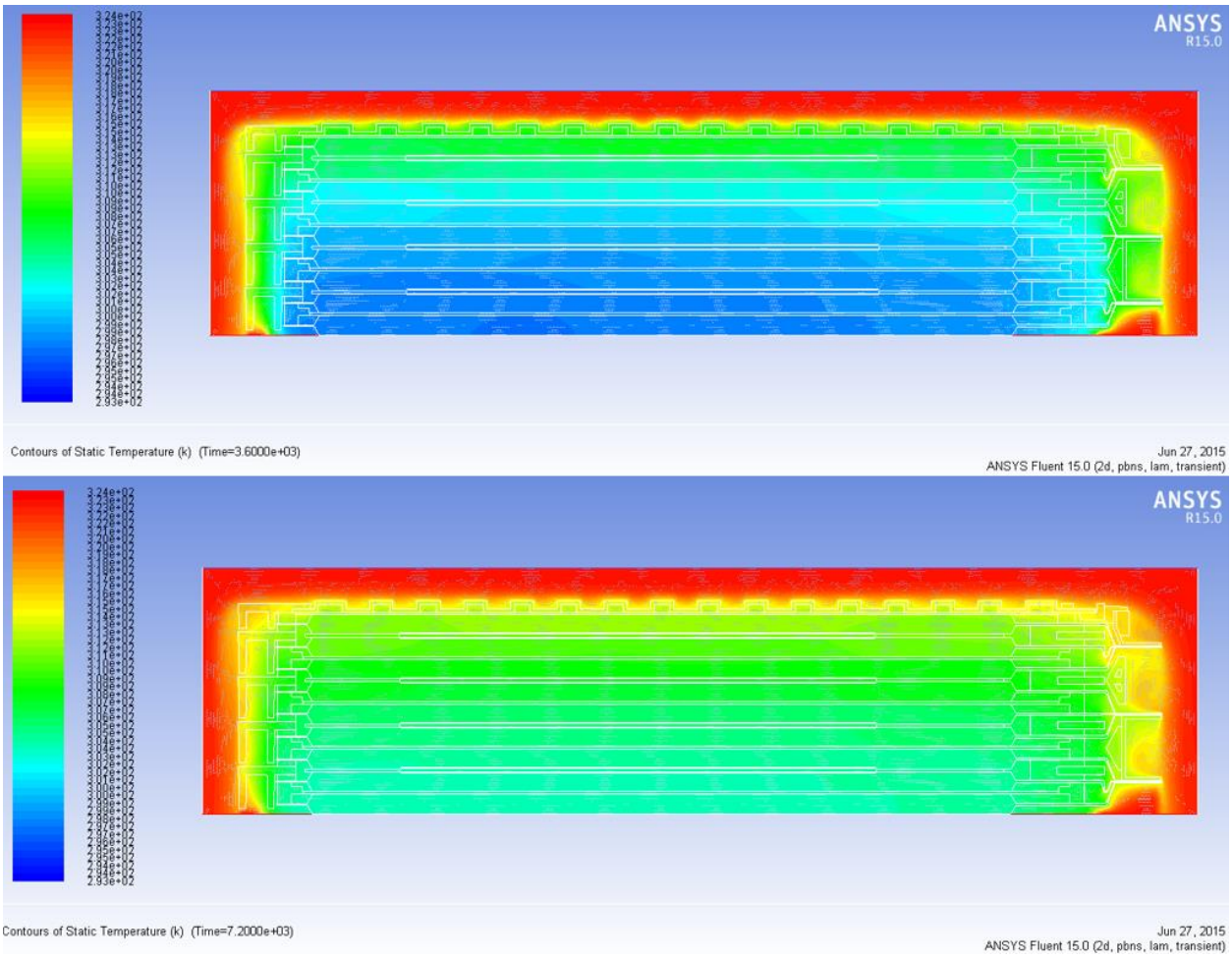

Figure 5-16, Vertical section, no cell heating or cooling. Top: 1 hr, Bottom: 2 hrs

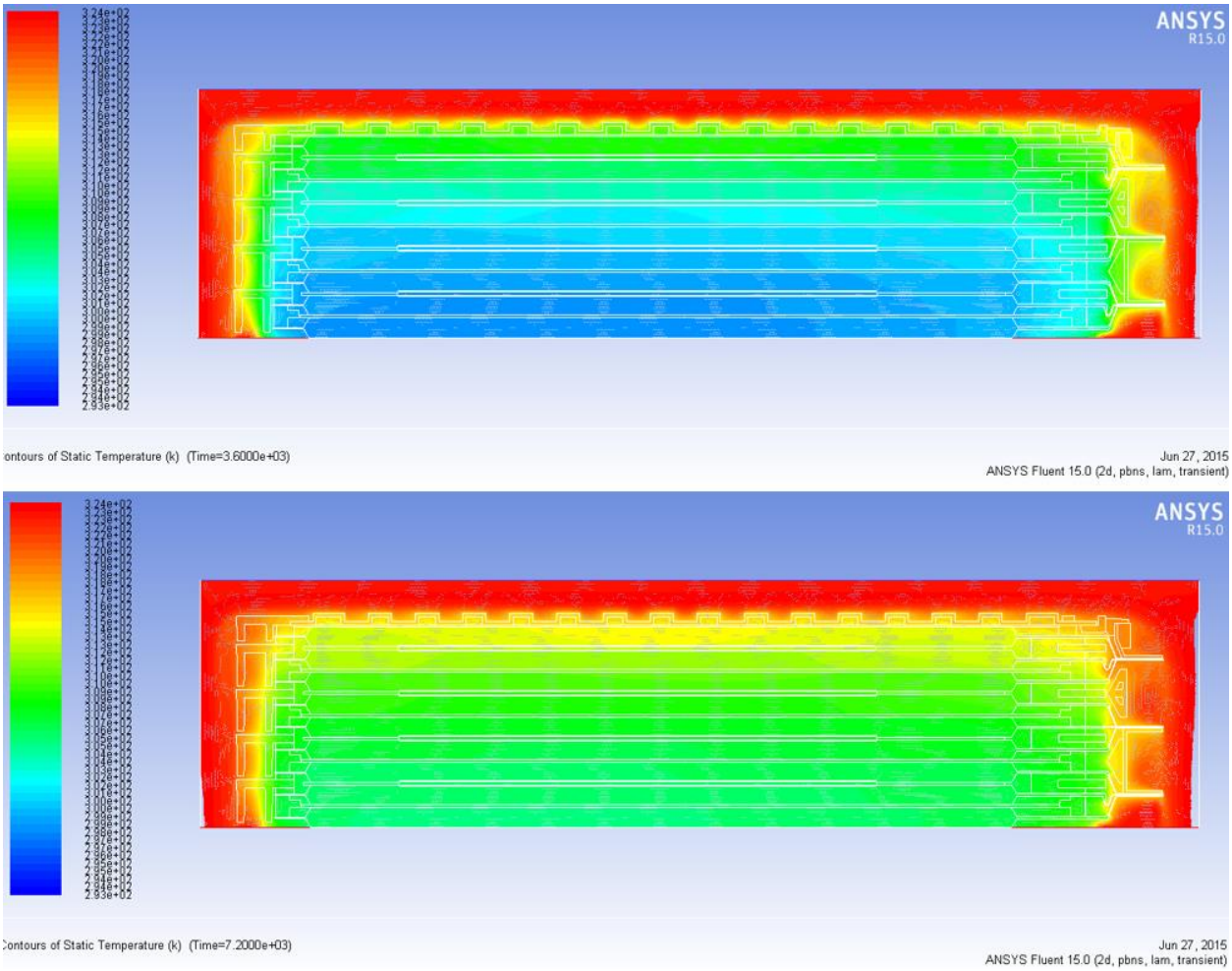

Figure 5-17, Vertical section with cell heating, no cooling. Top: 1 hr, Bottom: 2 hrs

Results summarized by means of the temperature rise within a module and the thermal time constant of the cells may be seen in Figure 5-18. These results demonstrate that by optimizing the constraint design within the cell module there can be significant improvement attributed to its thermal resistance. Such data can be compared between the stock module and optimized module in Table 5-1. Here it can be seen that heat transfer coefficient of the stock module has been lowered by a factor of ~4.5 thru better insulating the cell edges. It however should be noted the "stock module" column reports values from the original cross-section models described in section 5.2.1 which were not of the same fidelity as the optimized models explained in this section. It is therefore likely that the values are high compared to reality.

Such results can be integrated into the pack level model through means of the bulk thermal properties for the module as calculated. Then for cases where the cell module is generating heat, this quantity may be added to the solid through means of a volumetric heat generation rate. It is important to note that the values in Table 5-1 are representative of the larger module size found at the pack level.

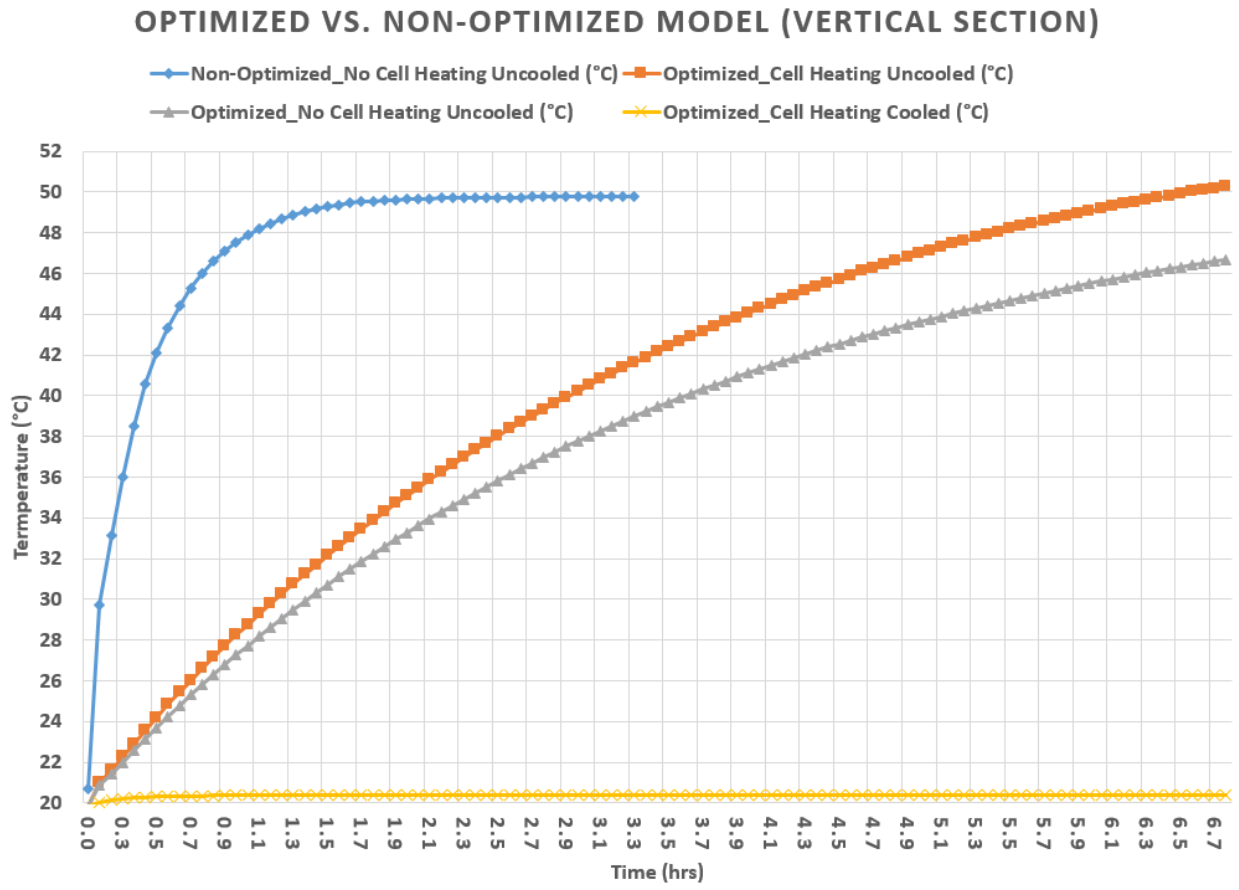

Figure 5-18, 2D temperature results comparison (optimized vs. non-optimized)

TABLE 5-1, THERMAL PROPERTIES: STOCK MODULE, FROM 2D RESULTS

Thermal properties: Lumped module, Stock configuration					
	Symbol	**Stock Module**	**Optimized Module**	**Optimized Module With Cell Heating**	**Units**
Heat Energy	Q	945.0	959.0	859.9	KJ
Temperature Change	ΔT	18.48	18.9	18.9	°C
Specific Heat	C_p	1272.50	1261.40	1249.1	J/kg K
Time Constant	τ	1890	11130	7020	s
Heat Transfer Coefficient	h	51.25	8.63	13.55	w/m² K
Heating Rate	$\bar{Q}$	500.1	86.2	122.5	W

5.3 CFD Modeling: Three Dimensional Pack Model

The objective of all work done prior to running a complete CFD analysis at the pack level was to increase its fidelity. Information gained through both the module level virtual analysis and the thermal chamber data helped to increase the fidelity of the final model. With confidence in the base cases that mirror what was experimentally ran using actual battery packs, it was then possible to expand the scope and perform simulations outside the cases tested physically.

Three variants of the 3D model were created for simulation. Each of the three models were solved in a subset of tests which consisted of changes to the parameters within the model. Once all models were ran through the same subset of test conditions, comparisons were made to analyze the effects of the pack construction changes on its thermal properties. The objective was ultimately providing an analysis and quantifying energy that can be saved in the BTMS by constructing the ESS with thermal management in mind.

5.3.1 50 °C Ambient Soak

The first model created was used as a baseline. It mirrored the stock pack, where the outer shell was composite. The second case ran included a ten millimeter thick layer of insulation along the bottom and using a composite baseplate. The third model created included ten millimeters of insulation inside of the fiberglass cover as well as insulation on the bottom with a composite baseplate.

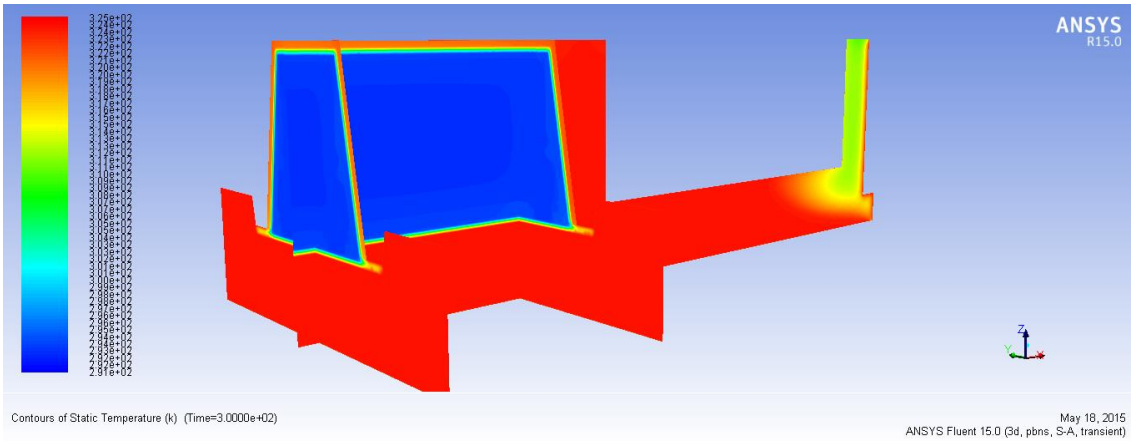

Figure 5-19, Initial timestep: insulated pack (50 °C soak)

The first case ran was similar to that of the testing performed in the thermal chamber. This considered a dormant pack soaked at room temperature (20 °C) that was placed in a 50 °C environment. For this the ambient air was flowing slowly to simulate a vehicle sitting in a hot parking lot in a dormant state (which had "cool" cells via previous activity of the BTMS). Additional heat inputs were added for vehicle sheet metal, and a small convective air current. Aside from that, the main heat load was created through the temperature differential between ambient and the pack internals. Figure 5-20 through Figure 5-22 summarize the results of this case ran on all three construction variants. Figure 5-20 shows the first indications of solver instability, where an initial temperature spike is seen in the bottom insulation only and no insulation case. In this run the data collected for temperature during the first hour of the simulation is inaccurate overshooting the expected temperature rise before becoming stagnant for hour two of the simulation. By 2.5 hours into the simulation the energy relaxation has rebounded, once again accurately portraying the results. For more information refer to the "Summary and Conclusions" section.

The results from Figure 5-20 show fully insulating the pack increased τ by a multiple of 6.75 from the base case, and by a factor of three from only insulating the bottom of the pack. Important to note for this case is that adding insulation to the bottom of the pack and replacing the heat sink metallic base plate with composite material increased the time constant by a factor of two. Figure 5-20 shows the time constants of the respective variants when soaked at 50 °C. When compared to the physical testing results, the fully insulated case modeled had the internals of the cell module reaching their time constant about 25% later. This is likely a combination of the thermocouple on the live test not being situated at the cell centers, and gaps in insulation coverage on the live test. To narrow the gap between result sets, the simulated model might be refined to accommodate electrical connectors and other thermal bridges which were not able to be covered in insulation. Similarly the cells heated about 20% slower in the uninsulated case simulations vs. live results.

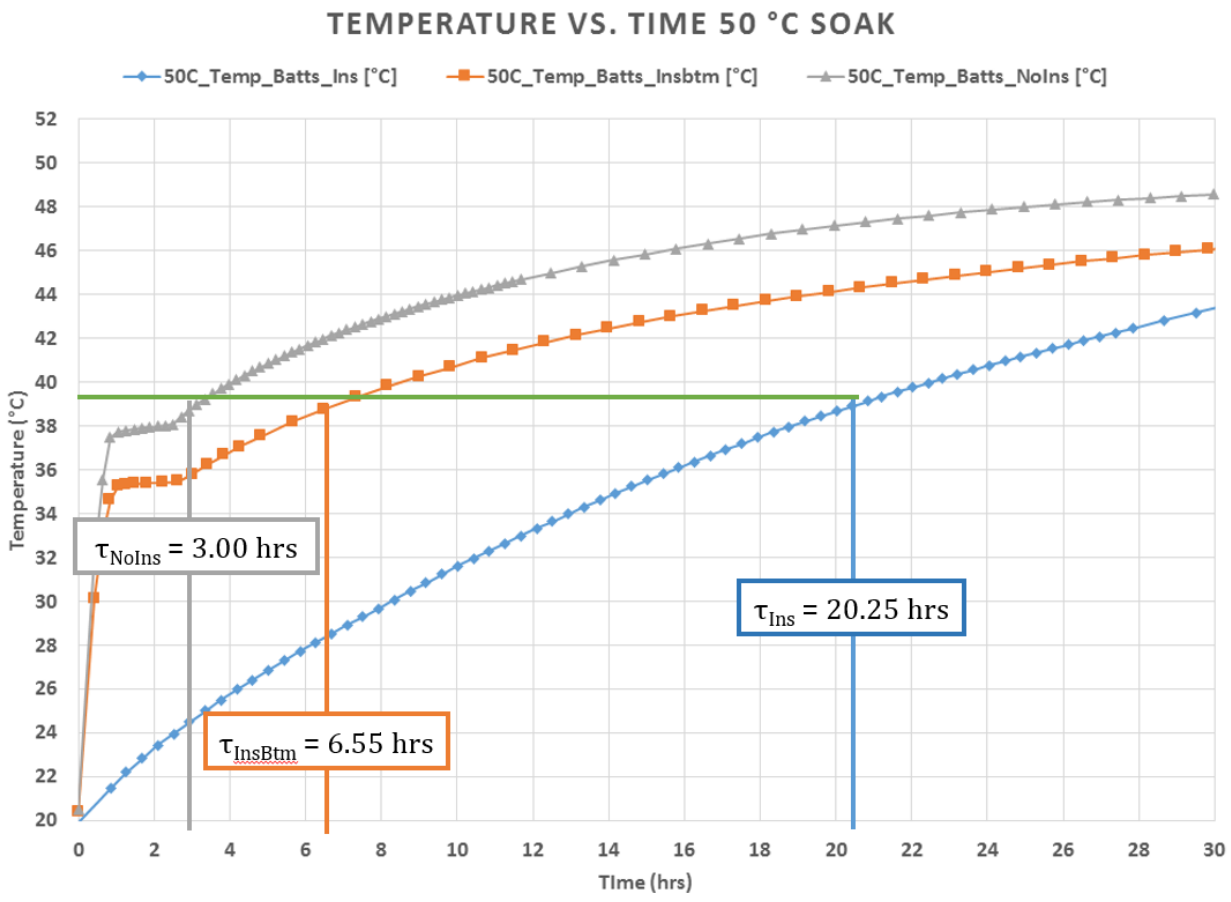

Figure 5-20, Simulated 50 °C soak temperature vs time

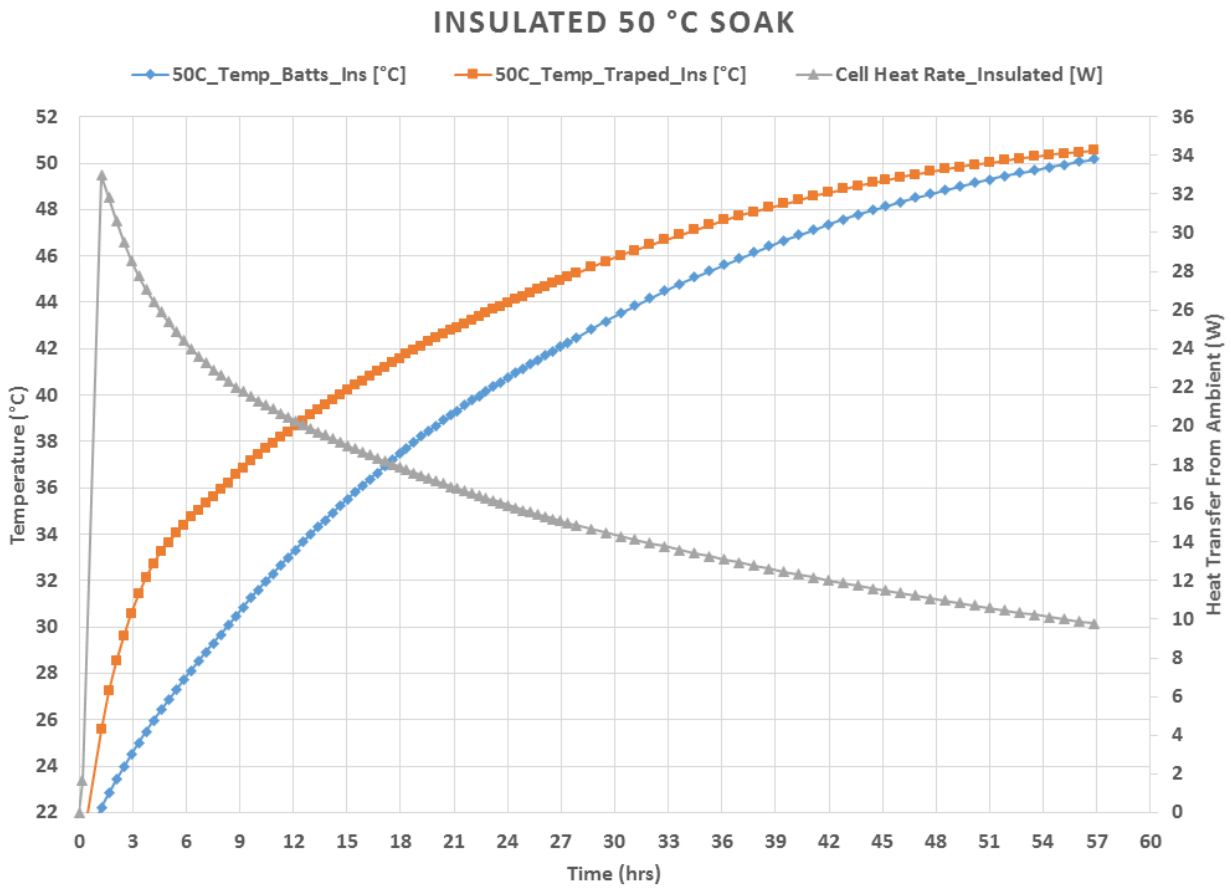

Figure 5-21, Simulated 50 °C soak insulated data

Table 5-2, 50°C soak summary

50°C Soak	Insulated	Bottom Insulation Only	No Insulation
Time Constant (hr)	20.25	6.55	3
Average Rate of Heat Transfer (W)	22	132	186
Maximum Rate of Heat Transfer (W)	33	332	391

Figure 5-21 through Figure A-11 show the cell temperatures and air temperatures on the vertical axis while displaying the rate of heat transfer to the pack on the secondary axis. The peak heating rate for the insulated variant is ~33 W while the bottom insulated and non-insulated variants hit 332 W and 391 W respectively. Using the average rate of heating up to the point of reaching the time constant yields: 22 W, 132 W, and 186 W for the insulated, bottom only insulated and non-insulated solutions respectively.

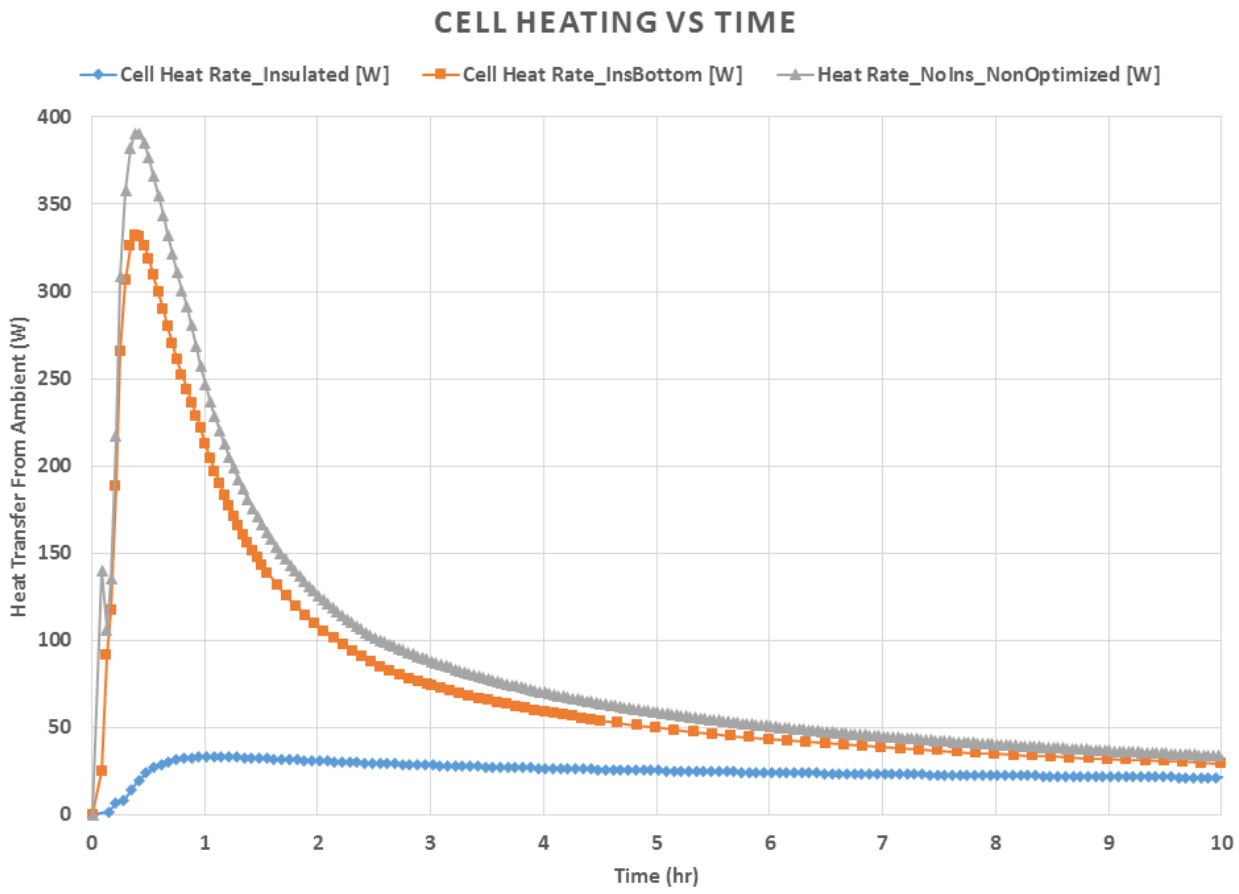

Figure 5-22, 50 °C soak heating data

5.3.2 Engine on Idling Variant

The worst case variant was thought to be a slow moving or stopped vehicle with the engine running. This would be considered a charge sustaining mode for the ESS. In solutions ran for the simulation there was no thermal energy being released by the cells. The heat flow measured is from a combination of the ambient air temperature, heated air flowing though the forward heat exchanger (radiator), radiant/convective heat from the engine/exhaust system, and radiant/convective heat from the road as a 50 °C ambient is being assumed for all cases.

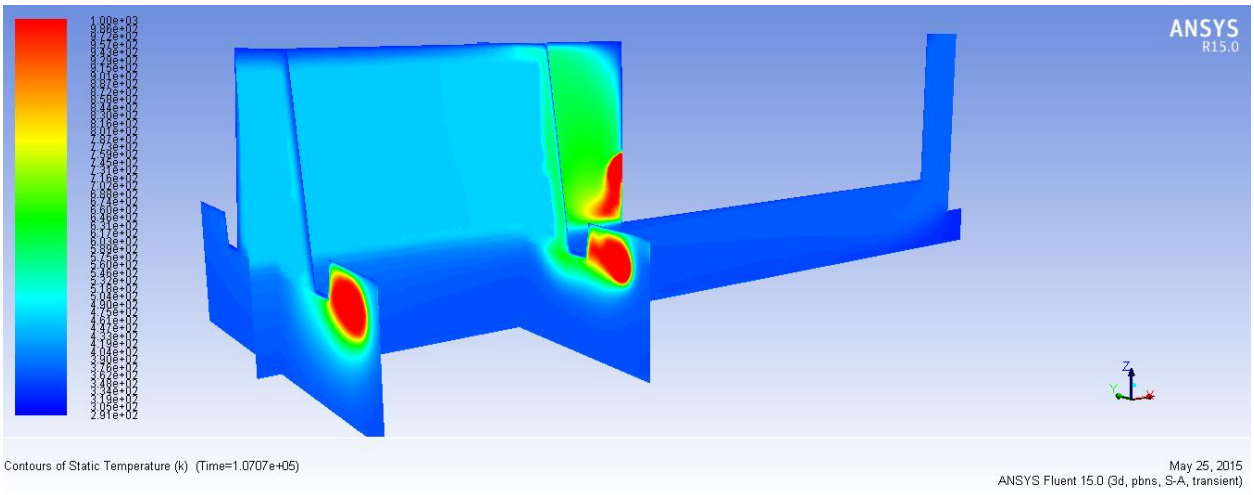

Figure 5-23, Visual representation of hot soak bottom insulation only

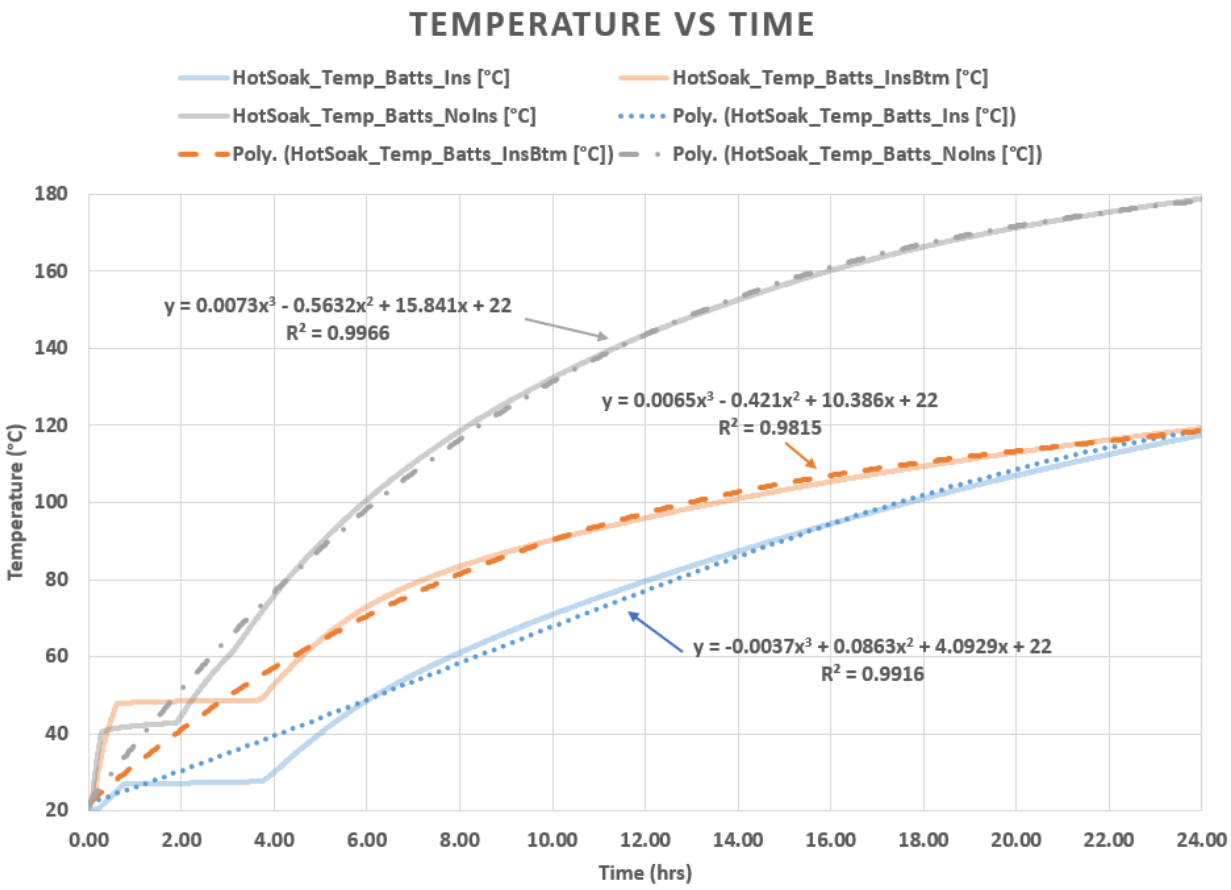

Figure 5-24, Hot soak temperature data for cells

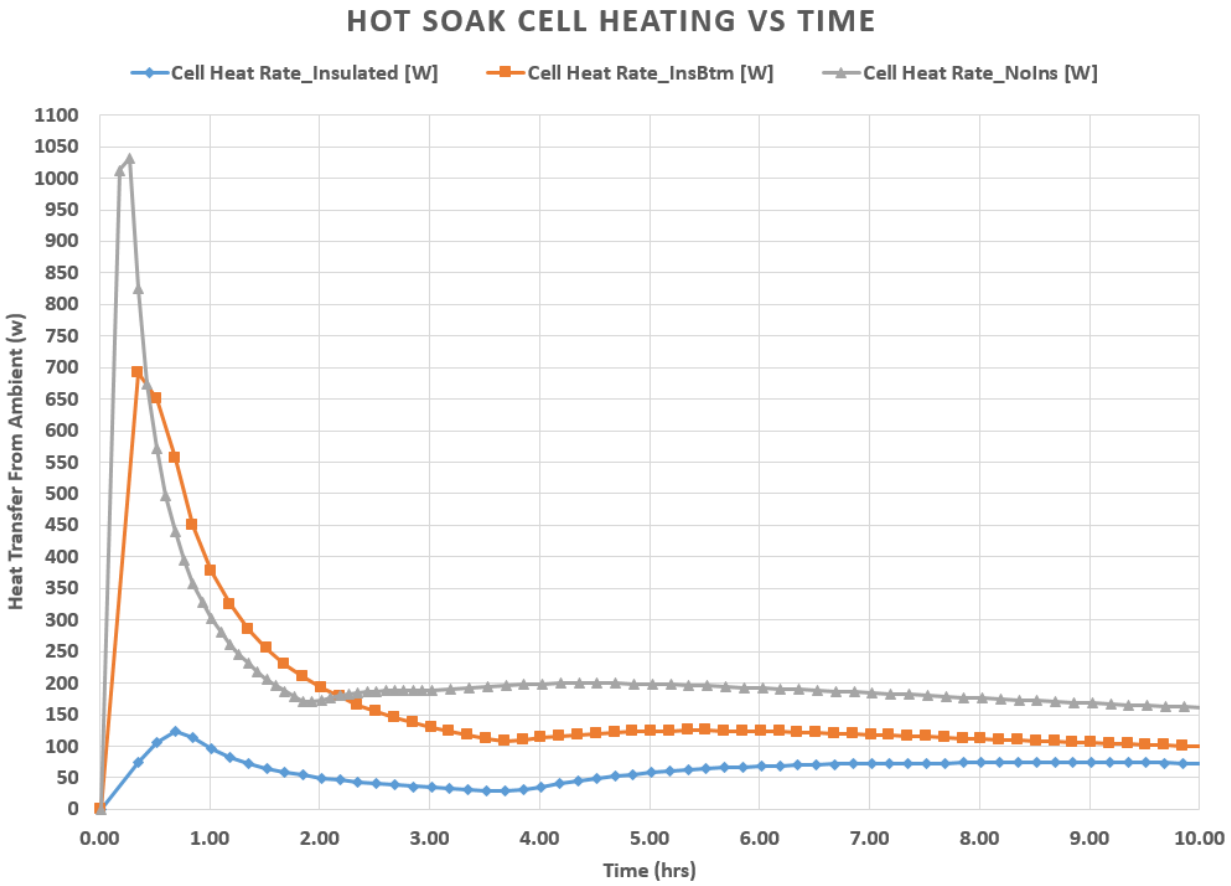

Figure 5-25, Hot soak heat data for cells

Figure 5-23 through Figure 5-25 show some of the relevant data from the solutions. In Figure 5-24 an initial spike and then relaxation of the component temperatures occurs. This is due to the relaxation factors given to the solver in order to obtain accurate energy flow results through the entire time period. Initially as the energy flow develops it quickly ramps and overshoots causing a brief temperature spike before settling and obtaining more accurate values. For this portion of the results a "best fit" approach was used to estimate what values should be used through these initial time steps by means of a 3rd order polynomial representing adjusted values through the entire time period. The equations used to define these "best fit" lines for the "Hot Soak" case can be seen in Figure 5-24. The version of ANSYS FLUENT used (version 12.0) did not allow for the solution initialization to iterate until flows were steady. Later versions of the software (version 14.0 and higher) allow the initialization of the solution to iterate until steady state is achieved which would likely remove this spike.

A script could also be written to dynamically change the relaxation factors during the initial time steps of the solution. These values represent the nose section of the ESS. Noting**Error! Reference source not found.**, the worst case would likely be in the rear of the vehicle where the heat from the exhaust system is not adequately shielded by the longitudinal rails. The uninsulated pack reached 50 °C in roughly 2.3 hours with a peak heating rate of 1.05 kW. Referencing cell heat generation rates from Figure 3-1, the cells could potentially be creating an additional 1.1 kW of heat. Introducing some factor of safety, the cooling system would likely have to be able to remove about 3 kW of heat during peak load conditions, and 1 kW nominal. The addition of insulation to the bottom plate reduces peak heat transfer from ambient to 690 W and ~250 W nominal. Fully insulating the pack reduces the ambient peak to 130 W and nominal to ~60 W. This would allow for the cooling system to be reduced in capacity to 1.5 kW peak output to maintain a fixed cell temperature within the packs. Such a design might allow alternative cooling methods to be considered and could slightly increase electric range of the vehicle without degrading cooling abilities. Thus important heat transfer reductions are possible not only in steady state values, but rather also peak heat flux.

5.3.3 Additional Variants

The only variants discussed in further detail are the hot soak (vehicle running) and the 50 °C ambient soak as they represent the two extremes on which cooling system design decisions may be based. The other variants looked at helped to further define thermal loads while the vehicle is moving and the abilities of the current cooling system to maintain temperature of the cells. It was found as expected that in all variants the stock cooling system was able to maintain the cells at a safe temperature.

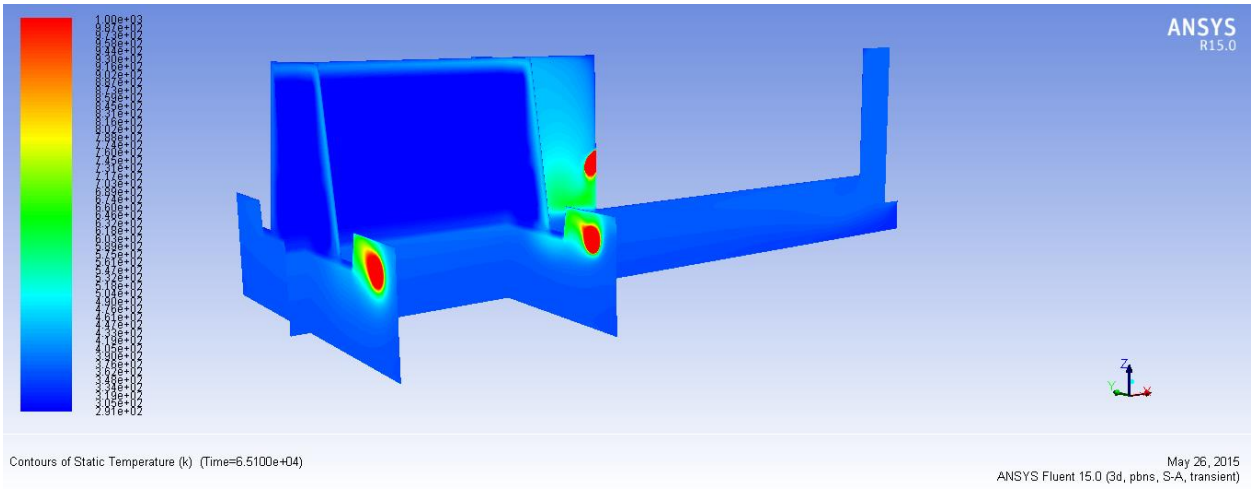

Figure 5-26, Temperature animation from cooled variant with engine running

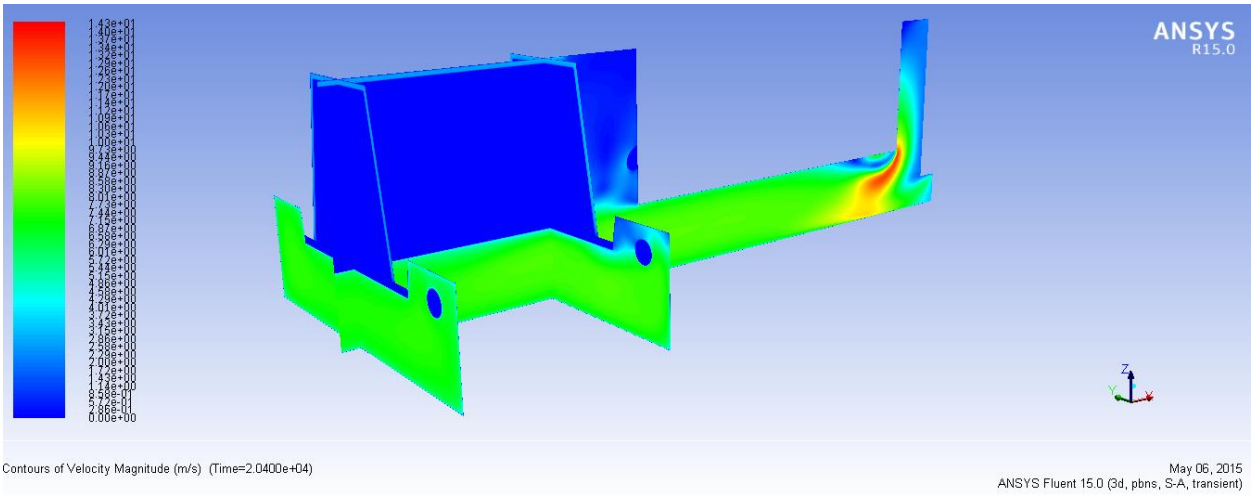

Figure 5-27, Velocity contour from moving vehicle variant

The case that simulated a moving vehicle yielded results similar to that of the stationary case. However the thermal loadings were slightly less in this instance. As the engine is running the main thermal load on the ESS comes from exhaust components. When the vehicle is moving, airflow developed dissipates the exhaust heat more effectively than when the vehicle is stationary (heat developed from engine and exhaust is consistent for both cases). Using real world data for the heat actually generated from exhaust and engine may prove this statement false. For purposes of the current research, heat generated by IC components was left constant across both cases. As with the materials, air flow, cooling power, and heat generation from the exhaust system; the road, and underbody can be modeled. For the time being their heating values also remain static through the simulation.

5.3.4 Effect of Optimized Module Construction

Additional simulations were run using the 2D parameters from the optimized module construction in the 3D models. Simulations were ran with the non-insulated and insulated 3D models in a 50° C soak environment with no flow and a hot soak environment with the engine on, and no vehicle movement. The results were then compared to those where the stock module was used.

There was no measurable improvement to the rate at which the cells heated in the 50° C environment once the pack was fully insulated. However in the case of a non-insulated pack the peak rate of heat transfer into the cells was lowered from 391 W to 185 W, more than a 50% improvement in peak heat load. This small (inexpensive) change represents a significant improvement to BTMS power requirements in the case of a non-insulated EV ESS.

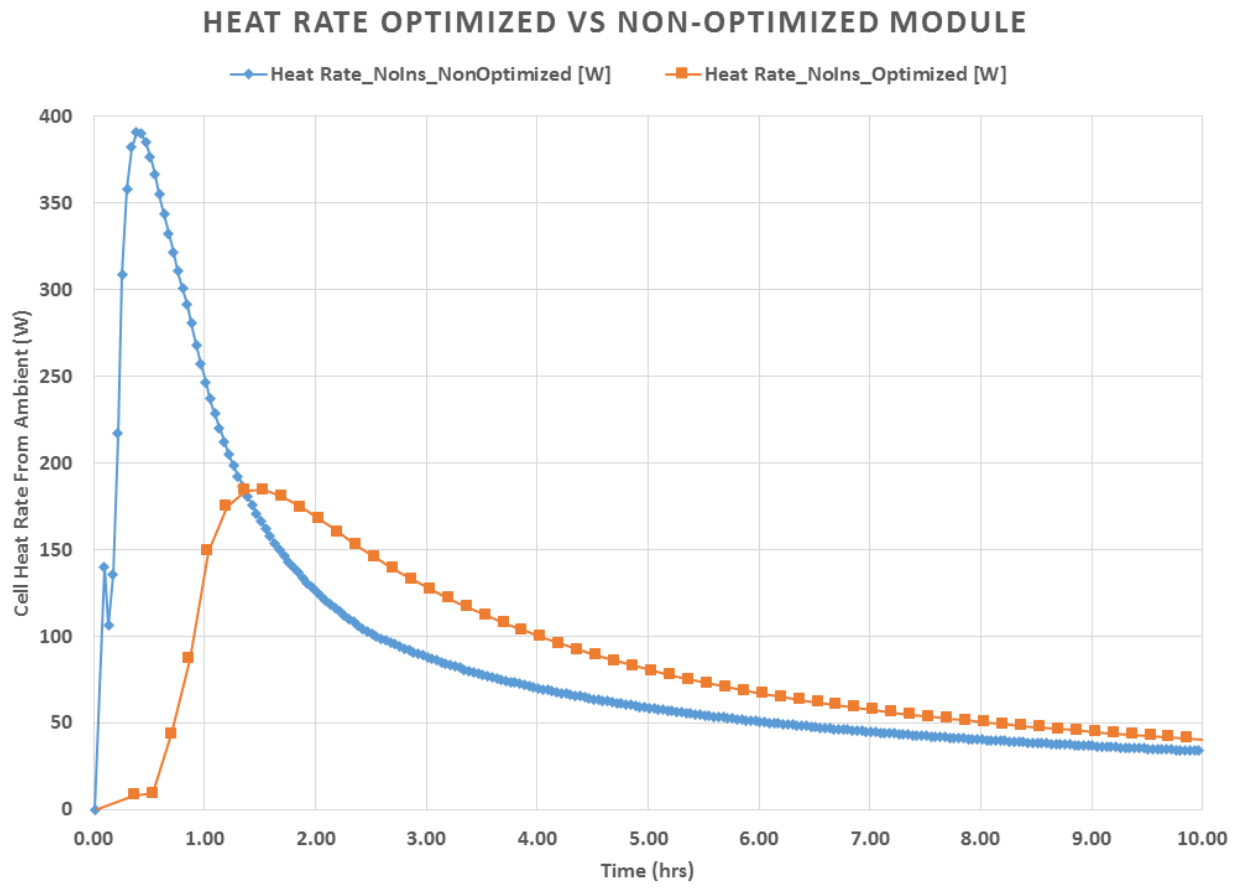

Figure 5-28, Cell heat rate, 50 °C soak: optimized vs non-optimized module

Improvements were seen in the more extreme hot soak case where the vehicle is considered to be moving at a low rate of speed while the engine is on. This case would be representative of being stuck in traffic with a low SOC on the pack forcing the IC engine to run. Figure 5-29 shows the temperature rise of the module in this scenario. Once again the temperature rise results are represented using a 3rd order polynomial "best fit" approach. The optimized module resists heat better initially eventually equalizing with the non-optimized construction. Once again we see some error in the simulation during the early portion of the run where the relaxation factors are rebounding. These gains demonstrate that altering the module construction is an additional technique that may be used for thermal optimization of the ESS, and at essentially zero material cost.

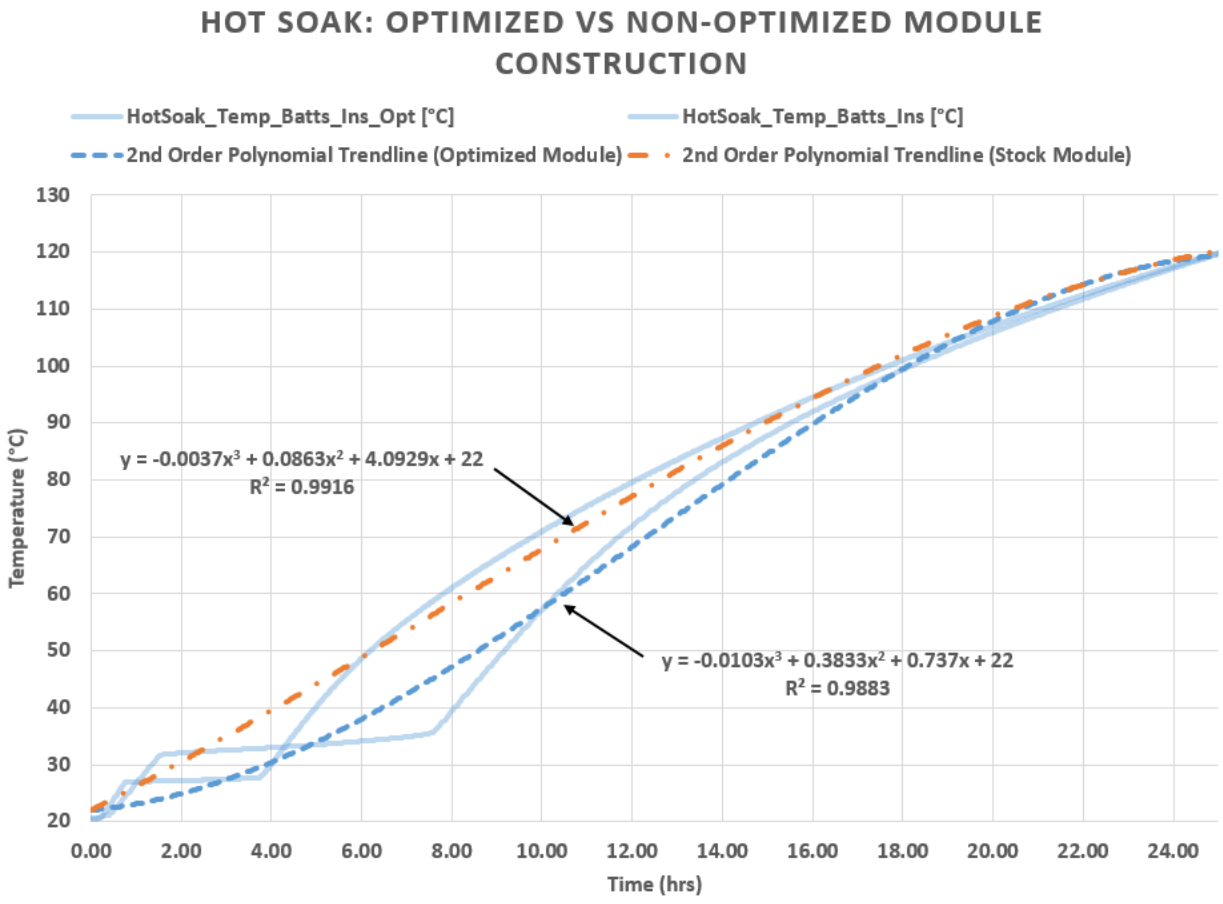

Figure 5-29, Hot soak: non otimized vs optimized module construction

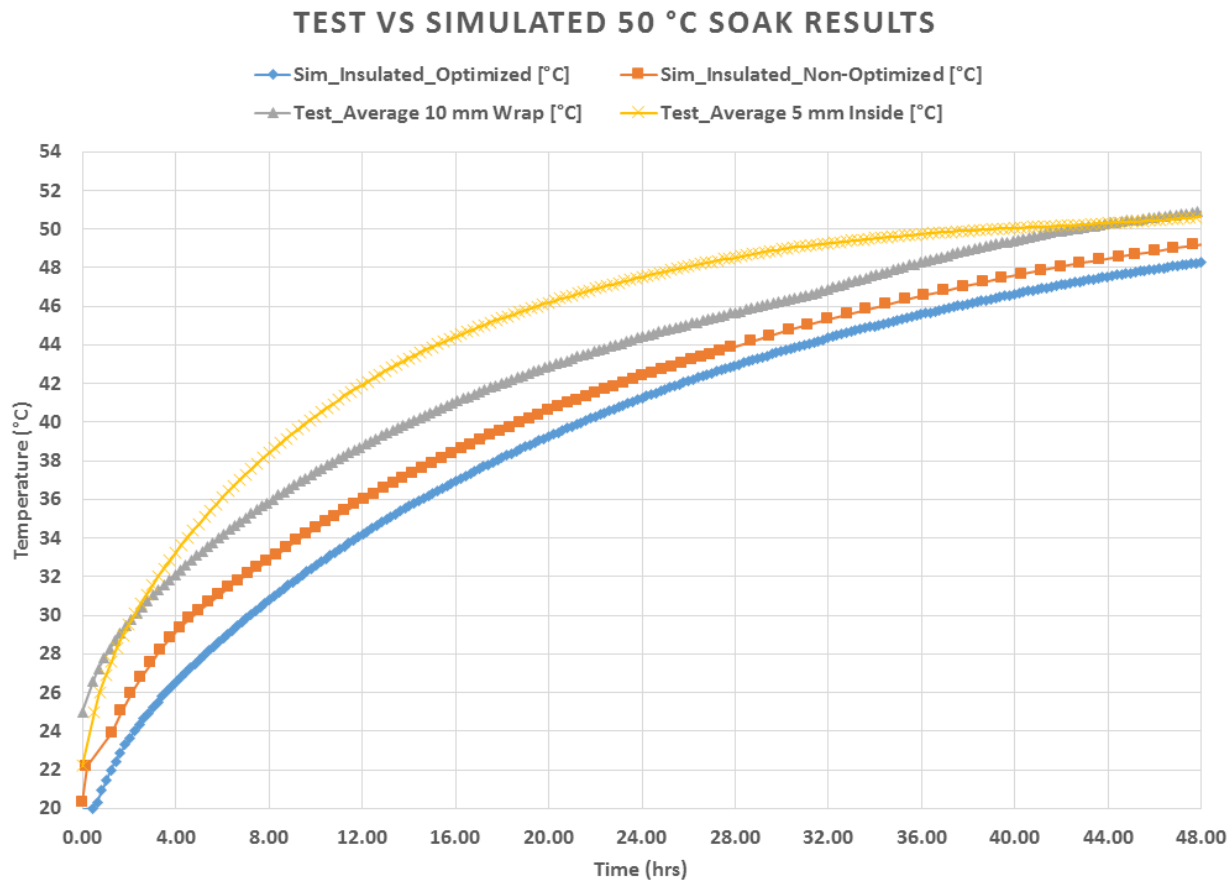

Figure 5-30, Live vs. modeled results 50°C Soak

Figure 5-30 shows some key simulated results vs. the thermal chamber data collected. This depicts that the accuracy of the simulated results are comparable to that of the physical tests performed on the modified production ESSs. The modeled data shows a slight increase in thermal isolation when compared to the data collected from the thermal chamber. This was expected as the simulated runs have a composite base plate instead of steel, and the improved module mounts. A slight improvement is also seen when using the "optimized" vs. the "stock" module configuration.

An important timeframe to note when comparing results is the initial 8 hour time period. Referring back to Figure 1-2, temperatures in an extreme climate may reach highs near 50 °C in hot months. However low temperatures in the same 24 hour period hit lows of 25 - 30° C. Limiting the temperature rise over a typical "hot" portion of the day can have significant

effect on the power requirements of a BTMS. Comparing the stock and fully optimized pack for an 8 hour period. The measured temperature rise within the stock pack (between cells within the module) was 26 °C when soaked to 20 °C and placed in a 50 °C environment. Comparing this to the results in Figure 5-30 the temperature rise for the fully optimized case was 11 °C for the same time period. This is significant for the case of preconditioning the cells as it now becomes feasible to condition cells while the vehicle is sitting because of the reduction in required power (possibly less than 100 Wh/day).

A summary of results is shown in Table 5-3 quantifying the effect of the various design modifications chosen for thermal isolation improvement. Referring to Table 1-1 the values relating to effectiveness have now been calculated and items may be selected based on the knowledge gained. Knowing that anything which does not drive complexity, cost, or mass is considered to be a free improvement, selections may be made. Optimization of the module construction and optimization of the pack construction to avoid thermal bridging are both items that may net improvement without driving additional costs. These two items combined could theoretically give a 30% overall improvement to thermal isolation. Combining all methods described, a 490% improvement is theoretically available.

TABLE 5-3, SUMMARY OF RESULTS

Modification	Thermal Time Constant	Increase from Baseline
Optimize Module Construction	**3.1 hours (2D FEA)**	**480% In 2D simulation 10% In 3D Simulation**
ESS Construction Optimization	**3 hours (3D FEA)**	**26%**
Adding Thermal Insulation to ESS Baseplate	**6.55 hours (3D FEA)**	**118%**
Adding 5 mm of Insulation (Aerogel)	**11.5 hours (Experimental)**	**202%**
Adding 10 mm of Insulation (Aerogel)	**15 hours (Experimental)**	**295%**
Summation of Changes	**22.4 hours (3D Optimized Module FEA)**	**490%**
Heat Load Reduction:	**390 W as compared to experimental stock configuration @ 30 °C ΔT exposure**	

Chapter 6. Summary and Conclusions

Understanding historical techniques and technologies employed in ESS design was integral in arriving at the final model used to demonstrate thermal isolation improvement potential. Comprehending the characteristics and limitations of various cell chemistries and cell construction strategies helped to identify a more optimal configuration for thermal management. Previous research demonstrating the advantages and limitations to each BTMS leads the ultimate choice towards ignoring forced air cooling for EREV, and EV cases along with most PHEV cases. Its limited thermal capacity is deemed insufficient to provide protection to the Li-ion cells in all cases. The research helped to identify alternatives to the vehicle's standard HVAC which could be used to provide thermal management in conjunction with a sufficiently optimized construction. PCMs although not used in the final scope of simulations presented could further improve thermal efficiency and provide additional reduction to peak thermal loads seen within an ESS.

Initial research also identified consumer cost of ownership to be a large factor in EV success. In order to reach a large enough portion of potential customers the cost of ownership must compare with a conventionally powered vehicle over a typical lifespan. This identified overall cost as something that must be considered when making thermal improvements to the ESS model.

Examining the construction of a mass produced ESS provided a means to identify where improvements can be made that would not drive a great increase in cost to the pack. Working with an OEM has provided insight into what types of improvements would be taken under consideration. Working with vehicle design has provided insight on how much importance is placed on material cost to determine whether a part makes it into production or not. In order to maintain margins required to justify bringing a vehicle to production, adding extra cost to a component needs to be offset from removing cost from another. Often this can affect customer facing components and interfaces which may lead to an overall reduction in the perceived quality of a vehicle.

Working in the electrification group testing ESSs has provided experience in identifying the type of scenarios and environments that packs must survive without losing useable capacity.

Often batteries face difficulties in the form of isolation loss due to a buildup of condensation when ambient temperature or humidity changes rapidly. When batteries are cycled at cold temperatures (< -30° C), or exposed to hot temperatures (> 40° C) for an extended period of time capacity loss occurs. Built in algorithms attempt to prevent this by current limiting the ESS output at temperature extremes. The need for current limiting could be lessened by employing the thermal isolation methods described in this thesis. Destructive testing must also be considered where packs must not harm vehicle occupants when exposed to open flames, such as in a wreck where a vehicle or fuel catches fire. Improvements identified in this thesis could also improve how the ESS reacts in these conditions without a large increase in piece cost.

With only an incremental increase in manufacturing complexity the thermal management system required can be downsized significantly. By using a composite construction with reduced thermal bridging and the addition of insulation materials the heat transfer can be cut by a factor of more than five without forcing a major redesign of an existing pack. Maintaining cell temperatures in a given range while cycling the pack with the engine turned on in an EREV mode may result in significant parasitic losses. In this case the refrigerant compressor may be consuming three or more kilowatts of available power sporadically. Through optimization of construction this load could be reduced by half without altering cell module design. This not only represents significant thermal management efficiency gains, but also enables manufacturers to explore alternatives to a compressor refrigerant system such as TE units for providing cooling to cells.

Current generation EVs and EREVs focus on robust design and the ability to last through the manufacturer warranty period with few problems. This has led to over engineering of many components sacrificing efficiency for assured longevity. The present opportunity is to optimize the EV power delivery system to lower cost, and increase range, while still being able to maintain cells at a safe temperature through all expected conditions. Given the costs associated with the raw materials used to create Li-ion cells, the ESS will likely remain the most expensive component for EV, and EREVs. Complex and costly cooling systems add unnecessary fixed costs to vehicles and should be replaced by purpose built modular systems able to be adapted and sized for various applications. Thermoelectric units with a coolant

pump present one such alternative. They are able to operate at a nominal capacity efficiently while being able to offer a peak output capable of keeping the cells in their safe temperature range given that the ΔT isn't too great between the cells and the ambient environment. Another parallel and synergistic opportunity is to employ PCM's to shave the significant peak heat flux rates seen in the simulation.

The testing completed assumed use of silica aerogel blankets as insulation. Another technique to achieve a thermal barrier would be to use a molded foam core fiberglass construction for the cover to reduce cost. This would allow the pack to be better protected from ambient without the associated cost and handling difficulty of silica aerogel blankets. Simply replacing the bottom structural plate of an ESS with a fiberglass composite can eliminate thermal bridging without increasing complexity significantly. Building it as a tub vs a plate can overcome the structural rigidity loss associated with employing less rigid materials.

An unexpected difficulty was faced when using the three dimensional solver within FLUENT to solve cases where there was a large temperature delta between the air temperature and the components at the beginning of the simulation. Initially temperatures would spike within components before settling for a brief period and once again accurately representing expected values. This was mitigated by fitting a third order polynomial to the data to predict what temperature values should have been through this initial period of the simulation. Depending on the temperature differential and which model variant was running this period lasted from two up to eight hours. The effect noted is believed to be caused by the relaxation factors set when initializing the solution. Here the response to new inputs can be varied from 0 - 1, where 0 is the slowest response. For these simulations the energy relaxation was set high which is believed to have caused the overshoot in temperature rise. Setting it low would smooth out the initial portion of the simulation where flows are stabilizing. The additional time required to generate heat flow within the model would however cause inaccuracies later on in the simulation where the temperatures are reaching an equilibrium. Running additional iterations per time step or a smaller time step value may also lead to more accurate temperature prediction during this initial phase of the simulation. Without additional computational power then available it would greatly increase the amount of time

to run a simulation. The simulations as presented took from days to weeks depending on the variant ran. With an increased timeframe for gathering results or removal of computational limitations it is expected that this inaccuracy could be eliminated from the results.

To expand on the learnings presented it would be useful to gain access to more computational processing power which would allow for a full ESS in the vehicle, to be modeled and have CFD analysis performed. Alternatively more models could be built to simulate different portions of the ESS as their environments can vary due to the proximity of heat sources, and varying airflow. With enough computing power the two dimensional and three dimensional models could be combined allowing for a better analysis of heat distribution and thermal loadings within the cell modules. Additional parameters could be created to vary environment variables and simulate real world drive cycles. Further testing in a climate controlled wind tunnel with a fully instrumented ESS would add fidelity and help to tune the simulated models. The ultimate goal being that the models could be built with enough fidelity that an ESS could be designed using data from the simulations, eliminating the need for some levels of costly development builds. This would also eliminate some testing allowing the design cycle to be shortened significantly. Other advantages are the ease of varying the construction material alternatives and employing techniques allowing for quicker optimization of the system.

6.1 Research Contributions and Future Goals

Improvement Factors Identified:

- Addition of insulation to the underside of ESS in an under vehicle mounted pack doubled the thermal time constant value while soaking to 50° C.
- Wrapping pack in an insulation blanket further improves this by 300%.
- Optimizing module construction (internal thermal bridging reduction) offers significant improvement to pack level thermal isolation.
- Combining all methods of thermal optimization described, the peak environmental load is reduced from 390 W to 30 W, while soaking at a 30° C delta T.
- Overall system cooling requirements can be reduced by 360 W through adding insulation and optimizing the module construction
- The BTMS nominal output may be downsized from 1.5 kW to 1 kW for the pack described, reducing parasitic loses and improving EV range.
- A significant improvement can be had by insulating rear (exposed) portion of pack and underside only
- Accuracy could be greatly improved with additional computational power

The end result of the research presented is to challenge traditional ESS construction and cooling/heating techniques by analyzing the pack from the module level up, identifying opportunities for thermal isolation improvement. The work also discusses in detail means of creating, and evaluating virtual models both structurally and thermally. Both the learnings derived from the virtual assessment, and the methods employed to create the virtual models can be used by industry and other researchers to optimize ESS designs.

The novel ideas presented include deploying alternate thermal management systems, thermal optimization in construction methods (pack level, and module level), and the methods outlined for virtual modelling. By designing the structures and conducting thermal

evaluations virtually, one can identify, and remedy problem areas without requiring much physical testing. This shortens the design cycle, and allows for faster generation and evaluation of design alternatives. The methods described ultimately allow for a more optimal pack design both thermally to reduce parasitic losses, and structurally to better protect the Li-ion cells without incurring significant production costs.

While this research focuses on a specific example (pack, and vehicle). The methods described are adaptable to a variety of cases. Similar approaches could be used to optimize any HEV, PHEV, EREV, or EV. It is also possible to use the results and methods presented to further expand the scope of the research to include component level modeling. This would allow for a high fidelity full system model.

Some future goals building upon the research presented would be to develop realistic heat generation profiles for cells while a vehicle is completing a US06 cycle. The data could be imported into the solution as a heat generation profile which when applied to the cell volume would give a more accurate representation of heat generation within a module during normal driving. Incorporating the power electronics required to operate the ESS should also be considered in future models to improve accuracy. The results when input into the 3D system level model using the methods described would increase the accuracy of the results. The same could be done for engine and exhaust heat profiles. Using user defined functions within FLUENT, the heating values could be varied dynamically, simulating a vehicle running repeating drive cycles. A cell level model would also add value to the overall simulation, the results could increase the accuracy of how heat flow is simulated within the module. The way it is currently constructed the cell heat generation is uniform throughout the cell. We know that in reality there is more heat generated near the anode and cathode of the cell.

Eventually the cooling system exterior to the pack could be brought into the system level model allowing for the heat transfer of the complete vehicle to be modeled. Using multiple smaller models to describe subsystems as presented allows larger systems to be represented accurately without demanding excessive computing power. Another advantage of using this approach is that making changes to the component level models can be done relatively quickly when separated from the system level. A full system level exergy analysis could then be conducted identifying where energy is wasted throughout the ESS and the subsystems it

requires. This would allow thermal optimization efforts to be focused on the components that are responsible for the most loss.

Appendix

A. Internal pack thermocouple placement: Live Testing

Internal Thermocouples:

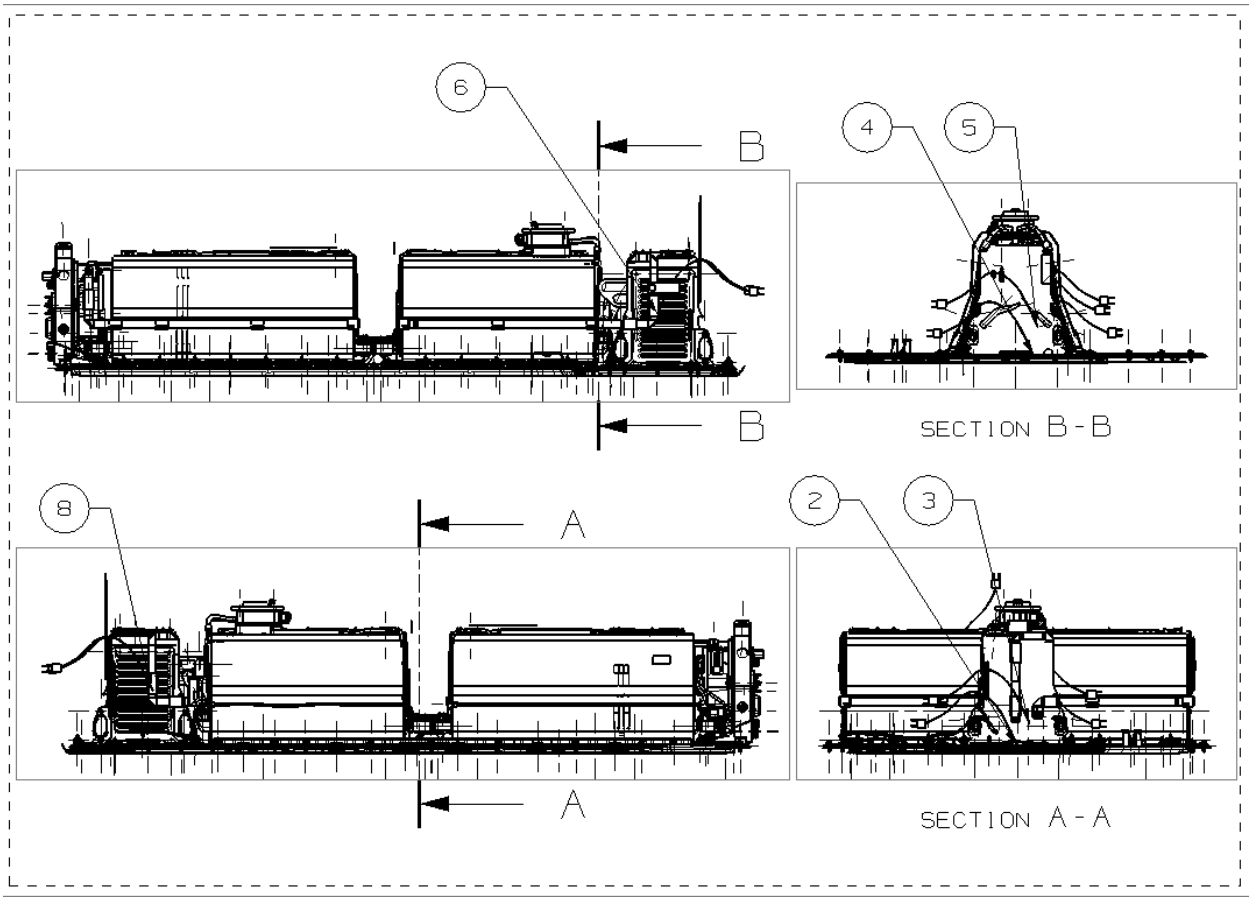

Bottom side of lid thermocouples:

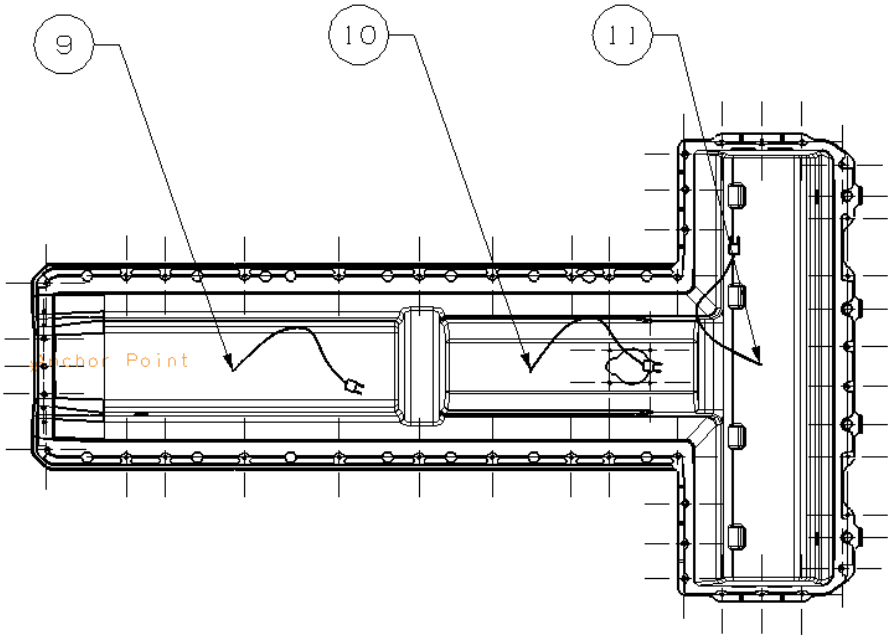

Top side of lid thermocouples:

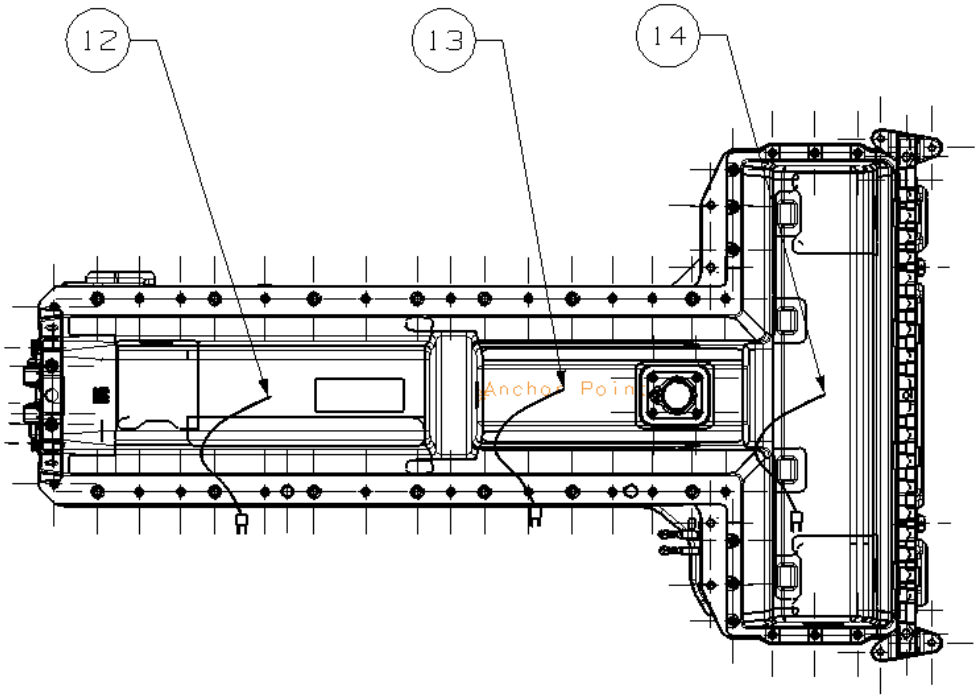

B. Cryogel® Z Specification Sheet

Cryogel® Z

aspen aerogels

PRODUCT DATA SHEET

HIGH PERFORMANCE, FLEXIBLE, INDUSTRIAL INSULATION FOR SUB-AMBIENT AND CRYOGENIC APPLICATIONS

Cryogel® Z flexible aerogel blanket insulation is engineered to deliver maximum thermal protection with minimal weight and thickness. Ideal for use in sub-ambient and cryogenic applications, Cryogel® Z incorporates an integral vapor retarder with zero water vapor permeability to ensure maximum protection of your assets.

Cryogel® Z insulation features unique silica aerogel within a flexible fiber blanket to deliver industry-leading thermal performance in an easy-to-handle and environmentally safe product.

Cryogel® Z's extremely low thermal conductivity reduces heat gain and liquid boil-off. The inherent flexibility of Cryogel® Z's blanket form minimizes installation labor, eliminates the need for contraction joints, and makes the product durable and resistant to mechanical abuse.

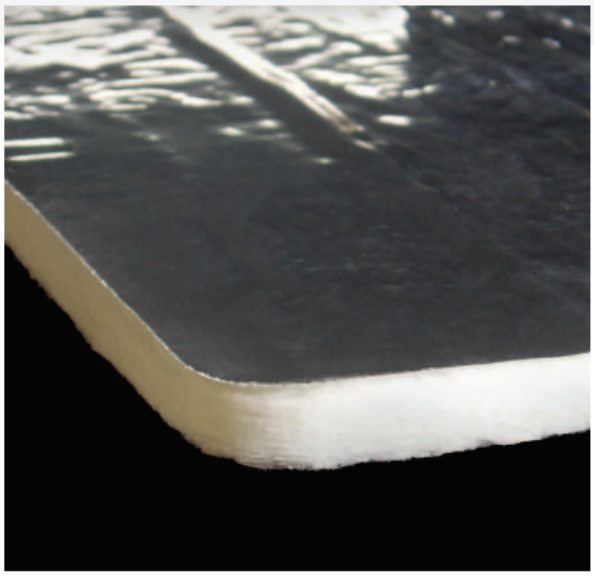

Physical Properties

Thicknesses*	0.20 in (5 mm)	0.40 in (10 mm)
Material Form*	57 in (1,450 mm) wide x 250 ft (76 m) long rolls	57 in (1,450 mm) wide x 150 ft (46 m) long rolls
Max. Use Temp.	257°F (125°C)	
Color	White	
Density*	10 lb/ft³ (0.16 g/cc)	
Hydrophobic	Yes	

*Nominal Values

Thermal Conductivity†

ASTM C 1728, Type I, Grade 1, Category B

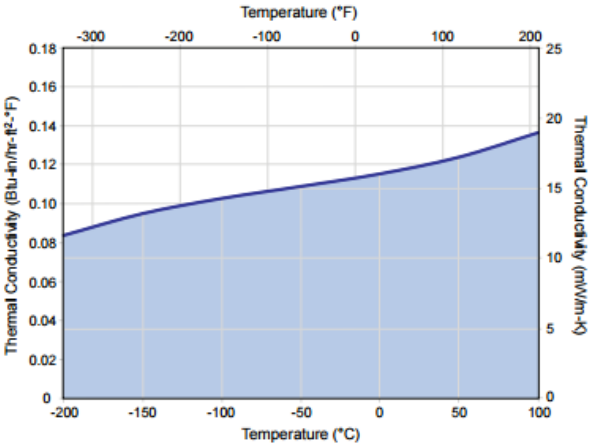

Mean Temp.	°F	-200	-100	0	75	100	200
	°C	-129	-73.3	-17.8	23.9	37.8	93.3
k	BTU-in/hr-ft²-°F	0.096	0.10	0.11	0.12	0.12	0.13
	mW/m-K	14	15	16	17	17	19

†Thermal conductivity typically measured at a compressive load of 2 psi.

Advantages

Superior Thermal Performance
Extremely low thermal conductivity (k-value) for improved efficiency and energy savings

Reduced Thickness and Profile
Can be installed at a fraction of the thickness of competing materials, enabling tighter packing of piping and equipment

Integral Vapor Retarder
Factory-laminated vapor retarder provides moisture protection, prevents damage from condensation and enhances process control

Eliminates Contraction Joints
Low-temperature flexibility eliminates the need for contraction joints, speeding installation and reducing complexity

Ease of Handling and Installation
Easily cut and conformed to complex patterns, Cryogel® Z excels in tight spaces with restricted access, allowing easier insulation of problem areas and improved adherence to site specifications

Physically Robust
Durable and flexible even at low temperatures, Cryogel® Z can recover from compression events and maintain performance, resulting in increased effectiveness over its lifetime

C. CYPLY® 1002 Reinforced Plastic Specifications

TECHNICAL DATASHEET

CYPLY® 1002 Reinforced Plastic

Mechanical properties at various temperatures, cont.

Orientation	Mechanical property	-60°F (-50°C)	70°F (21°C)	160°F (71°C)	250°F (121°C)
CROSSPLY	Flexural strength, PSI x 103	125 (865 MPa)	110 (760 MPa)	87 (600 MPa)	67 (460 MPa)
	Flexural modulus, PSI x 103	3.6 (24.8 GPa)	3.5 (24.1 GPa)	3.3 (22.8 GPa)	2.9 (20.0 GPa)
	Tensile strength, PSI x 103	85 (580 MPa)	70 (480 MPa)	65 (450 MPa)	61 (420 MPa)
	Tensile modulus, PSI x 106		3.4 (23.4 GPa)	3.4 (23.4 GPa)	2.7 (18.6 GPa)
	Compressive strength, PSI x 103	110 (760 MPa)	100 (690 MPa)	88 (605 MPa)	63 (435 MPa)

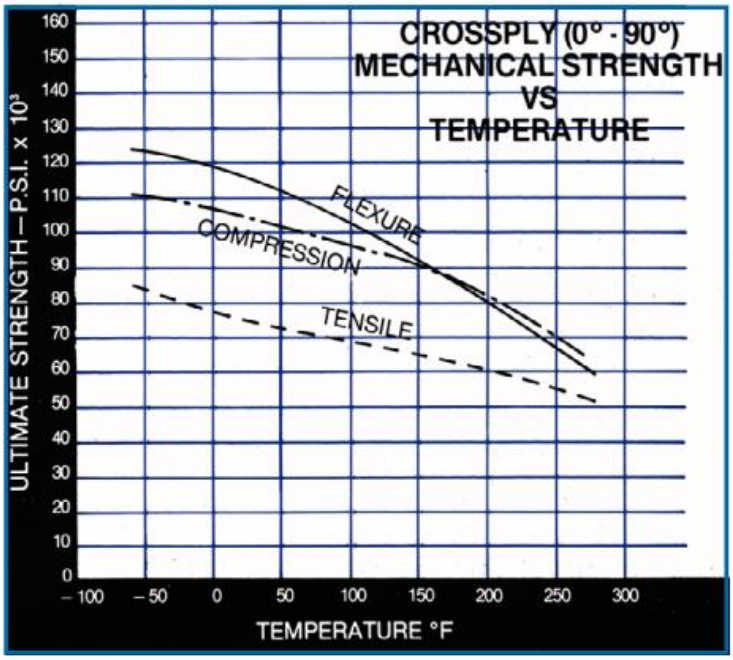

D. FLUENT Model Images

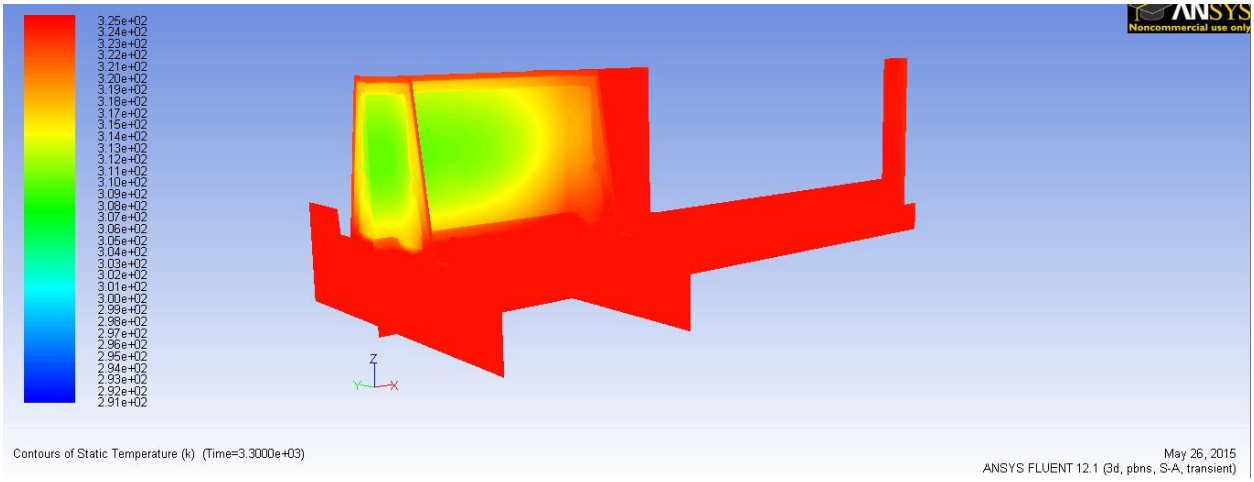

Figure A-1, 50 °C soak, no cooling, no insulation (~1 hr into test)

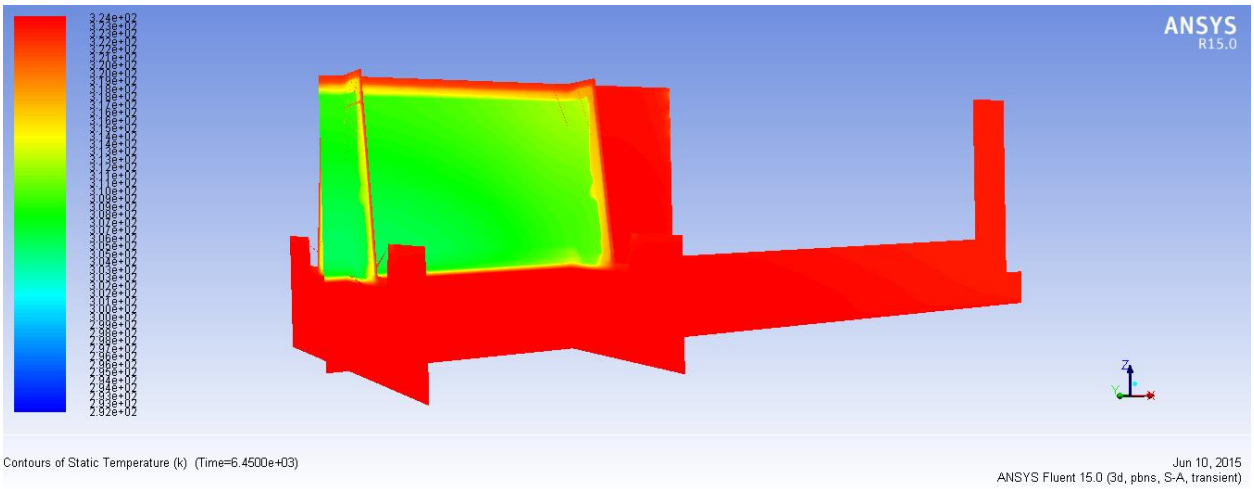

Figure A-2, 50 °C soak, no cooling, bottom insulation only (2 hours into test)

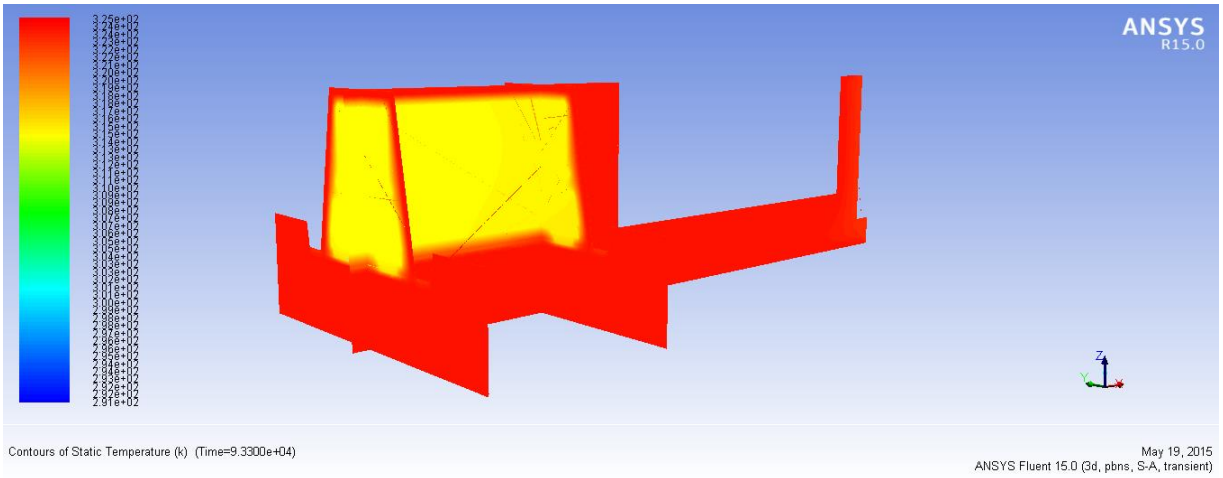

Figure A-3, 50 °C soak, no cooling, fully insulated (26 hours into test)

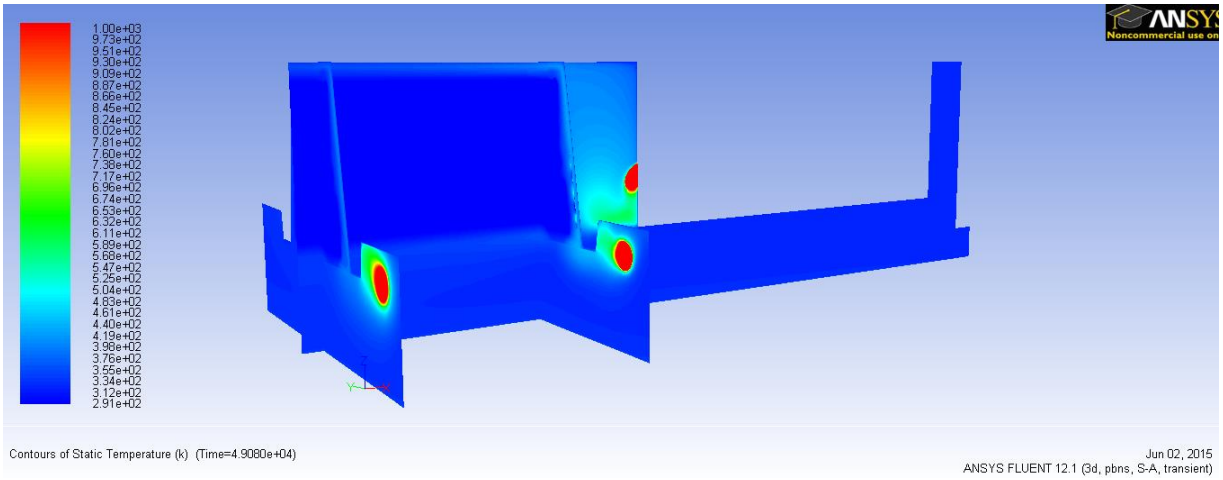

Figure A-4, Equilibrium temperature contours: cooled pack, no insulation

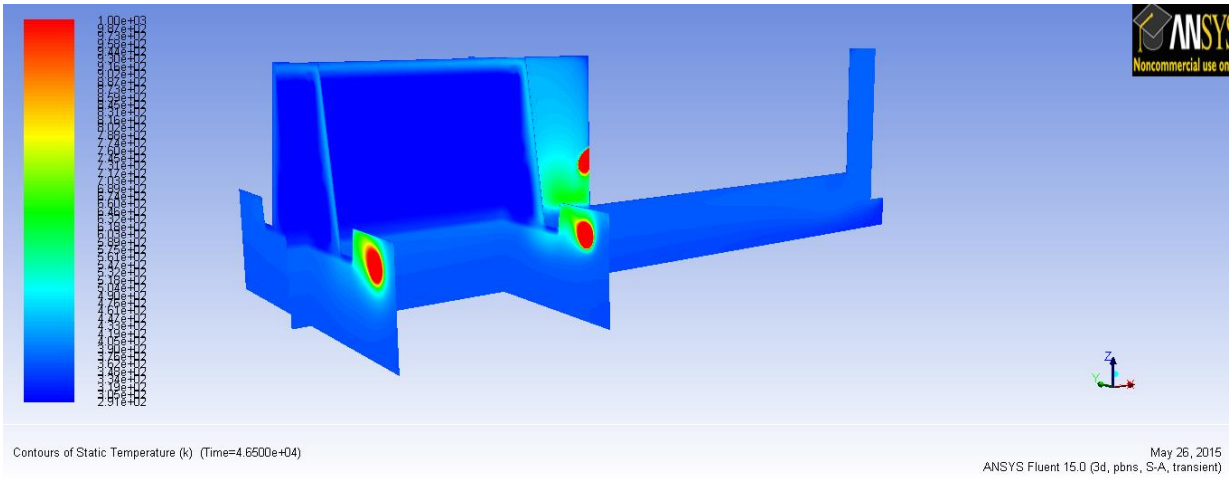

Figure A-5, Equilibrium temperature contours: cooled pack, bottom insulation only

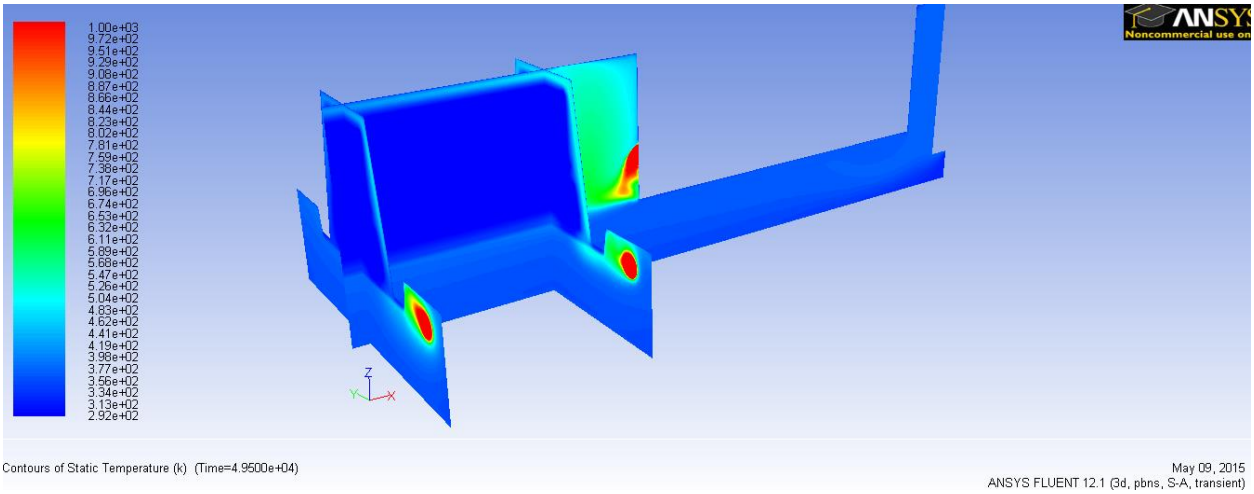

Figure A-6, Equilibrium temperature contours: cooled pack, fully insulated

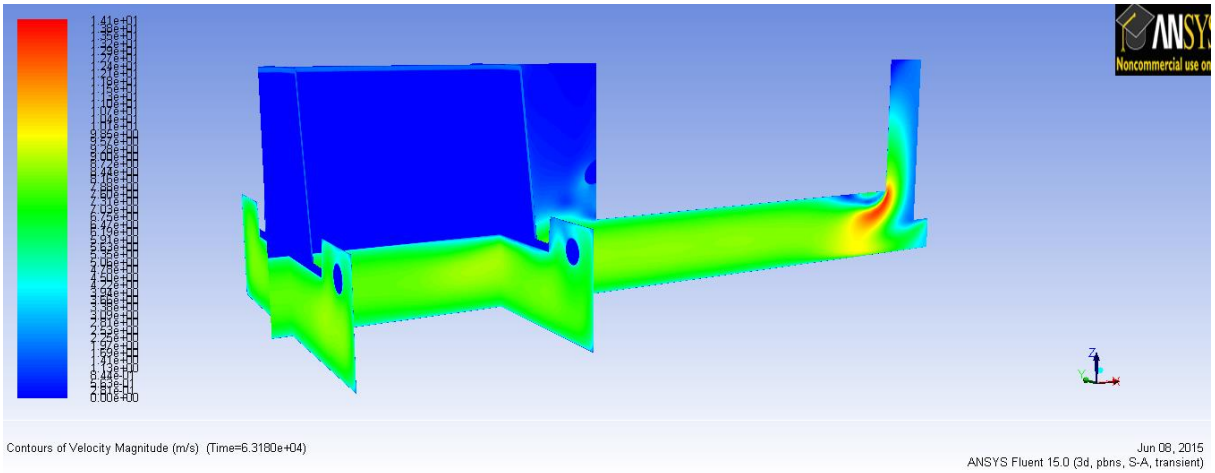

Figure A-7, Fully developed velocity profiles, moving vehicle

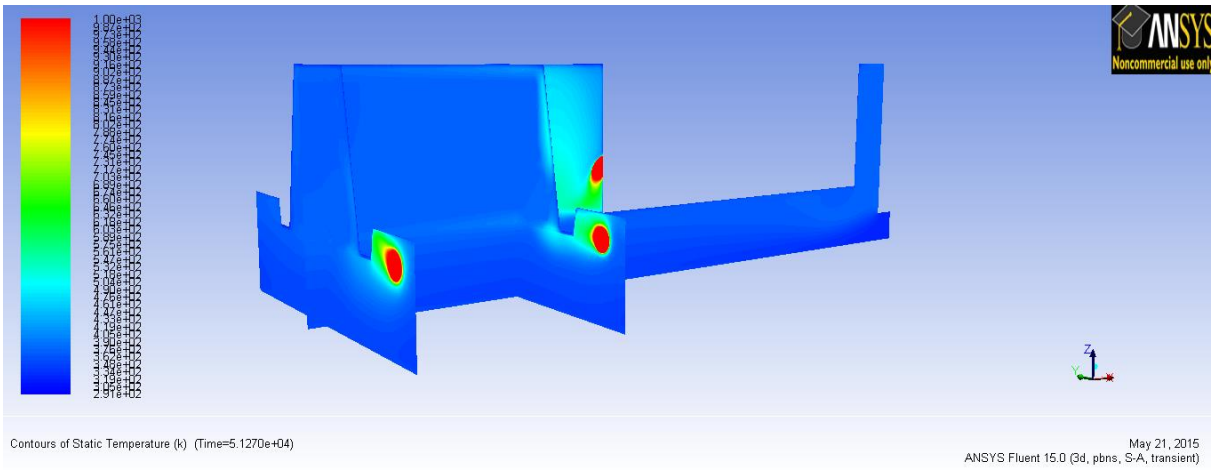

Figure A-8, Moving vehicle, no insulation, uncooled (14 hrs into test)

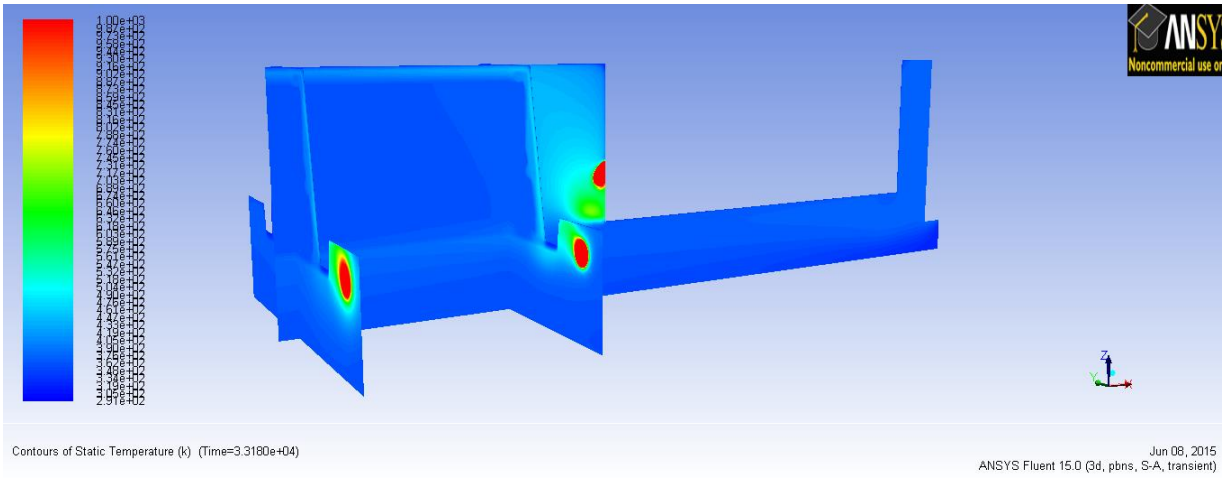

FIGURE A-9, MOVING VEHICLE, BOTTOM INSULATION ONLY, UNCOOLED (9 HRS INTO TEST)

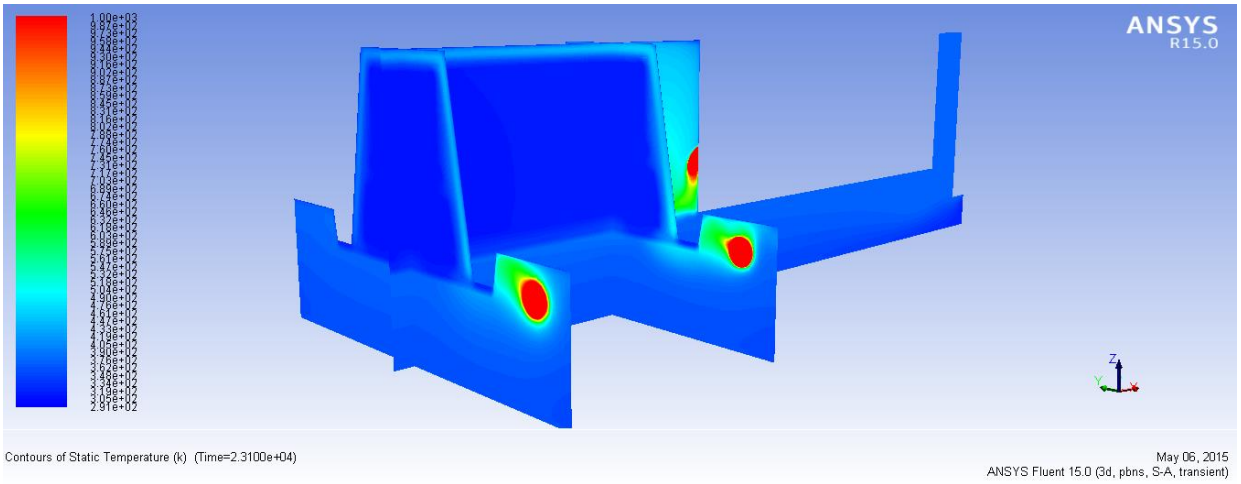

Figure A-10, Moving vehicle: fully insulated, uncooled (6.5 hrs into test)

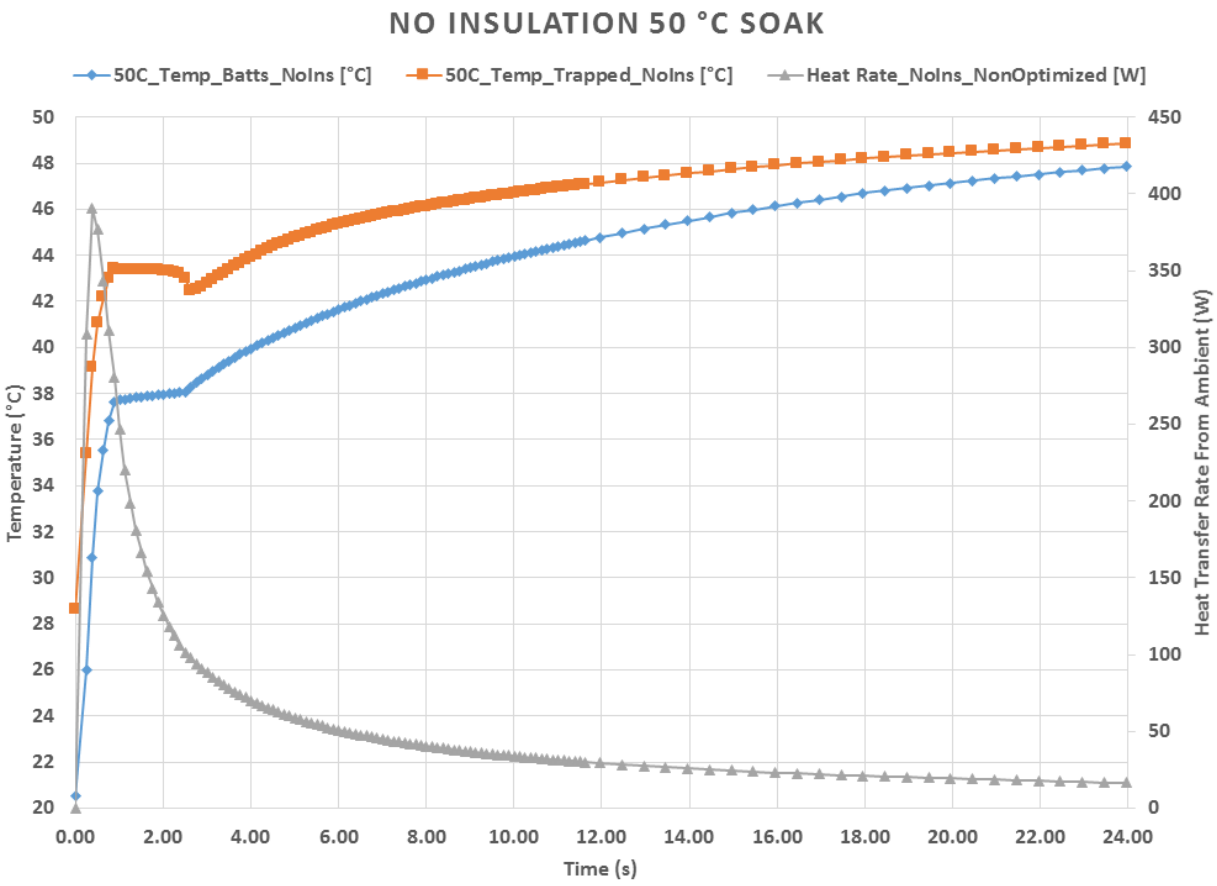

Figure A-11, 50 °C Soak with no insulation data

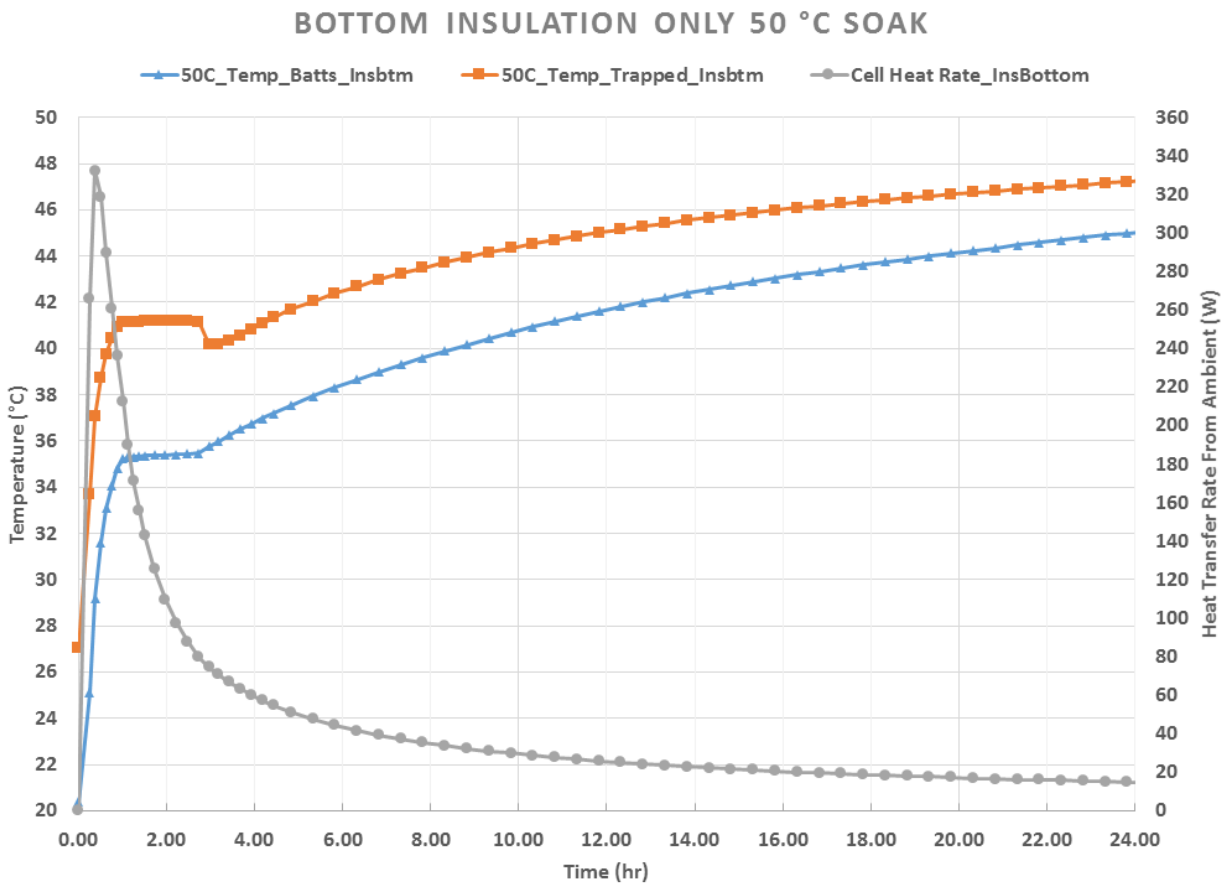

Figure A-12, Simulated 50 °C soak bottom insulation only data

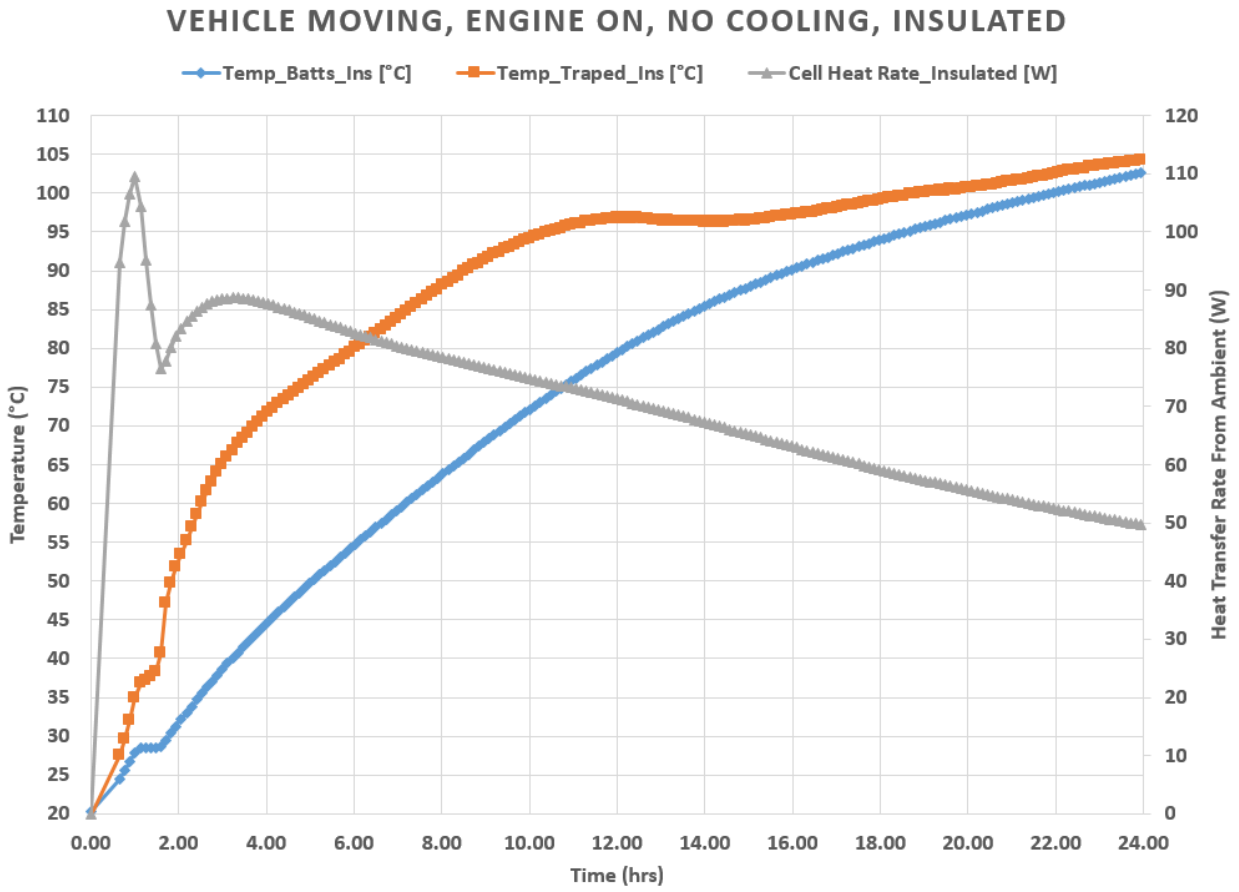

Figure A-13, Test data: moving vehicle, fully insulated

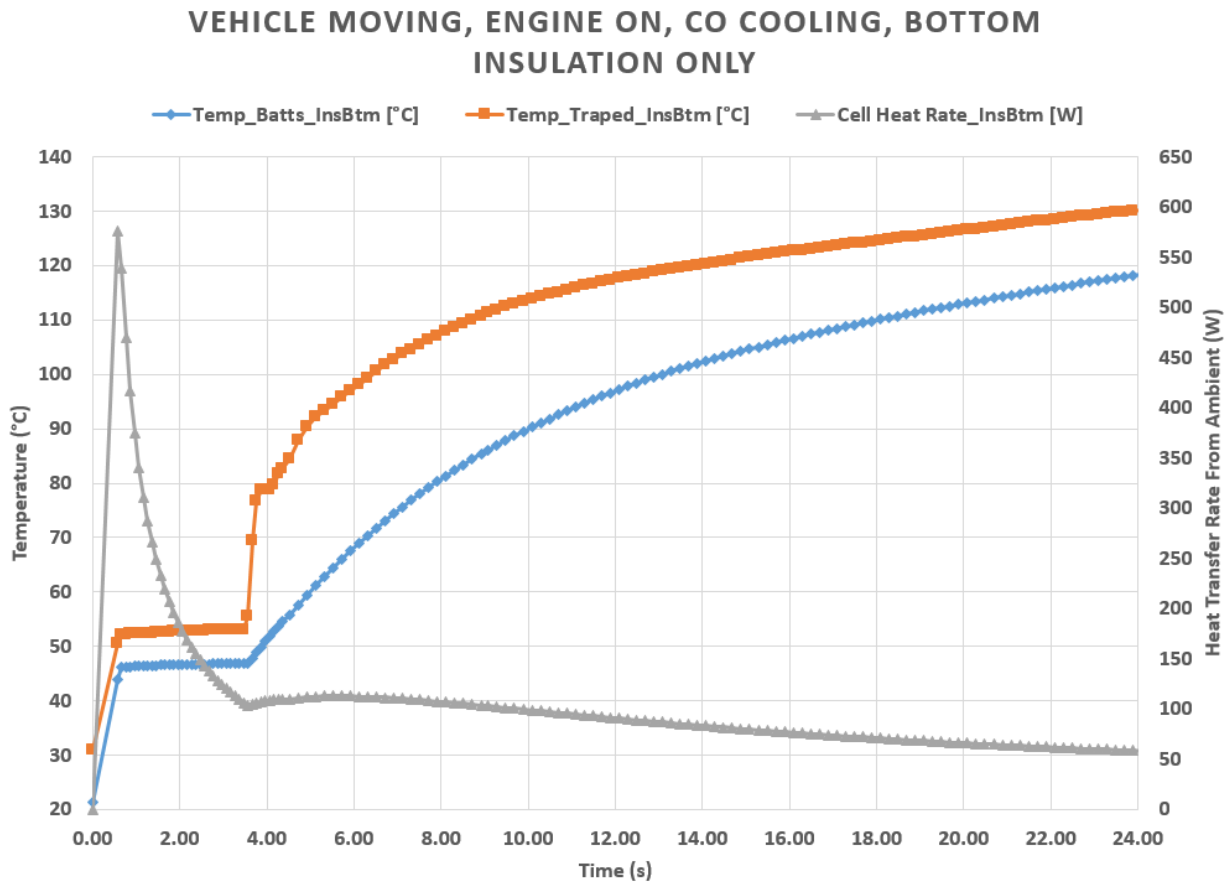

Figure A-14, Test data: moving vehicle, bottom insulation only

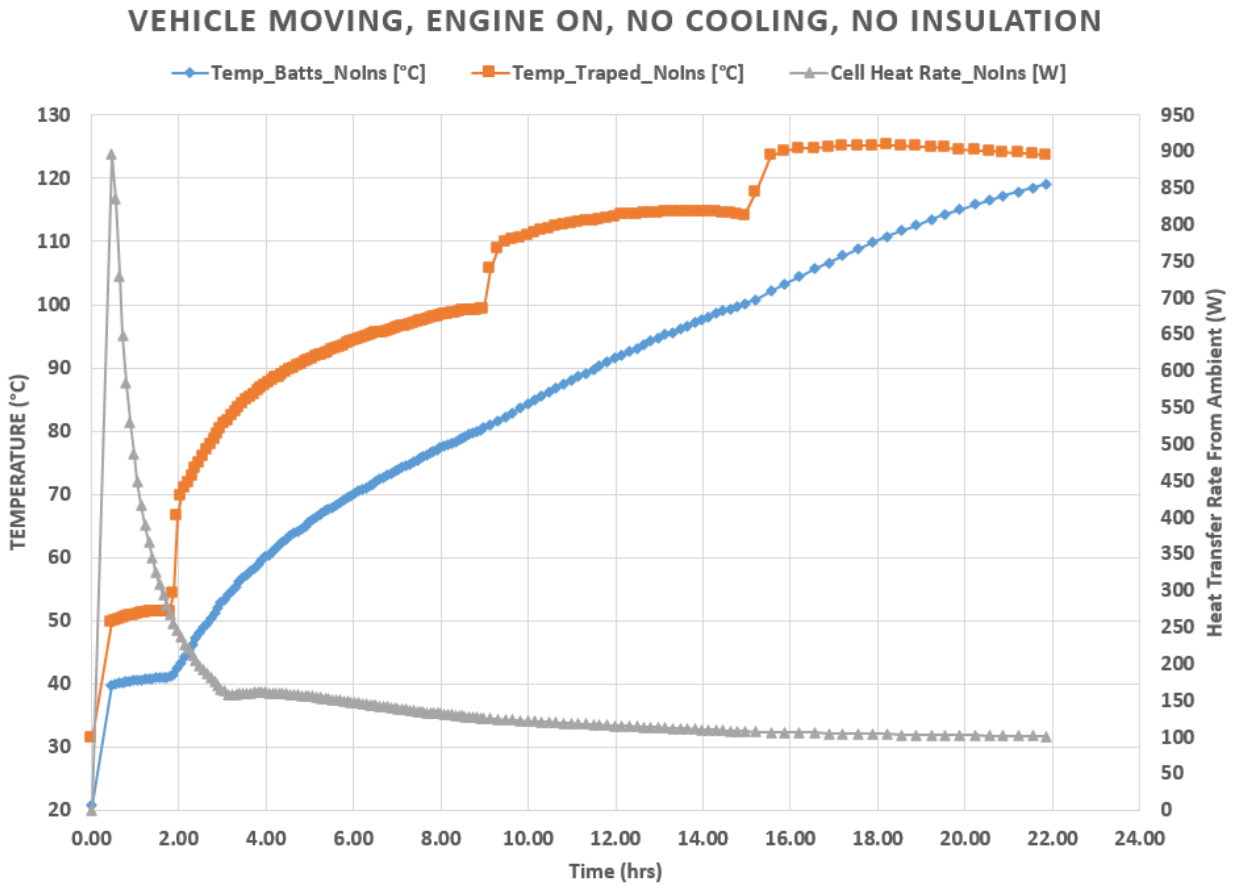

Figure A-15, Test data: moving vehicle, no insulation

Figure A-15 shows a unique case where there were three separate points in which the temperature rebounded for the air volume within an uninsulated pack. It is apparent that as the rate of heat transfer increases the relaxation factors need to be dynamically lessened to reduce overshoot.

Works Cited

[1] T. Badhauer, S. Garimella and T. F. Fuller, "A Critical Review of Thermal Issues in Lithium-Ion Batteries," *Journal of The Electrochemical Society,* vol. 1.158, pp. 1-25, 2011.

[2] S. Chen, C. Wang and Y. Wang, "Thermal Analysis of Lithium-ion Batteries," *Journal of Power Sources,* no. 140, pp. 111-124, 2004.

[3] K. Smith, M. Earleywine, E. Wood, J. Neubauer and A. Pesaran, "Comparison of Plug-In Hybrid Electric Vehicle Battery Life Across Geographies and Drive Cycles," *SAE International,* 2012.

[4] California Environmental Protection Agency, "Attachment A Status of ZEV Technology Commercialization," 25 November 2009. [Online]. Available: http://www.arb.ca.gov/msprog/zevprog/2009zevreview/attachment_a_tsd.pdf. [Accessed 17 October 2015].

[5] M. Hovis, "InsideEVs Exclusive Interview with General Motors EV1 Marketing Director John Dabels - Part 1," 2013. [Online]. Available: http://insideevs.com/insideevs-exclusive-interview-with-general-motors-ev1-marketing-director-john-dabels-part-1/. [Accessed 17 October 2015].

[6] C. Paine, Director, *Who Killed the Electric Car.* [Film]. USA: Plinyminor, Electric Entertainment, Papercut Films, 2006.

[7] Electric Transportation Applications, "General Motors EV1," U.S. Department of Energy, 1996. [Online]. Available: http://avt.inel.gov/pdf/fsev/eva/genmot.pdf. [Accessed 18 October 2015].

[8] A. Pesaran and G. Kim, "Battery Thermal System Design and Modeling," National Renewable Energy Laboratory, Washington, 2006.

[9] Electric Transportation Applications, "General Motors EV1 w/NiMH," U.S. Department of Energy, 1999. [Online]. Available: http://avt.inel.gov/pdf/fsev/eva/ev1_eva.pdf. [Accessed 18 October 2015].

[10] Green Car Congress, "Toyota Outlines RAV4 EV Policy," 16 July 2006. [Online]. Available: http://www.greencarcongress.com/2006/07/toyota_outlines.html. [Accessed 17 October 2015].

[11] R. Cogan, "Ford Ecostar EV," 1993. [Online]. Available: http://www.greencar.com/articles/fords-hot-ecostar-electric-car.php. [Accessed 2013].

[12] G. Berdichevsky, K. Kelly and E. Toomre, "The Tesla Roadster Battery System," 16 August 2006. [Online]. Available: http://www.casacota.cat/dispara2/TeslaRoadsterBatterySystem.pdf. [Accessed 11 October 2015].

[13] Tesla Motors, "2009 Tesla Roadster," 2008. [Online]. Available: https://web.archive.org/web/20081230181142/http://www.teslamotors.com/performance/tech_specs.php. [Accessed 18 October 2015].

[14] N. Bristow, "2011 Nissan Leaf US pricing officially announced: as low as $25,280*," 30 March 2011. [Online]. [Accessed 17 October 2015].

[15] Autocar, "Tokyo Video: Nissan Leaf," [Online]. Available: http://www.autocar.co.uk/car-news/new-cars/tokyo-video-nissan-leaf. [Accessed 23 July 2013].

[16] R. Matthe, L. Turner, M. Horst and A. Opel, "VOLTEC Battery System for Electric Vehicle with Extended Range," *SAE Internaltional,* no. 1373.1, pp. 1-19, 2001.

[17] Automotive Engineer, "Dana helps the Chevrolet Volt stay cool," 15 March 2011. [Online]. Available: https://ae-plus.com/technology/dana-helps-the-chevrolet-volt-stay-cool. [Accessed 18 October 2015].

[18] Car and Driver, "Tesla Mosel S Review," Car and Driver, 2015. [Online]. Available: http://buyersguide.caranddriver.com/tesla/model-s/specs#features. [Accessed 17 October 2015].

[19] J. Voelcker, "Tesla Model S Electic Car: Changes From 2012 Through 2015 (Updated)," 9 October 2015. [Online]. Available: http://www.greencarreports.com/news/1092439_tesla-model-s-electric-car-what-has-changed-since-2012. [Accessed 18 October 2015].

[20] A. G. Nandi, *Tesla: Supercharging the Future,* New York: New York University, 2013.

[21] T. Markel and A. Simpson, "Cost-Benefit Analysis of a Plus-In Hybrid Electric Vehicle Technology," in *22nd International Electric Vehicle Symposium*, Yokohama, 2006.

[22] A. Simpson, "Response to the CARB ZEV Expert Panel Position on Lithium-Ion Full-Performance Battery Electric Vehicles," Tesla Motors Inc, Palo Alto, 2008.

[23] "Relative Efficiency of Various Electric and Hybrid Drivetrains," Freedom Formula Foundation, Suntree, 2006.

[24] M. Rosen, "Comparative efficiency assessments for a range of hydrogen production processes," *International Journal of Hydrogen Energy,* vol. 23, no. 8, pp. 653-659, 1998.

[25] M. Eberhard and M. Tarpenning, "The 21st Century Electric Car," 6 October 2006. [Online]. Available: http://web.stanford.edu/group/greendorm/participate/cee124/TeslaReading.pdf. [Accessed 17 October 2015].

[26] Cadex Electronics Inc., "Advantages and limitations of the Different Types of Batteries - Battery University," 01 November 2010. [Online]. Available: http://batteryuniversity.com/learn/article/whats_the_best_battery. [Accessed 17 October 2015].

[27] L. Gaines and R. Cuenca, "Costs of Lithium-Ion Batteries for Vehicles," Argonne National Laboratory, Argonne, 2000.

[28] Harding Energy Inc., "Lithium Iron Phosphate," 2015. [Online]. Available: http://hardingenergy.com/lithium-iron-phosphate/. [Accessed 17 October 2015].

[29] F. B. Tudron, J. R. Akridge and V. J. Puglisi, "Lithium-Sulfur Rechargeable Batteries: Characteristics, State," 2004. [Online]. Available: http://www.sionpower.com/pdf/articles/PowerSources2004.pdf. [Accessed 17 October 2015].

[30] A. Pesaran, "Battery Thermal Management in EVs and HEVs," in *Advanced Automotive Battery Conference*, Las Vegas, 2001.

[31] R. Kizilel, R. Sabbah, R. Selman and S. Al-Hallaj, "An Alternative Cooling System to Enhance the Safety of Li-ion Battery Packs," *Journal of Power Sources,* no. 194, pp. 1105-1112, 2009.

[32] G. Jayaraman, G. Anderson, S. Kaushik and P. Klause, "Modeling of Battery Pack Thermal Management System for a Plug-In Hybrid Electric Vehicle," *SAE International,* vol. 0666.1, pp. 1-11, 2001.

[33] Y. Saito, "Thermal begaviors of Lithium-ion batteries during high-rate pulse cycling," *Journal of Power Sources,* no. 146, pp. 770-774, 2005.

[34] TE Technology Inc., 2010. [Online]. Available: https://tetech.com/wp-content/uploads/2013/11/HP-199-1.4-1.5.pdf. [Accessed 17 October 2015].

[35] Kokam, [Online]. Available: http://www.metricmind.com/audi/images/_0026_kokam.jpg. [Accessed 17 October 2015].

[36] M. Yue and H. Teng, "A Comparative Study of Thermal Characteristics of Lithium-ion Batteries for Vehicle Applications," *SAE International,* vol. 01.0668, pp. 1-12, 2011.

[37] Aspen Aerogels, "Cryogel_Z_DS," 2014. [Online]. Available: http://www.aerogel.com/_resources/common/userfiles/file/Data%20Sheets/Cryogel_Z_DS.pdf. [Accessed 17 October 2015].

[38] J. Brennan and G. Clark, "UOIT EcoCAR Technical Presentation," in *EcoCAR Challenge Final Competition*, Milford, 2011.

[39] Advanced Vehicle Technology Competitions, "EcoCAR The Next Challenge," 2015. [Online]. Available: http://avtcseries.org/competitions/ecocar/. [Accessed 19 October 2015].

[40] M. Moon, "GM powers data center with used Chevy Volt batteries," 17 June 2015. [Online]. Available: http://www.engadget.com/2015/06/17/gm-chevy-volt-old-batteries/. [Accessed 18 October 2015].

[41] A. Awarke, M. Jaeger, S. Pischinger and O. Oezdemir, "Comparison of Model Predictions with Temperature Data Sensed On-Board from the Li-ion Polymer Cells of an Electric Vehicle," *SAE International,* p. 9, 15 May 2012.

[42] P. Taheri and M. Bahrami, "Temperature Rise in Prismatic Polymer Lithium-Ion Batteries: An Analytic Approach," *SAE International Journal of Passenger Cars,* vol. 5, no. 1, pp. 164-176, 2012.

[43] A123 Systems, "AMP20 Lithium Ion Prismatic Cell," [Online]. Available: http://www.a123systems.com/Collateral/Images/English-US/AMP20.jpg. [Accessed 17 October 2015].

[44] Fluent Inc., "Pressure-Based Solver," in *Fluent 6.3 User's Guide*, 2006, p. Section 25.1.1.

[45] A. Pesaran and T. Markel, "Battery Requirements and Cost-Benefit Analysis for Plus-In Hybrid Vehicles," in *The 24th International Batter Seminar & Exhibit*, Fort Lauderale, 2007.

[46] M. Fetcenko, S. Ovshinsky, B. Reichman, K. Young, C. Fierro, J. Koch, A. Zallen, W. Mays and T. Ouchi, "Recent advances in NiMH battery technology," *Journal of Power Sources,* vol. 165, pp. 544-551, 2006.

[47] A. Taylor III, "Nissan's Leaf up close," Fortune, 17 February 2010. [Online]. Available: http://archive.fortune.com/galleries/2010/fortune/1002/gallery.nissan_leaf.fortune/. [Accessed 17 October 2015].

[48] S. Kahteeb, M. Farid, R. Selman and S. Al-Hallaj, "Design and simulation of a lithium-ion battery with a phase change material thermal management system for an electric scooter," *Journal of Power Sources,* no. 128, pp. 292-307, 2003.

[49] B. Black, "A Tale of Two Hybrids," 08 March 2007. [Online]. Available: http://evworld.com/article.cfm?storyid=1206&first=10228&end=10227. [Accessed 17 October 2015].

[50] O. P. Branko Remek, "Mechanical Efficiency of Small Engines for Passenger Cars," in *FISITA World Automotive Congress*, Seoul, 2000.

[51] A. Pesaran, A. Vlahinos and T. Stuart, "Cooling and Preheating of Batteries in Hybrid Electric Vehicles," in *The 6th ASME-JSME Thermal Engineering Joint Conference* , Kohala Coast, 2003.

[52] Crytec Engieered Materials, "Cyply 1002 Reinforces Plastic," [Online]. Available: http://www.redseal.com/download/Spec_Cyply2.pdf. [Accessed 17 October 2015].

[53] A. Mills and S. Al-Hallaj, "Simulation of a Passive Thermal Management System for Lithium-ion Battery Packs," *Journal of Power Sources,* no. 141, pp. 307-315, 2005.

[54] A. Alrashdan, A. Mayyas and S. Al-Hallah, "Thermo-Mechanical Behaviors of the Expanded Graphite-Phase Change Material Matrix Used for Thermal Management of Li-ion Battery Packs," *Journal of Power Sources,* no. 141, pp. 307-315, 2005.

[55] G. Guo, B. Long, B. Cheng, S. Zhou and P. Xu, "Three-Dimensional Thermal Finite Element Modelling of Lithium-ion Battery in Thermal Abuse Application," *Journal of Power Sources,* no. 195, p. 239302398, 2010.

[56] D. Ghosh, K. King, B. Schwemmin and D. Zhu, "Full Hybrid Electrical Vehicle Battery Pack System Design, CFD Simulation and Testing," *SAE Techical Paper,* p. 17, 12 April 2010.

[57] O. Gross and S. Clark, "Optimizing Electric Vehicle Battery Life Through Battery Thermal Management," *SAE International,* vol. 1.1370, pp. 1-16, 2011.

[58] A. Ingram, "Tesla's Battery Gigafactory May Achieve Nirvana: $100 Per Kilowatt-Hour, Report Says," 28 August 2014. [Online]. Available: http://www.greencarreports.com/news/1094102_teslas-battery-gigafactory-will-achieve-nirvana-100-per-kilowatt-hour-report-says. [Accessed 17 October 2015].

[59] J. B. Siegel, A. G. Stefanopoulou, P. Hagans, Y. ding and D. Gorsich, "Expansion of Lithium Ion Pouch Cell Batteries: Observations from Neutron Imaging," *Journal of the Electrochemical Society,* vol. 160, no. 8, pp. A1031-A1038, 2013.

[60] "EPA rating for 85 kWh Tesla Model S: 89 MPGe, 265-mile range," Green Car Congress, 21 June 2012. [Online]. Available: http://www.greencarcongress.com/2012/06/models-20120621.html. [Accessed 17 October 2015].

[61] Government of Canada, "Daily Data Report for January 2014," 22 September 2015. [Online]. Available:

http://climate.weather.gc.ca/climateData/dailydata_e.html?timeframe=2&Prov=ON&StationID=30435&dlyRange=2000-08-22|2015-10-17&Year=2014&Month=1&Day=01. [Accessed 18 October 2015].

[62] U.S. Advanced Battery Consortium, U.S. Department of Energy National Laboratory, "Electric Vehicle Battery Test Procedures Manual," January 1996. [Online]. Available: http://avt.inl.gov/battery/pdf/usabc_manual_rev2.pdf. [Accessed 18 October 2015].

[63] U.S. Department of Energy Vehicle Technologies Program, Battery Test Manual For Plug-In Hybrid Electric Vehicles, Idaho: U.S. Department of Energy National Laboratory, 2008.